Dynamical Casimir effect for gravitons in bouncing braneworlds

Marcus Ruser* and Ruth Durrer†
Département de Physique Théorique, Université de Genève,
24 quai Ernest Ansermet, 1211 Genève 4, Switzerland.
(Dated: April 5, 2007)

We consider a 2-brane system in a 5 dimensional Anti-de Sitter spacetime. We study particle creation due to the motion of the physical brane which first approaches the second static brane (contraction) and then recedes from it (expansion). We calculate the spectrum and the energy density of the generated gravitons. We show that the massless gravitons have a blue spectrum and that their energy density satisfies the nucleosynthesis bound with very mild constraints on the parameters. We also show that the Kaluza-Klein modes cannot provide the dark matter in an Anti-de-Sitter braneworld. However, for natural choices of parameters, back reaction from the KK-gravitons may well become important.

PACS numbers: 04.50.+h, 11.10.Kk, 98.80.Cq

I. INTRODUCTION

In recent times, the possibility that our observed Universe might represent a hypersurface in a higher dimensional spacetime has received considerable attention. The main motivation for this idea is the fact, that string theory [1, 2], which is consistent only in ten spacetime dimensions (or 11 for M–theory) allows for solutions where the standard model particles (like fermions and gauge bosons) are confined to some hypersurface (called the brane) and only the graviton can propagate in the bulk [2, 4]. Since gravity is not well constrained at small distances, the dimensions normal to the brane, the extra dimensions, can be as large as 0.1mm. The presence of two or more such extra-dimensions can provide a solution to the hierarchy problem, the problem of the huge difference between the Planck scale and the electroweak scale [3].

Here we consider another interesting consequence: within the context of braneworlds, cosmological evolution, i.e., the expansion of the Universe can be understood as motion of the brane which represents our Universe in the bulk. We consider a 5-dimensional Anti-de Sitter spacetime, as proposed in Randall Sundrum I [5], with two branes in it. For definiteness we keep the second brane at rest, while the first one, our universe, moves. This represents a spacetime with moving boundaries. Such moving boundaries can lead to particle creation via the dynamical Casimir effect [8]. We want to study the generation of gravitons in this context.

Previously, we have shown that in a radiation dominated universe, where the second, static brane is arbitrarily far away, no gravitons are produced [21]. It has also been shown that during a de Sitter phase of brane expansion, graviton production is basically like in four dimensional inflationary cosmology [22].

Motivated by the ekpyrotic Universe (see [23, 24] and Refs. therein) and similar ideas, we consider two branes which first approach each other. During this phase the physical brane, representing our Universe is contracting. We then suppose that some high energy mechanism which we do not want to specify in any detail, turns around the motion of the brane leading to an expanding Universe (see Fig. 1).

The Lanczos-Sen-Darmois-Israel-junction conditions [9, 10, 11, 12], relate the energy-momentum tensor on the brane to the extrinsic curvature and hence to the brane motion. Initially, the motion is very slow. Then the brane contracts, the energy density on the brane increases and the motion becomes faster. We do not model the transition from contraction to subsequent expansion in any detail, since this would require detailed assumptions about unknown physics, but we shall therefore ignore results which depend on the details of the transition. After some more or less close encounter, which we call the bounce, the physical brane moves away from the static brane, leading to an expanding universe. Expansion is first fast and then becomes slower as the energy density drops.

We consider the bulk graviton field initially to be in the vacuum state. We then evolve the graviton modes which are spin-2 on the brane through the bounce until late time, where we shall count the gravitons. The interactions dissappear at very early and at very late times, such that the entire process can be treated like an ordinary scattering process.

Similar results could be obtained for the free gravi-photon and gravi-scalar i.e. when we neglect the perturbations of the brane energy momentum tensor which also couple to these gravity wave modes which have spin-1 respectively spin-0 on the brane.

In this paper we address the following questions: What is the spectrum and energy density of the produced gravitons, the massless zero-mode and the Kaluza-Klein modes? Can the graviton production in such a brane universe lead to limits e.g. on the AdS curvature scale via the nucleosynthesis bound? Can the Kaluza-Klein

*Electronic address: marcus.ruser@physics.unige.ch
†Electronic address: ruth.durrer@physics.unige.ch

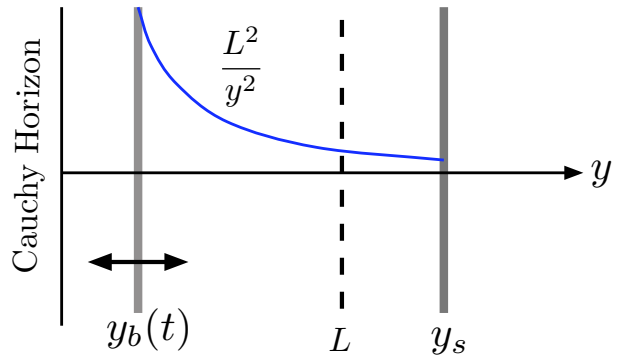

FIG. 1: Two branes in an AdS$_5$ spacetime. The physical brane is on the left. While it is approaching the static brane its scale factor is decreasing and when it moves away from the static brane it is expanding. The value of the scale factor of the brane metric as function of the extra dimension y is also indicated.

modes provide the dark matter or lead to stringent limits on these models? For this we investigate numerically graviton production due to the brane motion.

The reminder of the paper is organized as follows. In the next section we repeat the basic equations for the evolution of the background and perturbations. In Section III we present some basics of quantum particle creation in a space with moving boundaries and in Section IV we derive expressions for the energy density and the power spectrum of gravitons. In Section V we describe our numerical results. In Section VI we reproduce some of the numerical results with analytical approximations and we derive fits for the number of produced gravitons. We discuss our main results in Section VII and conclude in Section VIII. Some technical aspects are collected in appendices.

This rather long and technical paper is accompanied by a Letter [41] where we summarize the main results and comment on their interpretation and importance for braneworld cosmology.

II. GRAVITONS IN MOVING BRANEWORLDS

A. Tensor perturbations in AdS$_5$

We consider a AdS-5 spacetime. In Poincaré coordinates, the bulk metric is given by

$$\mathrm{d}s^2 = g_{AB}\mathrm{d}x^A\mathrm{d}x^B = \frac{L^2}{y^2}\left[-\mathrm{d}t^2 + \delta_{ij}\mathrm{d}x^i\mathrm{d}x^j + \mathrm{d}y^2\right] . \tag{2.1}$$

The physical brane (our Universe) is located at some time dependent position $y = y_b(t)$, while the static brane is at the fixed position $y = y_s$. The induced metric on the physical brane is given by

$$\begin{aligned} ds^2 &= \frac{L^2}{y_b^2(\eta)}\left[-\left(1-\left(\frac{dy_b}{dt}\right)^2\right)dt^2 + \delta_{ij}\mathrm{d}x^i\mathrm{d}x^j\right] \\ &= a^2(\eta)\left[-\mathrm{d}\eta^2 + \delta_{ij}dx^i dx^j\right] , \end{aligned} \tag{2.2}$$

where $a = L/y_b$ is the scale factor and η denotes the "conformal time" of an observer on the brane,

$$d\eta = \sqrt{1-\left(\frac{dy_b}{dt}\right)^2}\,dt \equiv \gamma^{-1}dt . \tag{2.3}$$

We have introduced

$$v \equiv \frac{dy_b}{dt} = -\frac{LH}{\sqrt{1+L^2H^2}} \qquad \text{and} \tag{2.4}$$

$$\gamma = \frac{1}{\sqrt{1-v^2}} = \sqrt{1+L^2H^2} . \tag{2.5}$$

Here H is the usual Hubble parameter,

$$H \equiv \dot{a}/a^2 \equiv a^{-1}\mathcal{H} = -L^{-1}\gamma v , \tag{2.6}$$

where an over-dot denotes the derivative w.r.t conformal time η. The bulk cosmological constant Λ is related to the curvature scale L by $\Lambda = -6/L^2$. The junction conditions on the brane lead to [26]

$$\kappa_5(\rho+\mathcal{T}) = 6\frac{\sqrt{1+L^2H^2}}{L} = 6L^{-1}\gamma , \tag{2.7}$$

$$\kappa_5(\rho+P) = -\frac{2L\dot{H}}{a\sqrt{1+L^2H^2}} - 2L^{-1}\dot{\gamma} , \tag{2.8}$$

$$\dot{\rho} = -3Ha(\rho+P) , \tag{2.9}$$

$$H^2 = \frac{\kappa_5^2}{18}\mathcal{T}\rho\left(1+\frac{\rho}{2\mathcal{T}}\right) + \frac{\kappa_5^2\mathcal{T}^2}{36} - \frac{1}{L^2} , \tag{2.10}$$

Equations (2.7) to (2.10) form the basis of brane cosmology and have been discussed at length in the literature (for a review, see [16] or [27]). The last equation is called the "modified Friedmann equation" for brane cosmology [17]. For usual matter with $\rho + P > 0$, ρ decreases during expansion and at sufficiently late time $\rho \ll \mathcal{T}$. The ordinary 4-dimensional Friedmann equation is then recovered if

$$\frac{\kappa_5^2\mathcal{T}^2}{12} = \frac{3}{L^2} \quad \text{and we set} \quad \kappa_4 = 8\pi G_4 = \frac{\kappa_5^2\mathcal{T}}{6} . \tag{2.11}$$

Here we have neglected a possible four-dimensional cosmological constant. Defining the string and Planck scales by

$$\kappa_5 = \frac{1}{M_5^3} = L_s^3 , \qquad \kappa_4 = \frac{1}{m_{\rm Pl}^2} = L_{\rm Pl}^2, \tag{2.12}$$

respectively, the Randall-Sundrum fine tuning condition $\kappa_5/L = \kappa_4$, which follwos from Eq. (2.11), leads to

$$\frac{L}{L_s} = \left(\frac{L_s}{L_{\rm Pl}}\right)^2 . \tag{2.13}$$

We shall be interested mainly in the radiation dominated low energy phase, hence in the period where

$$P = \frac{1}{3}\rho \quad \text{and} \quad v \ll 1 \quad \text{so that} \quad \gamma \simeq 1 \ , d\eta \simeq dt \ . \tag{2.14}$$

In such a period, the solutions to the above equations are of the form

$$a(t) = \frac{|t| + t_b}{L}, \tag{2.15}$$

$$y_b(t) = \frac{L^2}{|t| + t_b}, \tag{2.16}$$

$$v(t) = -\frac{\mathrm{sign}(t) L^2}{(|t| + t_b)^2} \simeq HL \ . \tag{2.17}$$

Negative times describe a contracting phase, while positive times describe radiation dominated expansion. At $t = 0$, the scale factor exhibits a kink and the evolution equations are singular. This is the bounce which we shall not model in detail, but we will have to introduce a cut-off in order to avoid ultraviolet divergencies in the total particle number and energy density which are due to this unphysical kink.

We now consider tensor perturbations on this background,

$$\mathrm{d}s^2 = \frac{L^2}{y^2}\left[-\mathrm{d}t^2 + (\delta_{ij} + 2h_{ij})\mathrm{d}x^i \mathrm{d}x^j + \mathrm{d}y^2\right] \ . \tag{2.18}$$

Tensor modes satisfy the traceless and transverse conditions, $h^i_i = \partial_i h^i_j = 0$. We decompose h_{ij} into spatial Fourier modes,

$$h_{ij}(t, \boldsymbol{x}, y) = \int \frac{d^3k}{(2\pi)^{3/2}} \sum_{\bullet=+,\times} e^{i\boldsymbol{k}\cdot\boldsymbol{x}} e^{\bullet}_{ij}(\mathbf{k}) h_\bullet(t, y; k) \ , \tag{2.19}$$

where $e^{\bullet}_{ij}(\mathbf{k})$ are unitary constant transverse-traceless polarization tensors which form a basis of the two polarization states $\bullet = +$ and $\bullet = \times$. For h_{ij} to be real we require

$$h^*_\bullet(t, y; \mathbf{k}) = h_\bullet(t, y; -\mathbf{k}). \tag{2.20}$$

The perturbed Einstein equations yield the equation of motion for the mode functions $h_\bullet$, which obey the Klein-Gordon equation for minimally coupled massless scalar fields in AdS_5 [18, 19, 20]

$$\left[\partial_t^2 + k^2 - \partial_y^2 + \frac{3}{y}\partial_y\right] h_\bullet(t, y; \mathbf{k}) = 0 \ . \tag{2.21}$$

In addition to the bulk equation of motion the modes also satisfy a boundary condition at the brane coming from the second junction condition,

$$\left[LH\partial_t h_\bullet - \sqrt{1 + L^2H^2}\partial_y h_\bullet\right]\Big|_{y_\mathrm{b}} = \gamma^{-1}\left(v\partial_t - \partial_y\right) h_\bullet\big|_{y_\mathrm{b}} = \frac{\kappa_5}{2} a P \Pi^{(T)}_\bullet \tag{2.22}$$

We are interested in the quantum production of free gravitons, not at the coupling of gravitational waves to matter. Therefore we shall set $\Pi^{(T)}_\bullet = 0$ in the sequel. This is not entirely correct for the evolution of gravity modes since at late times, when matter on the brane is no longer a perfect fluid and anisotropic stresses develop which slightly modify the evolution of gravitational waves. We neglect this subdominant effect in our treatment.

B. Mode expansion in the late time limit

We restrict ourselves to relatively late times, when $\rho\mathcal{T} \gg \rho^2$ and therefore $v \ll 1$. In this limit the conformal time on the brane agrees roughly with the 5D time coordinate t and we shall therefore not distinguish these times in this work. Furthermore, the boundary condition (2.22) reduces to a Neumann boundary condition. Consequently the graviton amplitude is subject to the boundary conditions

$$\partial_y h_\bullet|_{y_\mathrm{b}} = \partial_y h_\bullet|_{y_s} = 0 \ . \tag{2.23}$$

In order to achieve a canonical formulation, i.e. a description of the graviton field and its dynamics in terms of field modes, we introduce instantaneous eigenfunctions $\phi_n(t, y)$ of the spatial part of the differential operator (2.21)

$$\left[-\partial_y^2 + \frac{3}{y}\partial_y\right]\phi_\alpha(t, y) = -y^3\partial_y\left[y^{-3}\partial_y\phi_\alpha(t, y)\right] = m^2_\alpha(t)\phi_\alpha(t, y). \tag{2.24}$$

Imposing the boundary conditions (2.23) for the eigenfunctions $\phi_\alpha(t, y)$, equation (2.24) forms a Sturm-Liouville problem at any given time t. Consequently, the set of eigenfunctions $\{\phi_\alpha(t, y)\}_{\alpha=0}^\infty$ is complete and orthonormal with respect to the inner-product

$$(\phi_\alpha, \phi_\beta) = \int_{y_b}^{y_r} \frac{dy}{y^3}\phi_\alpha(t, y)\phi_\beta(t, y) = \delta_{\alpha\beta}. \tag{2.25}$$

The case $\alpha = 0$ with $m_0 = 0$ is the zero-mode, i.e. the massless four-dimensional graviton. Its general solution in accordance with the boundary conditions is just a constant with respect to the extra dimension, $\phi_0(t, y) = \phi_0(t)$, and is fully determined by the normalization condition $(\phi_0, \phi_0) = 1$:

$$\phi_0(t) = \sqrt{2}\frac{y_s y_b(t)}{\sqrt{y_s^2 - y_b^2(t)}}. \tag{2.26}$$

For $\alpha = i \in \{1, 2, 3, \cdots, \}$ with non-negative eigenvalues $m_i \neq 0$ the general solution of (2.24) is a combination of the Bessel functions $J_2(m_i(t)\, y)$ and $Y_2(m_i(t)\, y)$. Their particular combination is determined by the boundary condition at the moving brane. The remaining boundary condition at the static brane selects the possible values

for the eigenvalues $m_i(t)$, the Kaluza-Klein (KK) masses. For any three-momentum $\mathbf{k}$ these masses build up an entire tower of momenta in direction y, the fifth dimension. Explicitly, the solutions $\phi_i(t,y)$ for the KK-modes read [1]

$$\phi_i(t,y) = N_i(t) y^2 \mathcal{C}_2\left(m_i(t)\, y\right) \tag{2.27}$$

with

$$\mathcal{C}_\nu(m_i y) = Y_1(m_i y_b) J_\nu(m_i y) - J_1(m_i y_b) Y_\nu(m_i y). \tag{2.28}$$

The normalization reads

$$N_i(t, y_b, y_s) = \left[\frac{2}{y_s^2 \mathcal{C}_2^2(m_i\, y_s) - \left(2/(m_i \pi)\right)^2}\right]^{\frac{1}{2}} \tag{2.29}$$

where we have used that

$$\mathcal{C}_2(m_i\, y_b) = \frac{2}{\pi\, m_i\, y_b}\ . \tag{2.30}$$

It can be simplified further by using

$$\mathcal{C}_2(m_i\, y_s) = \frac{Y_1(m_i\, y_b)}{Y_1(m_i\, y_s)} \frac{2}{\pi\, m_i\, y_s} \tag{2.31}$$

leading to

$$N_i = \frac{m_i \pi}{\sqrt{2}} \left[\frac{Y_1^2(m_i y_s)}{Y_1^2(m_i y_b) - Y_1^2(m_i y_s)}\right]^{\frac{1}{2}}. \tag{2.32}$$

Note that it is possible to have $Y_1^2(m_i\, y_s) - Y_1^2(m_i\, y_b) = 0$. But then both $Y_1^2(m_i y_s) = Y_1^2(m_i y_b) = 0$ and Eq. (2.32) has to be understood as a limit. For that reason, the expression (2.29) for the normalization is used in the numerical simulations. Its denominator remains always finite.

The time-dependent KK-masses $\{m_i(t)\}$ are determined by the condition

$$\mathcal{C}_1\left(m_i(t) y_s\right) = 0 \tag{2.33}$$

and the rate of change $\dot{m}_i/m_i$ of a KK-mass can be directly related to the normalization,

$$\hat{m}_i \equiv \frac{\dot{m}_i}{m_i} = \hat{y}_b\, \frac{2}{m_i^2\, \pi^2}\, N_i^2 \tag{2.34}$$

where we have set

$$\widehat{y}_{\rm b}(t) \equiv \partial_t \ln\left(y_{\rm b}\right) = -v y_{\rm b}^{-1} \simeq -Ha = -\frac{\dot{a}}{a} \equiv -\mathcal{H}\ . \tag{2.35}$$

Because the zeros of the cross product of the Bessel functions J_1 and Y_1 are not known analytically in closed form, the KK-spectrum has to be determined by solving Eq. (2.33) numerically[2].

On account of the completeness of the eigenfunctions $\phi_\alpha(t,y)$ the gravitational wave amplitude $h_\bullet(t,y;\mathbf{k})$ can now be expanded in these eigenfunctions. The coefficients $q_{\alpha,\mathbf{k},\bullet}(t)$ are canonical variables,

$$h_\bullet(t,y;\mathbf{k}) = \sqrt{\frac{\kappa_5}{L^3}} \sum_{\alpha=0}^{\infty} q_{\alpha,\mathbf{k},\bullet}(t) \phi_\alpha(t,y). \tag{2.36}$$

In order to satisfy (2.20) we have to impose the same condition for the canonical variables, i.e. $q^*_{\alpha,\mathbf{k},\bullet} = q_{\alpha,-\mathbf{k},\bullet}$. The factor $\sqrt{\frac{\kappa_5}{L^3}}$ has been introduced in order to render the $q_{\alpha,\mathbf{k},\bullet}$'s canonically normalized.

C. Equations of motion

Inserting the expansion (2.36) into the wave equation, (2.21) leads to the equations of motion for the variables $q_{\alpha,\mathbf{k},\bullet}$

$$\begin{aligned}\ddot{q}_{\alpha,\mathbf{k},\bullet} \ &+\ \omega_{\alpha,k}^2 q_{\alpha,\mathbf{k},\bullet} + \sum_\beta \left[M_{\beta\alpha} - M_{\alpha\beta}\right] \dot{q}_{\beta,\mathbf{k},\bullet} \\ &+\ \sum_\beta \left[\dot{M}_{\alpha\beta} - N_{\alpha\beta}\right] q_{\beta,\mathbf{k},\bullet} = 0\ ,\end{aligned} \tag{2.37}$$

where we have introduced the time-dependent frequency of a graviton mode

$$\omega_{\alpha,k}^2 = \sqrt{k^2 + m_\alpha^2}\ \ ,\ \ k = |\mathbf{k}|\ , \tag{2.38}$$

and the coupling matrices $M_{\alpha\beta}$ and $N_{\alpha\beta}$. The mode couplings occur due to the time-dependent boundary condition $\partial_y h_\bullet(t,y)|_{y_b} = 0$ which forces the eigenfunctions $\phi_\alpha(t,y)$ to be explicitly time-dependent. This system of equations as well as the specific form of the coupling matrices $M_{\alpha\beta}$ and $N_{\alpha\beta}$ has been derived in detail in Ref. [21]. For completeness we repeat the formulae for the matrix elements in Appendix A. Here we just mention that $N = MM^T$, so that we only need to calculate M. The matrix M is determined by the brane motion, i.e., the cosmological evolution which leads to particle creation.

III. QUANTUM GENERATION OF FIVE-DIMENSIONAL TENSOR PERTURBATIONS

A. Preliminary remarks

In this section we present a treatment of quantum generation of tensor perturbations, i.e. graviton production,

[1] Note that we have changed the parametrization of the solutions with respect to [21] for technical reasons.

[2] Approximate expressions for the zeros can be found in [36].

based on the formulation of the dynamical Casimir effect. The this section is partly based on [28, 29, 30] where the dynamical Casimir effect is discussed for a scalar field as well as for the electromagnetic field.
Asymptotically, i.e. for $t \to \pm\infty$ when the physical brane approaches the Cauchy horizon, $y_b \to 0$, and moves very slowly, the coupling matrices vanish and the Kaluza-Klein masses are constant (for y_b close to zero, Eq. (2.33) reduces to $J_1(m_i y_s) = 0$):

$$\lim_{t\to\pm\infty} M_{\alpha\beta}(t) = 0 \ , \ \lim_{t\to\pm\infty} m_\alpha(t) = \text{const.} \ . \tag{3.1}$$

In this limit, the system (2.37) reduces to an infinite set of uncoupled harmonic oscillators which allows to introduce an unambiguous and meaningful particle concept, i.e. notion of (massive) gravitons.
As a matter of fact, in the numerical simulations we have to switch the brane motion on and off at finite times. These times are denoted by $t_{\rm in}$ and $t_{\rm out}$, respectively. We then introduce the vacuum state with respect to times $t \le t_{\rm in} < 0$ and $t \ge t_{\rm out} > 0$. In order to avoid spurious effects influencing the particle creation, we have to chose $t_{\rm in}$ small, respectively $t_{\rm out}$ large enough such that the couplings are effectively zero at those times. Checking the independence of the numerical results on the choice of $t_{\rm in}$ and $t_{\rm out}$ guarantees that these times correspond effectively to the real asymptotic states of the brane configuration.

B. Quantization, initial and final state

Canonical quantization of the gravity wave amplitude is performed by replacing the canonical variables $q_{\alpha,\mathbf{k},\bullet}$ by the corresponding operators $\hat{q}_{\alpha,\mathbf{k},\bullet}$

$$\hat{h}_\bullet(t,y;\mathbf{k}) = \sqrt{\frac{\kappa_5}{L^3}} \sum_\alpha \hat{q}_{\alpha,\mathbf{k},\bullet}(t)\phi_\alpha(t,y). \tag{3.2}$$

Adopting the Heisenberg picture it follows that $\hat{q}_{\alpha,\mathbf{k},\bullet}$ satisfies the same equation (2.37) as the canonical variable $q_{\alpha,\mathbf{k},\bullet}$.
Under the assumptions outlined above, the operator $\hat{q}_{\alpha,\mathbf{k},\bullet}$ can be written for times $t \le t_{\rm in}$ as

$$\hat{q}_{\alpha,\mathbf{k},\bullet}(t \le t_{\rm in}) = \frac{1}{\sqrt{2\omega^{\rm in}_{\alpha,k}}} \left[\hat{a}^{\rm in}_{\alpha,\mathbf{k},\bullet} e^{-i\,\omega^{\rm in}_{\alpha,k}\,t} + \hat{a}^{\rm in\dagger}_{\alpha,-\mathbf{k},\bullet} e^{i\,\omega^{\rm in}_{\alpha,k}\,t}\right] \tag{3.3}$$

where we have introduced the reference frequency

$$\omega^{\rm in}_{\alpha,k} \equiv \omega_{\alpha,k}(t \le t_{\rm in}). \tag{3.4}$$

The set of annihilation and creation operators $\{\hat{a}^{\rm in}_{\alpha,\mathbf{k},\bullet}, \hat{a}^{\rm in\dagger}_{\alpha,\mathbf{k},\bullet}\}$ corresponding to the particle (graviton) notion for $t \le t_{\rm in}$ is subject to the usual commutation relations

$$\left[\hat{a}^{\rm in}_{\alpha,\mathbf{k},\bullet}, \hat{a}^{\rm in\dagger}_{\alpha',\mathbf{k}',\bullet'}\right] = \delta_{\alpha\alpha'}\delta_{\bullet\bullet'}\delta^{(3)}(\mathbf{k}-\mathbf{k}') \ , \tag{3.5}$$

$$\left[\hat{a}^{\rm in}_{\alpha,\mathbf{k},\bullet}, \hat{a}^{\rm in}_{\alpha',\mathbf{k}',\bullet'}\right] = \left[\hat{a}^{\rm in\dagger}_{\alpha,\mathbf{k},\bullet}, \hat{a}^{\rm in\dagger}_{\alpha',\mathbf{k}',\bullet'}\right] = 0. \tag{3.6}$$

For times $t \ge t_{\rm out}$, i.e. after the motion of the brane, the operator $\hat{q}_{\alpha,\mathbf{k},\bullet}$ can be expanded in a similar manner,

$$\hat{q}_{\alpha,\mathbf{k},\bullet}(t \ge t_{\rm out}) = \tag{3.7}$$
$$= \frac{1}{\sqrt{2\omega^{\rm out}_{\alpha,k}}} \left[\hat{a}^{\rm out}_{\alpha,\mathbf{k},\bullet} e^{-i\,\omega^{\rm out}_{\alpha,k}\,t} + \hat{a}^{\rm out\,\dagger}_{\alpha,-\mathbf{k},\bullet} e^{i\,\omega^{\rm out}_{\alpha,k}\,t}\right].$$

with final state frequency

$$\omega^{\rm out}_{\alpha,k} \equiv \omega_{\alpha,k}(t \ge t_{\rm out}). \tag{3.8}$$

The annihilation and creation operators $\hat{a}^{\rm out}_{\alpha,\mathbf{k},\bullet}, \hat{a}^{\rm out\,\dagger}_{\alpha,\mathbf{k},\bullet}$, correspond to a meaningful definition of final state particles (they are associated with positive and negative frequency solutions for $t \ge t_{\rm out}$) and satisfy the same commutation relations as the initial state operators.
Initial $|0,{\rm in}\rangle \equiv |0, t \le t_{\rm in}\rangle$ and final $|0,{\rm out}\rangle \equiv |0, t \ge t_{\rm out}\rangle$ vacuum state are uniquely defined via

$$\hat{a}^{\rm in}_{\alpha,\mathbf{k},\bullet}|0,{\rm in}\rangle = 0 \ , \ \hat{a}^{\rm out}_{\alpha,\mathbf{k},\bullet}|0,{\rm out}\rangle = 0 \ , \ \ \forall\ \alpha,\ \mathbf{k},\ \bullet \ . \tag{3.9}$$

Note that the notations $|0, t \le t_{\rm in}\rangle$ and $|0, t \ge t_{\rm out}\rangle$ do not mean that the states are time-dependent, states do not evolve in the Heisenberg picture. These are the *vacuum states* for times $t \le t_{\rm in}$ and $t \ge t_{\rm out}$, respectively, defined by the annihilation properties (3.9). The operators counting the number of particles defined with respect to the initial and final vacuum state, respectively, are

$$\hat{N}^{\rm in}_{\alpha,\mathbf{k},\bullet} = \hat{a}^{\rm in\,\dagger}_{\alpha,\mathbf{k},\bullet}\hat{a}^{\rm in}_{\alpha,\mathbf{k},\bullet} \ , \ \ \hat{N}^{\rm out}_{\alpha,\mathbf{k},\bullet} = \hat{a}^{\rm out\,\dagger}_{\alpha,\mathbf{k},\bullet}\hat{a}^{\rm out}_{\alpha,\mathbf{k},\bullet} \ . \tag{3.10}$$

The number of gravitons created during the motion of the brane for each momentum $\mathbf{k}$, quantum number α and polarization state $\bullet$ is given by the expectation value of the number operator $\hat{N}^{\rm out}_{\alpha,\mathbf{k},\bullet}$ of final-state gravitons with respect to the initial vacuum state $|0,{\rm in}\rangle$:

$$\mathcal{N}^{\rm out}_{\alpha,\mathbf{k},\bullet} = \langle 0,{\rm in}|\hat{N}^{\rm out}_{\alpha,\mathbf{k},\bullet}|0,{\rm in}\rangle. \tag{3.11}$$

If the brane undergoes a non-trivial dynamics between $t_{\rm in} < t < t_{\rm out}$ it is $\hat{a}^{\rm out}_{\alpha,\mathbf{k},\bullet}|0,{\rm in}\rangle \neq 0$ in general, and thus, particle production takes place.
From (2.19), the expansion (3.2) and Eqs.(3.3), (3.7) it follows that the amplitude of the five-dimensional tensor perturbations in the initial and final state can be written as

$$\hat{h}_{ij}(t \le t_{\rm in}, \mathbf{x}, y) = \tag{3.12}$$
$$\sqrt{\frac{\kappa_5}{L^3}} \sum_{\bullet\alpha} \int \frac{d^3k}{(2\pi)^{3/2}} \frac{\hat{a}^{\rm in}_{\alpha,\mathbf{k},\bullet}\, e^{-i\,\omega^{\rm in}_{\alpha,k}\,t}}{\sqrt{2\omega^{\rm in}_{\alpha,k}}}\, u^\bullet_{ij,\alpha}(t_{\rm in}, \mathbf{x}, y, \mathbf{k}) + \text{h.c.}$$

and

$$\hat{h}_{ij}(t \ge t_{\rm out}, \mathbf{x}, y) = \tag{3.13}$$
$$\sqrt{\frac{\kappa_5}{L^3}} \sum_{\bullet\alpha} \int \frac{d^3k}{(2\pi)^{3/2}} \frac{\hat{a}^{\rm out}_{\alpha,\mathbf{k},\bullet}\, e^{-i\,\omega^{\rm out}_{\alpha,k}\,t}}{\sqrt{2\omega^{\rm out}_{\alpha,k}}}\, u^\bullet_{ij,\alpha}(t_{\rm out}, \mathbf{x}, y, \mathbf{k}) + \text{h.c.},$$

respectively, where we have introduced the basis functions

$$u^{\bullet}_{ij,\alpha}(t,\mathbf{x},y,\mathbf{k}) = e^{i\boldsymbol{k}\cdot\boldsymbol{x}}\, e^{\bullet}_{ij}(\mathbf{k})\,\phi_\alpha(t,y). \tag{3.14}$$

Note that on account of $(e^{\bullet}_{ij}(\mathbf{k}))^* = e^{\bullet}_{ij}(-\mathbf{k})$ one has $(u^{\bullet}_{ij,\alpha}(t,\mathbf{x},y,\mathbf{k}))^* = u^{\bullet}_{ij,\alpha}(t,\mathbf{x},y,-\mathbf{k})$.

C. Time evolution

During the motion of the brane the time evolution of the field modes is described by the system of coupled differential equations (2.37). To account for the inter-mode couplings mediated by the coupling matrix $M_{\alpha\beta}$ the operator $\hat{q}_{\alpha,\mathbf{k},\bullet}$ may be written as

$$\hat{q}_{\alpha,\mathbf{k},\bullet}(t) = \sum_\beta \frac{1}{\sqrt{2\omega^{\rm in}_{\beta,k}}}\left[\hat{a}^{\rm in}_{\beta,\mathbf{k},\bullet}\epsilon^{(\beta)}_{\alpha,k}(t) + \hat{a}^{\rm in\dagger}_{\beta,-\mathbf{k},\bullet}\epsilon^{(\beta)^*}_{\alpha,k}(t)\right]. \tag{3.15}$$

The complex functions $\epsilon^{(\beta)}_{\alpha,k}(t)$ also satisfy the system of coupled differential equations (2.37). With the ansatz (3.15) the quantized tensor perturbation reads

$$\hat{h}_{ij}(t,\mathbf{x},y) = \tag{3.16}$$
$$\sqrt{\frac{\kappa_5}{L^3}}\sum_{\bullet\alpha\beta}\int \frac{d^3k}{(2\pi)^{\frac{3}{2}}}\frac{\hat{a}^{\rm in}_{\beta,\mathbf{k},\bullet}}{\sqrt{2\omega^{\rm in}_{\beta,k}}}\epsilon^{(\beta)}_{\alpha,k}(t)u^{\bullet}_{ij,\alpha}(t,\mathbf{x},y,\mathbf{k}) + \text{h.c.}\,.$$

Due to the time-dependence of the eigenfunctions ϕ_α the time-derivative of the gravity wave amplitude contains additional mode coupling contributions. Using the completeness and orthnormality of ϕ_α it is easy to show that

$$\dot{\hat{h}}_\bullet(t,y;\mathbf{k}) = \sqrt{\frac{\kappa_5}{L^3}}\sum_\alpha \hat{p}_{\alpha,\mathbf{k},\bullet}(t)\phi_\alpha(t,y) \tag{3.17}$$

where

$$\hat{p}_{\alpha,\mathbf{k},\bullet}(t) = \dot{\hat{q}}_{\alpha,\mathbf{k},\bullet}(t) + \sum_\beta M_{\beta\alpha}\hat{q}_{\beta,\mathbf{k},\bullet}(t). \tag{3.18}$$

The coupling term comes from the time dependence of the mode functions ϕ_α. Accordingly, the time derivative $\dot{\hat{h}}_{ij}$ reads

$$\dot{\hat{h}}_{ij}(t,\mathbf{x},y) = \sqrt{\frac{\kappa_5}{L^3}}\sum_{\bullet\alpha\beta}\int \frac{d^3k}{(2\pi)^{\frac{3}{2}}}\frac{\hat{a}^{\rm in}_{\beta,\mathbf{k},\bullet}}{\sqrt{2\omega^{\rm in}_{\beta,k}}}\times \tag{3.19}$$
$$\times\left\{\dot{\epsilon}^{(\beta)}_{\alpha,k}(t) + \sum_\gamma M_{\gamma\alpha}(t)\epsilon^{(\beta)}_{\gamma,k}(t)\right\}u^{\bullet}_{ij,\alpha}(t,\mathbf{x},y,\mathbf{k}) + \text{h.c.}\,.$$

Comparing Eq. (3.12) and its time-derivative with Eqs. (3.16) and (3.19) at $t = t_{\rm in}$ one can read off the initial conditions for the functions $\epsilon^{(\beta)}_{\alpha,k}$:

$$\epsilon^{(\beta)}_{\alpha,k}(t_{\rm in}) = \delta_{\alpha\beta}\;\Theta^{\rm in}_{\alpha,k}\,, \tag{3.20}$$
$$\dot{\epsilon}^{(\beta)}_{\alpha,k}(t_{\rm in}) = \left[-i\omega^{\rm in}_{\alpha,k}\delta_{\alpha\beta} - M_{\beta\alpha}(t_{\rm in})\right]\;\Theta^{\rm in}_{\beta,k} \tag{3.21}$$

with phase

$$\Theta^{\rm in}_{\alpha,k} = e^{-i\omega^{\rm in}_{\alpha,k}\,t_{\rm in}}. \tag{3.22}$$

The choice of this phase for the initial condition is in principle arbitrary, we could as well set $\Theta^{\rm in}_{\alpha,k} = 1$. But with this choice, $\epsilon^{(\beta)}_{\alpha,k}(t)$ is independent of t_{in} for $t < t_{in}$ and therefore it is also at later times independent of t_{in} if only we choose t_{in} sufficiently early. This is especially useful for the numerical work.

D. Bogoliubov transformations

The two sets of annihilation and creation operators $\{\hat{a}^{\rm in}_{\alpha,\mathbf{k},\bullet},\ \hat{a}^{\rm in\,\dagger}_{\alpha,\mathbf{k},\bullet}\}$ and $\{\hat{a}^{\rm out}_{\alpha,\mathbf{k},\bullet},\ \hat{a}^{\rm out\,\dagger}_{\alpha,\mathbf{k},\bullet}\}$ corresponding to the notion of initial state and final state gravitons, respectively, are related via a Bogoliubov transformation. Matching the graviton amplitude Eq. (3.16) and its time-derivative Eq. (3.19) at $t = t_{\rm out}$ with the final state expression Eq. (3.13) and its corresponding time-derivative one finds

$$\hat{a}^{\rm out}_{\beta,\mathbf{k},\bullet} = \sum_\alpha\left[\mathcal{A}_{\alpha\beta,k}(t_{\rm out})\hat{a}^{\rm in}_{\alpha,\mathbf{k},\bullet} + \mathcal{B}^*_{\alpha\beta,k}(t_{\rm out})\hat{a}^{\rm in\,\dagger}_{\alpha,-\mathbf{k},\bullet}\right] \tag{3.23}$$

with

$$\mathcal{A}_{\beta\alpha,k}(t_{\rm out}) = \frac{\Theta^{\rm out^*}_{\alpha,k}}{2}\sqrt{\frac{\omega^{\rm out}_{\alpha,\rm k}}{\omega^{\rm in}_{\beta,\rm k}}}\left[\epsilon^{(\beta)}_{\alpha,k}(t_{\rm out}) + \frac{i}{\omega^{\rm out}_{\alpha,k}}f^{(\beta)}_{\alpha,k}(t_{\rm out})\right] \tag{3.24}$$

and

$$\mathcal{B}_{\beta\alpha,k}(t_{\rm out}) = \frac{\Theta^{\rm out}_{\alpha,k}}{2}\sqrt{\frac{\omega^{\rm out}_{\alpha,\rm k}}{\omega^{\rm in}_{\beta,\rm k}}}\left[\epsilon^{(\beta)}_{\alpha,k}(t_{\rm out}) - \frac{i}{\omega^{\rm out}_{\alpha,k}}f^{(\beta)}_{\alpha,k}(t_{\rm out})\right] \tag{3.25}$$

where we have introduced the function

$$f^{(\beta)}_{\alpha,k}(t) = \dot{\epsilon}^{(\beta)}_{\alpha,k}(t) + \sum_\gamma M_{\gamma\alpha}(t)\epsilon^{(\beta)}_{\gamma,k}(t) \tag{3.26}$$

and we stick to the phase $\Theta^{\rm out}_{\alpha,k}$ defined like $\Theta^{\rm in}_{\alpha,k}$ in (3.22) for completeness. Performing the matching for $t_{\rm out} = t_{\rm in}$ the Bogoliubov transformation should become trivial, i.e. the Bogoliubov coefficients are subject to vacuum initial conditions

$$\mathcal{A}_{\alpha\beta,k}(t_{\rm in}) = \delta_{\alpha\beta}\ \ ,\ \ \mathcal{B}_{\alpha\beta,k}(t_{\rm in}) = 0. \tag{3.27}$$

Evaluating the Bogoliubov coefficients (3.24) and (3.25) for $t_{\rm out} = t_{\rm in}$ by making use of the initial conditions (3.20) and (3.21) shows the consistency. Note that the Bogoliubov transformation (3.23) is not diagonal due to the inter-mode coupling. If during the motion of the brane the graviton field departs form its vacuum state one has $\mathcal{B}_{\alpha\beta,k}(t_{\rm out}) \neq 0$, i.e. gravitons have been generated.

By means of Eqs. (3.23) the number of generated final state gravitons (3.11), which is the same for every

polarization state, is given by

$$\mathcal{N}^{\rm out}_{\alpha,k}(t \geq t_{\rm out}) = \sum_{\bullet=+,\times} \langle 0,{\rm in}|\hat{N}^{\rm out}_{\alpha,\mathbf{k},\bullet}|0,{\rm in}\rangle = 2\sum_{\beta}|\mathcal{B}_{\beta\alpha,k}(t_{\rm out})|^2. \quad (3.28)$$

Later we will sometimes interpret $t_{\rm out}$ as a continuous variable $t_{\rm out} \to t$ such that $\mathcal{N}^{\rm out}_{\alpha,k} \to \mathcal{N}_{\alpha,k}(t)$, i.e. it becomes a continuous function of time. We call $\mathcal{N}_{\alpha,k}(t)$ the instantaneous particle number [see Appendix B]. This quantity may be considered as the number of created particles in case the motion of the brane would stop at time t. However, a physical interpretation should be made with caution (discontinuity in the brane velocity when switching off the brane dynamics).

E. The first order system

The basic idea of our numerical approach is to derive a system of differential equations for the Bogoliubov coefficients directly. However, it turns out that, for technical reasons, it is simpler to work with functions $\xi^{(\beta)}_{\alpha,k}(t), \eta^{(\beta)}_{\alpha,k}(t)$ defined through

$$\xi^{(\beta)}_{\alpha,k}(t) = \epsilon^{(\beta)}_{\alpha,k}(t) + \frac{i}{\omega^{\rm in}_{\alpha,k}} f^{(\beta)}_{\alpha,k}(t) \quad (3.29)$$

$$\eta^{(\beta)}_{\alpha,k}(t) = \epsilon^{(\beta)}_{\alpha,k}(t) - \frac{i}{\omega^{\rm in}_{\alpha,k}} f^{(\beta)}_{\alpha,k}(t) \quad (3.30)$$

rather than $\mathcal{A}_{\alpha\beta,k}$, $\mathcal{B}_{\alpha\beta,k}$. These new functions are related to the Bogoliubov coefficients via

$$\mathcal{A}_{\beta\alpha,k}(t_{\rm out}) = \frac{\Theta^{{\rm out}^*}_{\alpha,k}}{2}\sqrt{\frac{\omega^{\rm out}_{\alpha,{\rm k}}}{\omega^{\rm in}_{\beta,{\rm k}}}}\left[\Delta^{+}_{\alpha,k}(t_{\rm out})\xi^{(\beta)}_{\alpha,k}(t_{\rm out}) + \Delta^{-}_{\alpha,k}(t_{\rm out})\eta^{(\beta)}_{\alpha,k}(t_{\rm out})\right] \quad (3.31)$$

$$\mathcal{B}_{\beta\alpha,k}(t_{\rm out}) = \frac{\Theta^{\rm out}_{\alpha,k}}{2}\sqrt{\frac{\omega^{\rm out}_{\alpha,{\rm k}}}{\omega^{\rm in}_{\beta,{\rm k}}}}\left[\Delta^{-}_{\alpha,k}(t_{\rm out})\xi^{(\beta)}_{\alpha,k}(t_{\rm out}) + \Delta^{+}_{\alpha,k}(t_{\rm out})\eta^{(\beta)}_{\alpha,k}(t_{\rm out})\right] \quad (3.32)$$

where we have defined

$$\Delta^{\pm}_{\alpha,k}(t) = \frac{1}{2}\left[1 \pm \frac{\omega^{\rm in}_{\alpha,k}}{\omega_{\alpha,k}(t)}\right]. \quad (3.33)$$

With the aid of the system of second order differential equations for $\epsilon^{(\beta)}_{\alpha,k}$ it follows that the functions $\xi^{(\beta)}_{\alpha,k}(t)$, $\eta^{(\beta)}_{\alpha,k}(t)$ satisfy the following system of first order differential equations:

$$\dot{\xi}^{(\beta)}_{\alpha,k}(t) = -i\left[a^{+}_{\alpha\alpha,k}(t)\xi^{(\beta)}_{\alpha,k}(t) - a^{-}_{\alpha\alpha,k}(t)\eta^{(\beta)}_{\alpha,k}(t)\right] - \sum_{\gamma}\left[c^{-}_{\alpha\gamma,k}(t)\xi^{(\beta)}_{\gamma,k}(t) + c^{+}_{\alpha\gamma,k}(t)\eta^{(\beta)}_{\gamma,k}(t)\right] \quad (3.34)$$

$$\dot{\eta}^{(\beta)}_{\alpha,k}(t) = -i\left[a^{-}_{\alpha\alpha,k}(t)\xi^{(\beta)}_{\alpha,k}(t) - a^{+}_{\alpha\alpha,k}(t)\eta^{(\beta)}_{\alpha,k}(t)\right] - \sum_{\gamma}\left[c^{+}_{\alpha\gamma,k}(t)\xi^{(\beta)}_{\gamma,k}(t) + c^{-}_{\alpha\gamma,k}(t)\eta^{(\beta)}_{\gamma,k}(t)\right] \quad (3.35)$$

with

$$a^{\pm}_{\alpha\alpha,k}(t) = \frac{\omega^{\rm in}_{\alpha,k}}{2}\left\{1 \pm \left[\frac{\omega_{\alpha,k}(t)}{\omega^{\rm in}_{\alpha,k}}\right]^2\right\}, \quad (3.36)$$

$$c^{\pm}_{\gamma\alpha,k}(t) = \frac{1}{2}\left[M_{\alpha\gamma}(t) \pm \frac{\omega^{\rm in}_{\alpha,k}}{\omega^{\rm in}_{\gamma,k}}M_{\gamma\alpha}(t)\right]. \quad (3.37)$$

The vacuum initial conditions (3.27) entail the initial conditions

$$\xi^{(\beta)}_{\alpha,k}(t_{\rm in}) = 2\,\delta_{\alpha\beta}\,\Theta^{\rm in}_{\alpha,k}\,, \quad \eta^{(\beta)}_{\alpha,k}(t_{\rm in}) = 0. \quad (3.38)$$

With the aid of Eq. (3.32), the coefficients $\mathcal{B}_{\alpha\beta,k}(t_{\rm out})$ and therefore the number of produced gravitons can be directly deduced from the solutions to this system of coupled first order differential equations.

In the next section we will show how interesting observables like the power spectrum and the energy density of the amplified gravitational waves are expressed in terms of the number of created gravitons.

The system (3.34, 3.35) of coupled differential equations forms the basis of our numerical simulations. Details of the applied numerics are collected in Appendix C. Other work on this subject [31, 32, 33, 34, 35] uses a Wronskian formulation to determine graviton production. In these works partial differential equations have to be solved which is in general less accurate than a system or ordinary differential equations. Another advantage of the formalism outlined here relies on the fact that the coupling matrices allow us to keep track of the inter mode couplings which can easily be switched on and off, as we shall see in Section V. This makes the relevant physical effects much more transparent.

IV. POWER SPECTRUM AND ENERGY DENSITY

A. Four dimensional perturbation

By solving the system of coupled differential equations formed by Eqs. (3.34) and (3.35) the time evolution of the quantized five-dimensional tensor perturbation $\hat{h}_{ij}(t,\mathbf{x},y)$ during the brane dynamics can be completely reconstructed. Accessible to observations is however, only the imprint which the five-dimensional perturbations have left on the brane, i.e. in our universe. Of particular interest is therefore the part of the five-dimensional tensor perturbation which resides on the brane. The amplitude measured on the brane is given by evaluating the five-dimensional perturbation at the

brane position $y = y_b$:

$$\hat{h}_{ij}(t,\mathbf{x},y_b) = \int \frac{d^3k}{(2\pi)^{3/2}} \sum_{\bullet} e^{i\mathbf{x}\mathbf{k}\cdot x} e^{\bullet}_{ij}(\mathbf{k}) \hat{h}_{\bullet}(t,y_b,\mathbf{k}). \tag{4.1}$$

The expansion of the universe (motion of the brane) enters this expression via the eigenfunctions $\phi_\alpha(t, y_b(t))$. The zero-mode function $\phi_0(t)$, given Eq. (2.26), does not depend on the extra dimension y. Noting that $\mathcal{C}_2(m_n y_b)$ is a Wronskian, we read off from Eqs. (2.27) that the eigenfunctions on the brane $\phi_n(t, y_b)$ are

$$\phi_\alpha(t,y_b) = \sqrt{2}\,\frac{L}{a}\,\mathcal{Y}_\alpha(a) \tag{4.2}$$

where we have used that $y_b = L/a$ and we define "correction" function for the zero-mode

$$\mathcal{Y}_0(a) = \sqrt{\frac{y_s^2}{y_s^2 - y_b^2}} \tag{4.3}$$

and the Kaluza-Klein-modes

$$\mathcal{Y}_n(a) = \sqrt{\frac{Y_1^2(m_n y_s)}{Y_1^2(m_n y_b) - Y_1^2(m_n y_s)}}. \tag{4.4}$$

One immediately is confronted with an interesting observation: the function $\mathcal{Y}_\alpha(a)$ behaves differently with the expansion of the universe for the zero-mode $\alpha = 0$ and the KK-modes $\alpha = n$. This is evident in particular in the asymptotic regime $y_s \gg y_b$, i.e. $y_b \to 0$ for $t \to \infty$ where, exploiting the asymptotics of Y_1, one finds

$$\mathcal{Y}_0(a) \simeq 1\ ,\ \ \mathcal{Y}_n(a) \simeq \frac{L}{a}\frac{\pi m_n}{2}|Y_1(m_n y_s)|, \tag{4.5}$$

i.e. $\mathcal{Y}_0$ is constant while $\mathcal{Y}_n \propto 1/a$. For large n we can approximate $m_n \simeq n\pi/y_s$ and $Y_1(m_n y_s) \simeq Y_1(n\pi) \simeq 1/(\pi\sqrt{n})$, so that

$$\mathcal{Y}_n(a) \simeq \frac{L m_n}{2\sqrt{n}a},\ \ \mathcal{Y}_n^2(a) \simeq \frac{\pi L^2 m_n}{4 y_s a^2}\ . \tag{4.6}$$

Consequently, the amplitude of the KK-modes on the brane will decrease faster with the expansion of the universe than the amplitude of the zero-mode. This leads to interesting consequences for the observable power spectrum and energy density and has a clear physical interpretation.

B. Power spectrum

We define the power spectrum $\mathcal{P}(k)$ of gravitational waves as

$$\frac{(2\pi)^3}{k^3}\mathcal{P}(k)\delta^{(3)}(\mathbf{k}-\mathbf{k}') = \sum_{\bullet=\times,+} \left\langle 0,\mathrm{in}|\hat{h}_{\bullet}(t,y_b;\mathbf{k})\hat{h}^{\dagger}_{\bullet}(t,y_b;\mathbf{k}')|0,\mathrm{in}\right\rangle, \tag{4.7}$$

i.e. we consider the expectation value of the field operator $\hat{h}_\bullet$ with respect to the initial vacuum state at the position of the brane $y = y_b(t)$. In order to get a physically meaningful power spectrum, averaging over several oscillations of the gravitational wave amplitude has to be performed. Equation (4.7) then describes the observable power spectrum imprinted by the five-dimensional tensor perturbations on the brane, i.e. in our universe. The explicit calculation of the expectation value involving a "renormalization" of a divergent contribution is carried out in detail in Appendix B. The final result reads

$$\mathcal{P}(k) = \frac{2}{a^2}\frac{k^3}{(2\pi)^3}\frac{\kappa_5}{L}\sum_\alpha \mathcal{R}_{\alpha,k}(t)\,\mathcal{Y}_\alpha^2(a). \tag{4.8}$$

The function $\mathcal{R}_{\alpha,k}(t)$ can be expressed in terms of the Bogoliubov coefficients (3.24) and (3.25) if we consider t_{out} as a continuous variable t:

$$\mathcal{R}_{\alpha,k}(t) = \frac{\mathcal{N}_{\alpha,k}(t) + \mathcal{O}^{\mathcal{N}}_{\alpha,k}(t)}{\omega_{\alpha,k}(t)}. \tag{4.9}$$

$\mathcal{N}_{\alpha,k}(t)$ is the instantaneous particle number which is obtained by replacing t_{out} in Eq. (3.28) by t and the function $\mathcal{O}^{\mathcal{N}}_{\alpha,k}(t)$ is defined in Eq. (B9). It is important to note that $\mathcal{N}_{\alpha,k}(t)$ cannot in general be interpreted as a physical particle number. For example zero-modes with wave numbers such that $kt < 1$ cannot be considered as particles. They have not performed several oscillations and their energy density cannot be defined in a meaningful way. Equivalently, expressed in terms of the complex functions $\epsilon^{(\beta)}_{\alpha,k}$, one finds

$$\mathcal{R}_{\alpha,k}(t) = \sum_\beta \frac{|\epsilon^{(\beta)}_{\alpha,k}(t)|^2}{\omega^{\mathrm{in}}_{\beta,k}} - \frac{1}{\omega_{\alpha,k}(t)} + \mathcal{O}^{\epsilon}_{\alpha,k}(t), \tag{4.10}$$

with $\mathcal{O}^{\epsilon}_{\alpha,k}$ given in Eq. (B10). The result (4.8) together with (4.9) or (4.10) holds at all times.

If one is interested in the power spectrum at early times $kt \ll 1$, it is not sufficient to take only the instantaneous particle number $\mathcal{N}_{\alpha,k}(t)$ in Eq. (4.9) into account. This is due to the fact that even if the mode functions $\epsilon^{(\beta)}_{\alpha,k}$ are already oscillating, the coupling matrix entering the Bogoliubov coefficients might still undergo a nontrivial time dependence [cf. Eq. (6.15)]. Later on, [cf, e.g., Figs. 5, 6, 8] we will see explicitly that in the radiation dominated bounce studied in this work, particle creation especially of the zero-mode, only stops on sub-Hubble times, $kt > 1$, even if the mode functions are plane waves right after the bounce. Therefore, in order to determine the perturbation spectrum of the zero-mode, we have to make use of the full expression expression (4.10) and may not use (4.11), given below.

At late times, $kt \gg 1$ ($t \geq t_{\mathrm{out}}$) when the brane moves slowly, the couplings $M_{\alpha\beta}$ go to zero and particle creation has ceased both functions $\mathcal{O}^{\mathcal{N}}_{\alpha,k}$ and $\mathcal{O}^{\epsilon}_{\alpha,k}$ do not contribute to the observable power spectrum after averaging

over several oscillations. Furthermore, the instantaneous particle number then equals the (physically meaningful) number of created final state gravitons $\mathcal{N}^{\rm out}_{\alpha,k}$ and, close to the Cauchy horizon, the KK-masses are constant. Consequently, the observable power spectrum at late times can be written as

$$\mathcal{P}(k, t > t_{\rm out}) = \frac{2\,\kappa_4}{a^2}\frac{k^3}{(2\pi)^3}\sum_\alpha \frac{\mathcal{N}^{\rm out}_{\alpha,k}}{\omega^{\rm out}_{\alpha,{\rm k}}}\mathcal{Y}^2_\alpha(a)\ , \qquad (4.11)$$

where we have used that $\kappa_5/L = \kappa_4$. The dependence on the wave number k is completely determined by the spectral behavior of the number of created gravitons $\mathcal{N}^{\rm out}_{\alpha,k}$. It is useful to decompose the power spectrum in its zero-mode and Kaluza-Klein contributions:

$$\mathcal{P}(k) = \mathcal{P}_0(k) + \mathcal{P}_{KK}(k). \qquad (4.12)$$

In the late time regime, using Eqs. (4.11) and (4.5) the zero-mode power spectrum reads

$$\mathcal{P}_0(k, t > t_{\rm out}) = \frac{2\,\kappa_4}{a^2}\frac{k^2}{(2\pi)^3}\mathcal{N}^{\rm out}_{0,k}. \qquad (4.13)$$

As expected for a four-dimensional tensor perturbation, on sub-Hubble scales the power spectrum decreases with the expansion of the universe as $1/a^2$. By contrast, the KK-mode power spectrum for late times, given by

$$\mathcal{P}_{\rm KK}(k) = \frac{k^3}{a^4}\frac{\kappa_4 L^2}{16\pi}\sum_n \mathcal{N}^{\rm out}_{n,k}\frac{m_n^2}{\omega^{\rm out}_{{\rm n,k}}}Y_1^2(m_n y_s), \qquad (4.14)$$

decreases as $1/a^4$, i.e. with a factor $1/a^2$ faster than $\mathcal{P}_0$. The gravity wave power spectrum at late times is therefore dominated by the zero-mode power spectrum and looks four dimensional. Contributions to it coming from five-dimensional effects are scaled away rapidly as the universe expands due to the $1/a^4$ behavior of $\mathcal{P}_{\rm KK}$. In the limit of large masses $m_n y_s \gg 1$, $n \gg 1$ and for wave lengths $k \ll m_n$ such that $\omega_{n,k} \simeq m_n$, the late-time KK-mode power spectrum can be approximated by

$$\mathcal{P}_{\rm KK}(k) = \frac{k^3}{a^4}\frac{\kappa_4 L^2}{16\pi^2 y_s}\sum_n \mathcal{N}^{\rm out}_{n,k} \qquad (4.15)$$

where we have inserted Eq. (4.6) for $\mathcal{Y}^2_n(a)$.

C. Energy density

For a usual four-dimensional tensor perturbation $h_{\mu\nu}$ on a background metric $g_{\mu\nu}$ an associated effective energy momentum tensor can be defined unambiguously by [37]

$$T_{\alpha\beta} = \frac{1}{\kappa_4}\langle h_{\mu\nu,\alpha}h^{\mu\nu}{}_{,\beta}\rangle\ , \qquad (4.16)$$

where the bracket stands for averaging over several periods of the wave. The energy density of gravity waves is the 00-component of the effective energy momentum tensor. We can use the same effective energy momentum tensor to calculate the energy density corresponding to the imprint left by the five-dimensional perturbations on the brane, i.e. for the perturbation $h_{ij}(t, \mathbf{x}, y_b)$ given in Eq. (4.1). For this it is important to note that at late times for which we want to calculate the energy density the conformal time η of an observer on the brane is identical to the bulk time t we have been working with so far. Consequently, the energy density of gravitational radiation amplified during the brane motion is given by (in the TT-gauge employed here)

$$\rho = \frac{1}{\kappa_4\, a^2}\left\langle\left\langle 0, {\rm in}|\dot{\hat{h}}_{ij}(t, \mathbf{x}, y_b)\dot{\hat{h}}^{ij}(t, \mathbf{x}, y_b)|0, {\rm in}\right\rangle\right\rangle. \qquad (4.17)$$

Here the outer bracket denotes averaging which (in contrast to the power spectrum) we embrace from the very beginning. We are only interested in the energy density at late times $kt \gg 1$ ($t \geq t_{\rm out}$) where the mode couplings vanish and particle creation has ceased. The factor $1/a^2$ comes from the fact that an overdot indicates the derivative with respect to bulk time which is conformal time on the brane. A detailed calculation is carried out in Appendix B leading to

$$\rho = \frac{2}{a^4}\sum_\alpha \int \frac{d^3k}{(2\pi)^3}\omega_{\alpha,k}\mathcal{N}_{\alpha,k}(t)\mathcal{Y}^2_\alpha(a)\ . \qquad (4.18)$$

At late times $t \geq t_{\rm out}$ the energy density is therefore given by

$$\rho = \frac{2}{a^4}\sum_\alpha \int \frac{d^3k}{(2\pi)^3}\omega^{\rm out}_{\alpha,{\rm k}}\,\mathcal{N}^{\rm out}_{\alpha,k}\,\mathcal{Y}^2_\alpha(a). \qquad (4.19)$$

This expression looks at first sight very similar to a "naive" definition of energy density as integration over momentum space and summation over all quantum numbers α of the energy $\omega^{\rm out}_{\alpha,{\rm k}}\,\mathcal{N}^{\rm out}_{\alpha,k}$ of created particles. (Note that the graviton number $\mathcal{N}^{\rm out}_{\alpha,k}$ already contains the contributions of both polarizations [see Eq. (3.28)] and the additional factor 2 is due to our normalization of the scale factor.) However, the important difference is the appearance of the function $\mathcal{Y}^2_\alpha(a)$ which exhibits a different dependence on the scale factor for the zero-mode compared to the KK-modes as we have seen before.
Decomposing the energy density into zero-mode and Kaluza-Klein contributions

$$\rho = \rho_0 + \rho_{KK} \qquad (4.20)$$

we find for the massless, i.e. four-dimensional, graviton in the late time regime the expected expression for the energy density which behaves as radiation, i.e. decreases as $1/a^4$ as the universe expands:

$$\rho_0 = \frac{2}{a^4}\int \frac{d^3k}{(2\pi)^3}\,k\,\mathcal{N}^{\rm out}_{0,k}. \qquad (4.21)$$

The energy density of the KK-modes at late times, however, is found to be

$$\rho_{\rm KK} = \frac{L^2}{a^6}\frac{\pi^2}{2}\sum_n \int \frac{d^3k}{(2\pi)^3}\omega^{\rm out}_{n,k}\,\mathcal{N}^{\rm out}_{n,k}\,m_n^2 Y_1^2(m_n y_s), \tag{4.22}$$

scaling like $1/a^6$. As the universe expands the energy density of massive gravitons on the brane is therefore rapidly diluted and the total energy density of gravitational waves in our universe at late times is dominated by the massless four-dimensional graviton. In the large mass limit $m_n y_s \gg 1$,$n \gg 1$ the KK-energy density can be approximated

$$\rho_{{\rm KK},n} \simeq \frac{\pi L^2}{2a^6 y_s}\int \frac{d^3k}{(2\pi)^3}\,\mathcal{N}^{\rm out}_{n,k}\,\omega^{\rm out}_{n,k} m_n\ . \tag{4.23}$$

Due to the factor m_n coming from the function $\mathcal{Y}_i^2$, for the summation over the KK-tower to converge, the number of produced gravitons $\mathcal{N}^{\rm out}_{n,k}$ has to decrease faster than $1/m_n^3$ for large masses and not just faster than $1/m_n^2$ as one might naively expect.

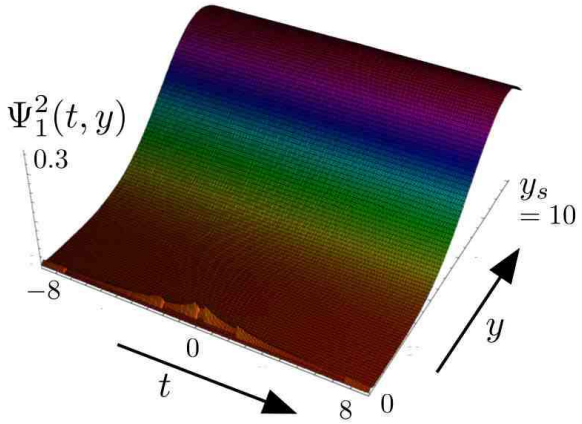

FIG. 2: The evolution of $\Psi_1(t,y) = \phi_1(t,y)/y^{3/2}$ which corresponds to the probability to find the first KK-graviton at time t at the position y in the AdS-bulk. The static brane is at $y_s = 10L$ and the maximal brane velocity is given by $v_b = 0.1$.

D. Escaping of massive gravitons and localization of gravity

The rapid decrease (compared to the zero-mode) of the power spectrum ($\mathcal{P}_{\rm KK} \propto 1/a^4$) and of the energy density ($\rho_{\rm KK} \propto 1/a^6$) of the KK-modes with the expansion of the universe has a simple physical interpretation. It is a direct consequence of the warping of the fifth dimension. Let us define the (spatial) "wave function"

$$\Psi_n(t,y) = \frac{\phi_n(t,y)}{y^{3/2}} \tag{4.24}$$

which satisfies $\int_{y_b}^{y_s} dy \Psi_n^2(t,y) = 1$. From the expansion of the gravity wave amplitude Eq. (2.36) and the normalization condition $(\phi_n,\phi_n) = 1$ where the inner product (ϕ_n,ϕ_n) is defined in Eq. (2.25) it is clear that $\Psi_n^2(t,y)$ gives the probability to find the corresponding KK-graviton for a given time t at position y in the AdS-bulk. In Fig. 2 we plot the evolution of $\Psi_1^2(t,y)$ under the influence of the brane motion Eq. (2.16) with $|v(0)| \equiv v_b = 0.1$. The second brane is placed at $y_s = 10L$. Thereby y ranges from $y_b(t)$ to y_s and, for simplicity, we have set $\Psi_1^2 = 0$ for $y < y_b(t)$. The time-dependent KK-mass m_1 has been determined numerically from Eq. (2.33). As it becomes clear from this Figure, Ψ_1^2 is effectively localized close to the static brane. The probability to find a KK-mode is therefore larger in a region with less warping.

Since the effect of the brane motion on Ψ_1^2 is hardly visible in Fig. 2 we also show the behavior of Ψ_1^2 close to the physical brane in Fig. 3. Ψ_1^2 peaks also at the physical brane but with an amplitude roughly ten times smaller than at the second brane. While the brane, coming from $t \to -\infty$ approaches the point of closest encounter Ψ_1^2 slightly increases and peaks at the bounce $t = 0$ where, as we will see in the next section, the production of KK-particles takes place. Afterwards, for $t \to \infty$, when the brane is moving back towards the Cauchy horizon, the amplitude Ψ_1^2 decreases again and so does the probability to find a KK-particle at the position of the physical brane, i.e. in our universe. From Eqs. (4.2) and (4.5) it follows that $\Psi_n^2(t,y_b) \propto 1/a$. If KK-gravitons are created in our universe during the brane motion, the weight of their wave function lies in the region of less warping, far from the brane, as the universe expands. In other words, the KK-particle escape from the brane into the bulk, when the brane moves back to the Cauchy horizon.

The power spectrum and the energy density imprinted by the KK-modes on the brane decrease faster with the expansion of the universe than for any kind of matter (including massless gravitons) confined on the brane.

The parameter settings used in Figures 2 and 3 are typical parameters which we use in the numerical simulations. However, the effect of escaping KK-particles is illustrated even better if the second brane is closer to the moving brane. In Figure 4 we show Ψ_1^2 for the same parameters as in Figures 2 and 3 but now with $y_s = L$. In this case, the probability to find a KK-particle on the physical brane is of the same order as in the region close to the second brane during times close to the bounce. However, as the universe expands, Ψ_1^2 rapidly decreases at the position of the physical brane, hence KK-particles generated during the bounce at the position of the moving brane escape into the bulk. This scaling behavior of the power spectrum and energy density of the KK-modes on the brane is entirely a consequence of the geometry of the bulk space-time, i.e. of the warping L^2/y^2 of the

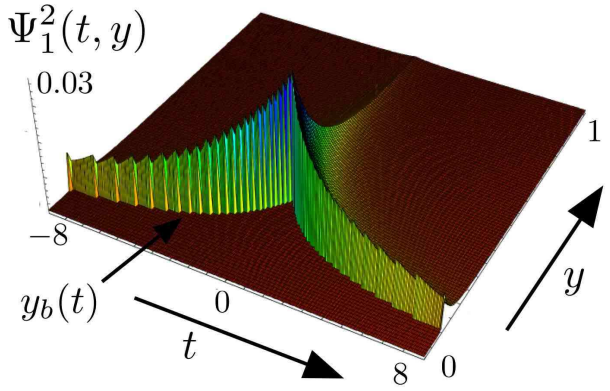

FIG. 3: Evolution of $\Psi_1(t,y)$ as in Fig. 2 but zoomed into the bulk-region close to the moving brane.

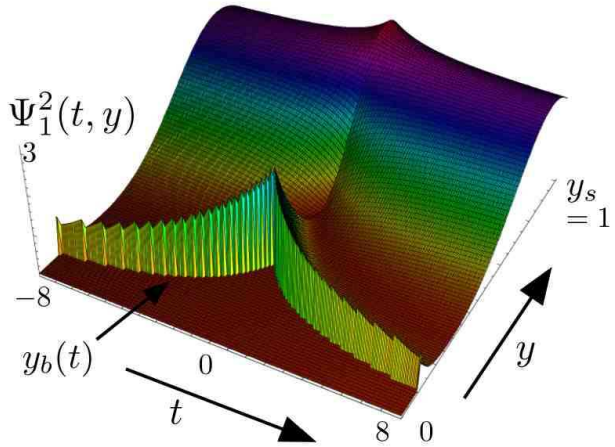

FIG. 4: Evolution of $\Psi_1(t,y)$ for $y_s = L$ and $v_b = 0.1$.

metric (2.1). It does not depend on a particular type of brane motion [3]. It is simply a manifestation of the localization of gravity on the brane: as time evolves, the KK-gravitons, which are traces of the 5D nature of gravity, escape into the bulk and only the zero-mode which corresponds to the usual 4D graviton remains on the brane. An immediate consequence of this particular scaling behavior is that KK-gravitons in an AdS brane world cannot play the role of dark matter. Their energy density in our universe decays much faster with the expansion than that of ordinary matter which is restricted to reside on the brane. This remains true also in the 1-brane model, Randall-Sundrum II [6], and is also true for other fields which are 'confined to the brane'. We actually expect it to hold in most brane-models with warped extra dimension.

[3] Actually, it should also be true in the high energy case which we do not consider here.

V. NUMERICAL SIMULATIONS

A. Preliminary remarks

The scale factor $a(t)$ of the universe, the corresponding motion of the brane in the bulk $y_b(t)$ and its velocity $v(t)$ are given by Eqs. (2.15)-(2.17). A quantity of particular importance is the maximal velocity of the brane which is reached at the bounce $t = 0$:

$$v_b = |\dot{y}_b(0)| = \frac{L^2}{t_b^2}. \tag{5.1}$$

In the numerical simulations we set $L = 1$, i.e. all quantities afflicted with dimensions are measured in units of the AdS curvature scale. Starting at initial time $t_{\rm in} \ll 0$ where the initial vacuum state $|0, {\rm in}\rangle$ is defined we evolve the system (3.34,3.35) up to final time $t_{\rm out}$. We set $t_{\rm in} = -2\pi N_{\rm in}/k$ with $1 \ll N_{\rm in} \in \mathbb{N}$, such that $\Theta^{\rm in}_{0,k} = 1$. This implies $\xi_0^{(0)}(t_{\rm in}) = 2$, i.e. independent of the 3D-momentum k a (plane wave) zero-mode solution always performs a fixed number of oscillations between $t_{\rm in}$ and the bounce at $t = 0$. We calculate the final particle spectrum at $t = t_{\rm out}$ $[\mathcal{N}^{\rm out}_{\alpha,k}]$ at late times when the brane approaches the Cauchy horizon and particle creation has ceased. This quantity is physically well defined and leads to the late-time power spectrum (4.11) and energy density (4.19) on the brane. For illustrative purposes, we will also plot the instantaneous particle number $\mathcal{N}_{\alpha,k,\bullet}(t)$ which also determines the power spectrum at all times [cf Eq.(4.9)]. In this section we will use the term *particle number* for both, the instantaneous particle number $\mathcal{N}_{\alpha,k,\bullet}(t)$ as well as the final state graviton number $\mathcal{N}^{\rm out}_{\alpha,k,\bullet}$, keeping in mind that only the latter is physically meaningful.

There are two physical input parameters for the numerical simulation; the maximal brane velocity v_b (i.e. t_b) and the position of the static brane y_s. The latter determines the number of KK-modes which fall within a particular mass range. On the numerical side we have to specify $N_{\rm in}$ and $t_{\rm out}$ as well as the maximum number of KK-modes $n_{\rm max}$ which we take into account, i.e. after which KK-mode we truncate the system of differential equations. The independence of the numerical results on the choice of the time parameters is checked and the convergence of the particle spectrum with increasing $n_{\rm max}$ is investigated. More detailed information on numerical issues including accuracy considerations are collected in Appendix C.

One strong feature of the brane motion (2.16) is its kink at the bounce $t = 0$. In order to study how particle

production depends on the kink we will compare the motion (2.16) with the following motion which has a smooth transition ($L = 1$):

$$y_b(t) = \begin{cases} (|t| + t_b - t_s)^{-1} & \text{if } |t| > t_s \\ a + (b/2)t^2 + (c/4)t^4 & \text{if } |t| \leq t_s \end{cases} \qquad (5.2)$$

with the new parameter t_s in the range $0 < t_s < t_b$. This motion is constructed such that its velocity at $|t| = t_s$ is the same as the velocity of the kink motion at the bounce. This will be the important quantity determining the number of produced gravitons. For $t_s \to 0$ the motion with smooth transition approaches (2.16). The parameters a, b and c are obtained by matching the motions and the first and second derivatives. Matching also the second derivative guarantees that possible spurious effects contributing to particle production are avoided. The parameter t_s has to be chosen small enough, $t_s \ll 1$, such that the maximal velocity of the smooth motion is not much larger than v_b in order to have comparable situations.

For reasons which will become obvious in the next two sections we discuss the cases $k \ll 1$ and $k \gg 1$ separately.

B. Generic results and observations for long wavelengths $k \ll 1$

Figure 5 displays the results of a numerical simulation for three-momentum $k = 0.01$, asymptotic inter-brane distance $y_s = 10$ and maximal brane velocity $v_b = 0.1$. Depicted is the graviton number for one polarization $\mathcal{N}_{\alpha,k,\bullet}(t)$ for the zero-mode and the first ten KK-modes as well as the evolution of the scale factor $a(t)$ and the position of the physical brane $y_b(t)$. Initial and final time are $N_{\rm in} = 5$ and $t_{\rm out} = 2000$, respectively. The KK-particle spectrum will be discussed in detail later.

One observes that the zero-mode particle number increases slightly with the expansion of the universe towards the bounce at $t = 0$. Close to the bounce $\mathcal{N}_{0,k,\bullet}(t)$ increases drastically, shows a local peak at the bounce and, after a short decrease, grows again until the mode is sub-horizon ($kt \gg 1$). Inside the horizon $\mathcal{N}_{0,k,\bullet}(t)$ is oscillating around a mean value with diminishing amplitude. This mean value which is reached asymptotically for $t \to \infty$ corresponds to the number of generated final state zero-mode gravitons $\mathcal{N}^{\rm out}_{0,k,\bullet}$. Production of KK-mode gravitons takes effectively place only at the bounce in a step-like manner and the graviton number remains constant right after the bounce.

In Fig. 6 we show the numerical results obtained for the same parameters as in Fig. 5 but without coupling of the zero-mode to the KK-modes, i.e. $M_{i0} \equiv 0$ (and thus also $N_{i0} = N_{0i} = 0$). We observe that the production of zero-mode gravitons is practically not affected by the artificial decoupling [4]. Note that even if $M_{0j} \equiv 0$ (see Appendix A) which is in general true for Neumann boundary conditions, the zero-mode q_0 couples in Eq. (2.37) to the KK-modes via $N_{0j} = M_{00}M_{j0}$ and through the anti-symmetric combination $M_{\alpha\beta} - M_{\beta\alpha}$. In contrast, the production of the first ten KK-modes is heavily suppressed if $M_{i0} \equiv 0$. Their corresponding final-state graviton numbers $\mathcal{N}^{\rm out}_{n,k,\bullet}$ are reduced by four orders of magnitude. This shows that the coupling to the zero-mode is essential for the production of massive gravitons. Later

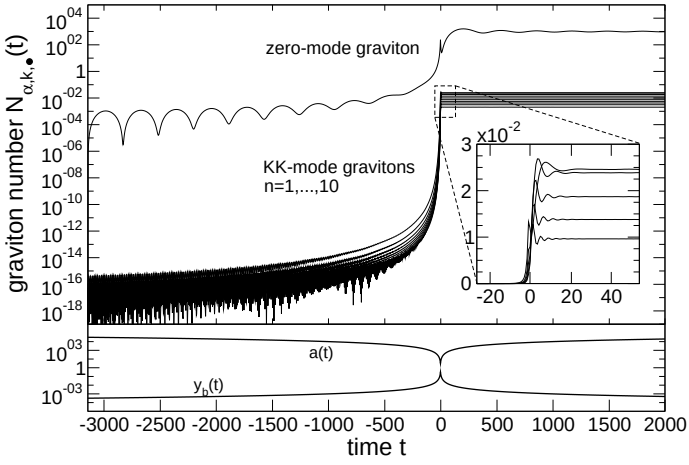

FIG. 5: Evolution of the graviton number $\mathcal{N}_{\alpha,k,\bullet}(t)$ for the zero-mode and the first ten KK-modes for three-momentum $k = 0.01$ and $v_b = 0.1$, $y_s = 10$.

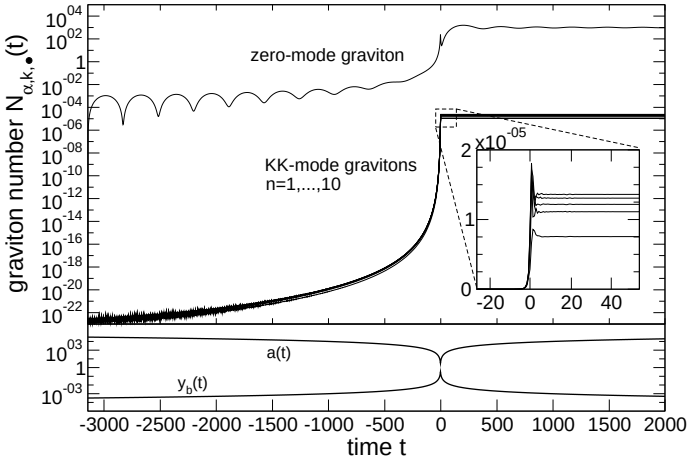

FIG. 6: $\mathcal{N}_{n,k,\bullet}(t)$ for the zero-mode and the first ten KK-modes for the parameters of Fig. 5, but without coupling of the zero-mode to the KK-modes, i.e. $M_{i0} \equiv 0$.

[4] Quantitatively it is $\mathcal{N}_{0,k,\bullet}(t = 2000) = 965.01$ with and $\mathcal{N}_{0,k,\bullet}(t = 2000) = 965.06$ without M_{i0}. Note that this difference lies indeed within the accuracy of our numerical simulations (see Appendix C).

we will show that this is true for light KK-gravitons only. If their masses exceed $m_i \sim 1$, they evolve indepently of the four-dimensional graviton and their evolution is entirely driven by the intermode couplings M_{ij}. It will also turn out that the time-dependent KK-mass $m_i(t)$ plays only an inferior role for the generation of massive KK-modes. On the other hand, the effective decoupling of the evolution of the zero-mode from the KK-modes occurs in general as long as $k \ll 1$ is satisfied, i.e. for long-wavelengths. We will see that it is no longer true for short wavelengths $k \gg 1$.

The effective decoupling of the zero-mode evolution from the KK-modes makes it is possible to derive an analytical expression for the number of zero-mode gravitons, their power spectrum and energy density. The calculations are carried out in Section VI.

In summary we emphasize the important observation that for long wavelengths the amplification of the four dimensional gravity wave amplitude during the bounce is not affected by the evolution of the KK-gravitons. We can therefore study the zero-mode separately from the KK-modes in this case.

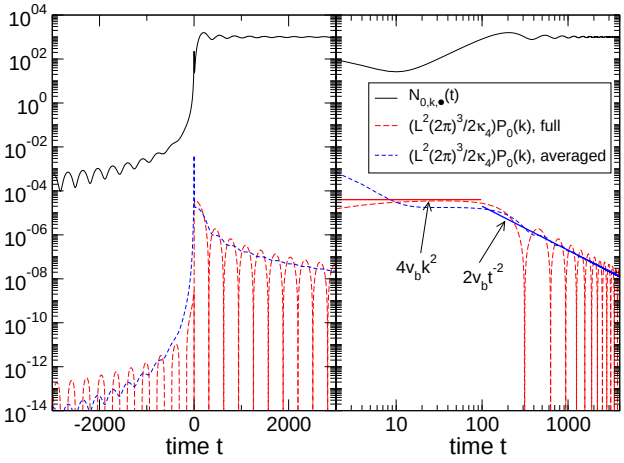

FIG. 7: Time evolution of the number of created zero-mode gravitons $\mathcal{N}_{0,k,\bullet}(t)$ and of the zero-mode power spectrum (4.8): (a) for the entire integration time; (b) for $t > 0$ only. Parameters are $k = 0.01$, $y_s = 10$ and $v_b = 0.1$. Initial and final time of integration are given by $N_{\rm in} = 10$ and $t_{\rm out} = 4000$, respectively. The power spectrum is shown with and without the term $\mathcal{O}^{\mathcal{N}}_{0,k,\bullet}$, i.e. before and after averaging, respectively, and compared with the analytical results.

C. Zero-mode: long wavelengths $k \ll 1$

In Figure 7 we show the numerical results for the number of generated zero-mode gravitons $\mathcal{N}_{0,k,\bullet}(t)$ and the evolution of the corresponding power spectrum $\mathcal{P}_0(k)$ on the brane for momentum $k = 0.01$, position of the static brane $y_s = 10$ and maximal brane velocity $v_b = 0.1$. The results have been obtained by solving the equations for the zero mode alone, i.e. without the couplings to the KK-modes, since, as we have just shown, the evolution of the four-dimensional graviton for long wavelengths is not influenced by the KK-modes. Thereby the power spectra is shown before and after averaging over several oscillations, i.e. employing Eq. (4.9) with and without the term $\mathcal{O}^{\mathcal{N}}_{0,k}$, respectively. Right after the bounce where the generation of gravitons is initiated and which is responsible for the peak in $\mathcal{N}_{0,k,\bullet}$ at $t = 0$, the number of gravitons first decreases again. Afterwards $\mathcal{N}_{0,k,\bullet}$ grows further until the mode enters the horizon at $kt = 1$. Once on sub-horizon scales $kt \gg 1$, the number of produced gravitons oscillates with a diminishing amplitude and asymptotically approaches the final state graviton number $\mathcal{N}^{\rm out}_{0,k,\bullet}$. During the growth of $\mathcal{N}_{0,k,\bullet}(t)$ after the bounce, the power spectrum remains practically constant. Within the range of validity it is in good agreement with the analytical prediction (6.21) yielding $L^2(2\pi)^3/(2\kappa_4)\mathcal{P}_0(k) = 4v_b(kL)^2$. When particle creation has ceased, the full power spectrum Eq.(4.8) starts to oscillate with an decreasing amplitude. The time-averaged power spectrum obtained by using Eq. (4.9) without the $\mathcal{O}^{\mathcal{N}}_{0,k}$-term is perfectly in agreement with the analytical expression Eq. (6.19) which yields $L^2(2\pi)^3/(2\kappa_4)\mathcal{P}_0(k) = 2v_b/t^2$. Note that at early times, the time-averaged power spectrum behaves not in the same way as the full one, demonstrating the importance of the term $\mathcal{O}^{\mathcal{N}}_{0,k}$ at early times.

Figure 8 shows a summary of numerical results for the number of created zero-mode gravitons $\mathcal{N}_{0,k,\bullet}(t)$ for different values of the three-momentum k. The maximum velocity at the bounce is $v_b = 0.1$ and the second brane is at $y_s = 10$. Those values are representative. Other values in accordance with the considered low-energy regime do not lead to a qualitatively different behavior. Note that the evolution of the zero-mode does practically not depend on the value of y_s as long as $y_s \gg y_b(0)$ (see below). Initial and finial integration times are given by $N_{\rm in} = 5$ and $t_{\rm out} = 20000$, respectively. For sub-horizon modes we compare the final graviton spectra with the analytical prediction (6.16). Both are in perfect agreement. On super-horizon scales where particle creation has not ceased yet $\mathcal{N}_{0,k,\bullet}$ is independent of k. The corresponding time-evolution of the power spectra $\mathcal{P}_{0,k}(t)$ is depicted in Fig. 9. For the sake of clarity, only the results for $t > 0$, i.e. after the bounce, are shown in both figures.

The numerical simulations and the calculations carried out in Section VI reveal that the power spectrum for the four-dimensional graviton for long wavelengths is scale invariant on sub-horizon scales and decaying like $1/a^2$ but blue on super-horizon scales. However, the analytical calculations rely on the assumption that $y_b \ll y_s$ and $t_{\rm in} \to \infty$. Figure 10 shows the behavior of the number of generated zero-mode gravitons of momentum $k = 0.01$ in dependence on the inter-brane distance and the initial integration time. The maximal brane velocity at the bounce is $v_b = 0.1$ which implies that at the bounce the moving brane is at $y_b(0) = \sqrt{v_b} \simeq 0.316$ ($L = 1$). In case

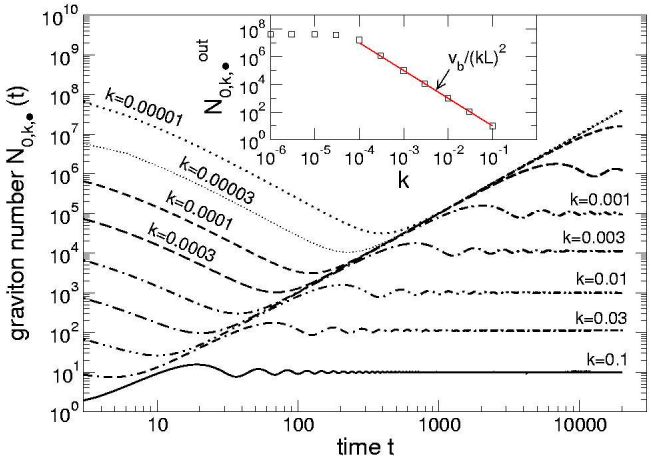

FIG. 8: Numerical results for the time evolution of the number of created zero-mode gravitons $\mathcal{N}_{0,k,\bullet}(t)$ after the bounce $t > 0$ for different three-momenta k. The maximal brane velocity at the bounce is $v_b = 0.1$ and the second brane is positioned at $y_s = 10$. In the final particle spectrum the numerical values are compared with the analytical prediction Eq. (6.16). Initial and final time of integration are given by $N_{\rm in} = 5$ and $t_{\rm out} = 20000$, respectively.

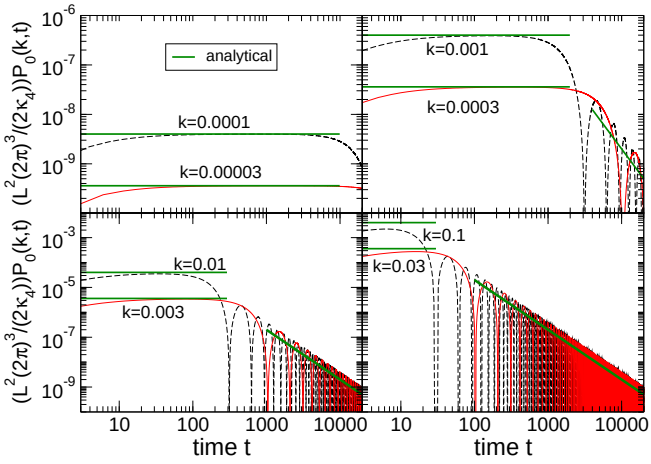

FIG. 9: Evolution of the zero-mode power spectrum after the bounce $t > 0$ corresponding to the values and parameters of Fig. 8. The numerical results are compared to the analytical predictions Eqs. (6.19) and (6.21).

of a close encounter of the two branes as for $y_s = 0.35$, the production of massless gravitons is strongly enhanced compared to the analytical result. But as soon as $y_s \geq 1$, (i.e. $y_s \geq L$) the numerical result is very well described by the analytical expression Eq. (6.15) derived under the assumption $y_s \gg y_b$. For $y_s \geq 10$ the agreement between both is very good. From panels (b) and (c) one infers that the numerical result becomes indeed independent of the initial integration time when increasing $N_{\rm in}$. Note that in the limit $N_{\rm in} \gg 1$, the numerical result is slightly larger than the analytical prediction but the difference between both is negligibly small. This confirms the correctness and accuracy of the analytical expressions derived in Section VI for the evolution of the zero-mode graviton.

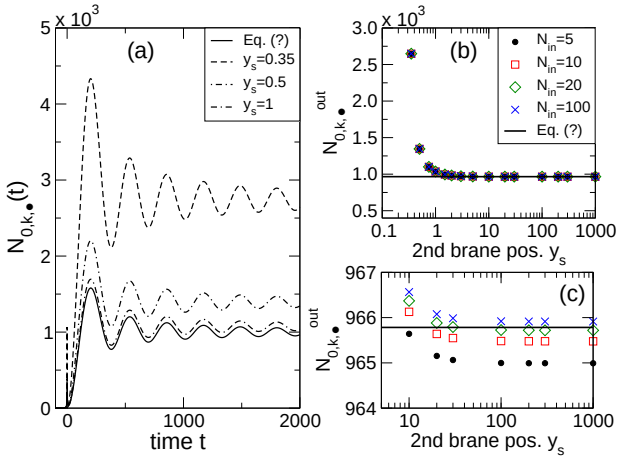

FIG. 10: Dependence of the zero-mode particle number on inter-brane distance and initial integration time for momentum $k = 0.01$, maximal brane velocity $v_b = 0.1$ in comparison with the analytical expression Eq. (6.15). (a) Evolution of the instantaneous particle number $\mathcal{N}_{0,k,\bullet}(t)$ with initial integration time given by $N_{\rm in} = 5$ for $y_s = 0.35, 0.5$ and 1. (b) Final zero-mode graviton spectrum $\mathcal{N}_{0,k,\bullet}(t_{\rm out} = 2000)$ for various values of y_s and $N_{\rm in}$. (c) Close-up view of (b) for large y_s.

D. Kaluza-Klein-modes: long wavelengths $k \ll 1$

Because the creation of KK-gravitons ceases right after the bounce [cf Fig. 5] we can stop the numerical simulation and read out the number of produced KK-gravitons $\mathcal{N}^{\rm out}_{n,k,\bullet}$ at times $t_{\rm out}$ for which the zero-mode is still superhorizon.

Even though Eq. (2.33) cannot be solved analytically, the KK-masses can be approximated by $m_n \simeq n\pi/y_s$. This expression is the better the larger the mass. Consequently, for the massive modes the position of the second brane y_s determines how many KK-modes belong to a particular mass range Δm.

In Figure 11 we show the KK-graviton spectra $\mathcal{N}^{\rm out}_{n,k,\bullet}$ for three-momentum $k = 0.001$ and second brane position $y_s = 100$ for maximal brane velocities $v_b = 0.1, 0.3$ and 0.5. For any velocity v_b two spectra obtained with $n_{\rm max} = 60$ and 80 KK-modes taken into account in the simulation are compared to each other. This reveals that the numerical results are stable up to a KK-mass $m_n \simeq 1$.

One infers that first, $\mathcal{N}^{\rm out}_{n,k,\bullet}$ grows with increasing mass until a maximum is reached. The position of the maximum shifts slightly towards larger masses with increasing brane velocity v_b. Afterwards, $\mathcal{N}^{\rm out}_{n,k,\bullet}$ declines with growing mass. Until the maximum is reached, the numerical

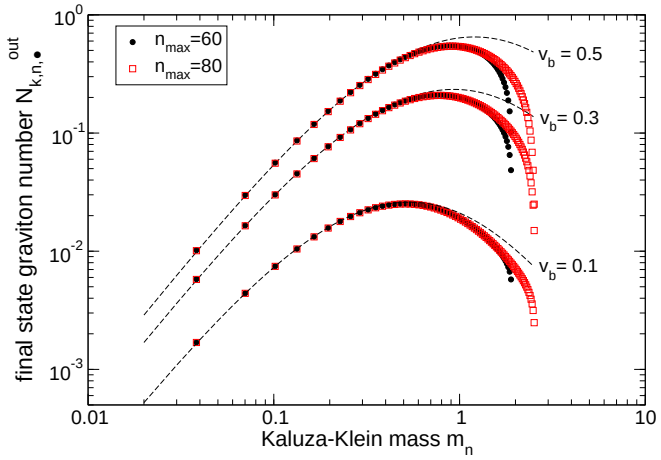

FIG. 11: Final state KK-graviton spectra for $k = 0.001$, $y_s = 100$, different maximal brane velocities v_b and $N_{\rm in} = 1$, $t_{\rm out} = 400$. The numerical results are compared with the analytical prediction Eq. (6.33) (dashed line).

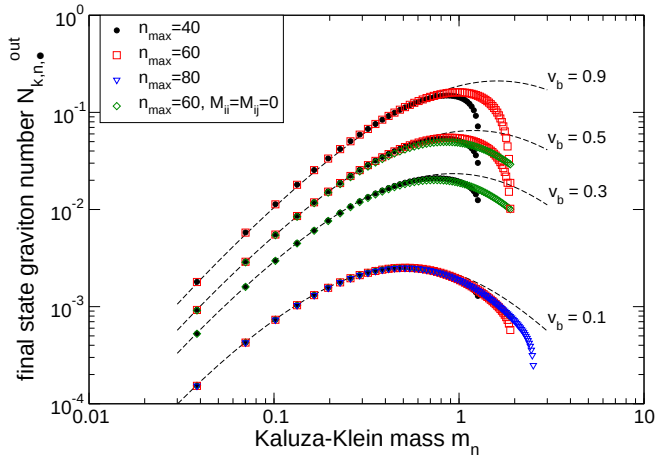

FIG. 12: Final state KK-graviton spectra for $k = 0.01$, $y_s = 100$, different v_b and $N_{\rm in} = 1$, $t_{\rm out} = 400$. The numerical results are compared with the analytical prediction Eq. (6.33) (dashed line). For $v_b = 0.3, 0.5$ the spectra obtained without KK-intermode and self-couplings ($M_{ii} = M_{ij} = 0$) are shown as well.

results for the KK-particle spectrum are very stable. This already indicates that the KK-intermode couplings mediated by M_{ij} are not very strong in this mass range. In Figure 12 we show the final KK-particle spectrum for the same parameters as in Fig. 11 but for three-momentum $k = 0.01$ and the additional velocity $v_b = 0.9$ [5]. The same qualitative behavior is observed as in Fig. 11. In addition we show numerical results obtained without the KK-intermode couplings, i.e. we have set $M_{ij} = 0$ by hand. One infers that for KK-masses, depending slightly on the velocity v_b, but at least up to $m_n \simeq 1$ the numerical results for the spectra do not change when switching off the KK-intermode couplings. Consequently, the evolution of *light*, i.e. $m_n \leq 1$, KK-gravitons is practically not affected by the KK-intermode coupling. In addition one finds that also the time-dependence of the KK-masses is not important for the production of those light KK-gravitons which will later be demonstrated explicitely. Thus the production of *light* KK-gravitons is driven by the zero-mode evolution only. This allows us to find an analytical expression for the number of produced light KK-gravitons in terms of exponential integrals Eq. (6.33). It is based on several approximations and particularly valid up to masses $m_n \simeq 1$. In Figs. 11 and 12 the analytical prediction for the spectrum of final state gravitons has already been included (dashed lines). Within its range of validity it is in excellent agreement with the numerical results obtained by including the full KK-intermode couplings. It perfectly describes the dependence of $\mathcal{N}^{\rm out}_{n,k,\bullet}$ on the three-momentum k and the maximal velocity v_b. For small velocities $v_b \sim 0.1$ it is also able to reproduce the position of the maximum. This proves that the KK-intermode coupling is negligible for the light KK-masses and their production is entirely driven by their coupling to the evolution of the four-dimensional graviton. Since the analytical expression has been derived for real asymptotic initial conditions $t_{\rm in} \to -\infty$, its agreement with the numerics gives us confidence that the (finite) initial time used in the numerical simulations is large enough. No spurious initial effects contribute to the shown particle spectra. Note, that the numerical values for $\mathcal{N}^{\rm out}_{n,k,\bullet}$ in the shown examples are all smaller than one. However, for smaller values of k than the ones which we consider here for purely numerical reasons, the number of generated KK-mode particles is enhanced since $\mathcal{N}^{\rm out}_{n,k,\bullet} \propto 1/k$ as can be inferred from Eq. (6.33) in the limit $k \ll m_n$.

If one goes to smaller values of y_s, less KK-modes belong to a particular mass range. Hence, with the same or similar number of KK-modes as taken into account in the simulations before, we can study the behavior of the final particle spectrum for larger masses. Those simulations will reveal the asymptotical behavior of $\mathcal{N}^{\rm out}_{n,k,\bullet}$ for $m_n \to \infty$ and therefore the behavior of the total graviton number and energy density. Due to the kink in the brane motion we cannot expect that the energy density of produced KK-mode gravitons is finite when summing over arbitrarily high frequency modes. Eventually we will have to introduce a cut-off setting the scale at which our kink-approximation is no longer valid. This is the scale at which the effects of the underlying unspecified high-energy physics become important which drive the transition from contraction to expansion. The dependence of the final particle spectrum on the kink will be studied later on in this section in detail.

[5] Such a high brane velocity is of course not consistent with a Neumann boundary condition Eq. (2.23) at the position of the moving brane.

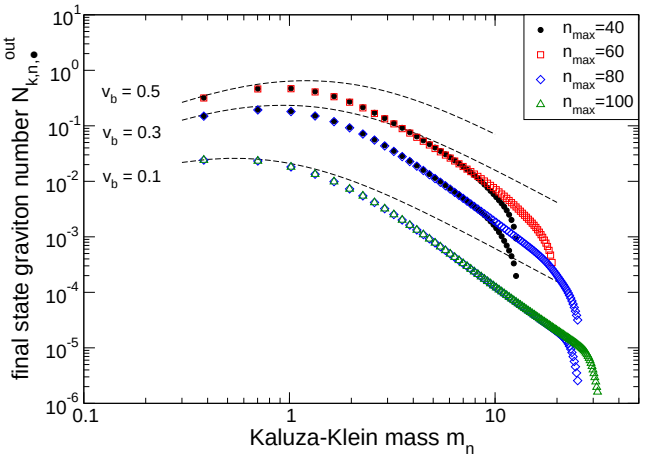

FIG. 13: Final state KK-graviton spectra for $k = 0.01$, $y_s = 10$, different maximal brane velocities v_b and $N_{\rm in} = 2$, $t_{\rm out} = 400$. The numerical results are compared with the analytical prediction Eq. (6.33) (dashed line).

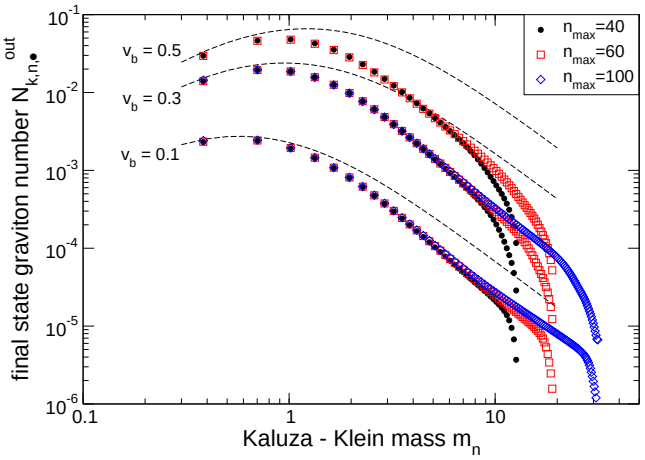

FIG. 14: Final state KK-graviton spectra for $k = 0.1$, $y_s = 10$, different maximal brane velocities v_b and $N_{\rm in} = 2$, $t_{\rm out} = 400$. The numerical results are compared with the analytical prediction Eq. (6.33) (dashed line).

In Figures 13 and 14 we show final KK-graviton spectra for $y_s = 10$ and three-momentum $k = 0.01$ and $k = 0.1$, respectively. The analytical expression Eq. (6.33) is depicted as well and the spectra are always shown for at least two values of $n_{\rm max}$ to indicate up to which KK-mass the numerical results are stable. Now, only two KK-modes are lighter than $m_n = 1$. For those modes the analytical expression Eq. (6.33) is valid and in excellent agreement with the numerical results, in particular for small maximal brane velocities $v_b \sim 0.1$. As before, the larger the velocity v_b the stronger the effect of the truncation of the system at $n_{\rm max}$.

For $k = 0.01$ the spectrum seems to follow a power law decrease right after the maximum in the spectra. In case of $v_b = 0.1$ the spectrum is numerically stable up to masses $m_n \simeq 20$. In the region $5 \leq m_n \leq 20$ the spectrum is very well fitted by a power law $\mathcal{N}^{\rm out}_{n,k,\bullet} \propto m_n^{-2.7}$. Also for the larger velocities the decline of the spectrum is given by the same power within the mass ranges where the spectrum is numerically stable. For $k = 0.1$, however, the decreasing spectrum bends over at a mass around $m_n \simeq 10$ towards a less steep decline. This is in particular visible in the two cases with $v_b = 0.1$ and 0.3 where the first 100 KK-modes have been taken into account in the simulation. The behavior of the KK-mode particle spectrum can therefore not be described by a single power law decline for masses $m_n > 1$. It shows more complicated features instead, which depend on the parameters. We will see that this bending over of the decline is related to the coupling properties of the KK-modes and to the kink in the brane motion.

Before we come to a detailed discussion of those issues we briefly confront numerical results of different y_s to demonstrate a scaling behavior. In the upper panel of Figures 15 and 16 we compare the final KK-mode spectra for several positions of the second brane $y_s = 3, 10, 30$ and 100 obtained for maximal brane velocity $v_b = 0.1$ for $k = 0.01$ and 0.1, respectively. One observes that the shapes of the spectra are basically identical. The bending over in the decline of the spectrum at masses $m_n \sim 1$ is very well visible for $k = 0.1$ and $y_s = 3, 10$. For a given KK-mode n the number of particles produced in this mode is larger the smaller y_s. But the smaller y_s, the less KK-modes belong to a given mass interval Δm. The energy transferred into the system by the moving brane, which is basically defined by the maximum brane velocity v_b, is the same in all cases. Therefore, the energy of the produced final state KK-gravitons belonging to a given mass interval Δm should also be the same, independent of how many KK-modes are contributing to it. This is demonstrated in the lower panels of Figs. 15 and 16 where the energy (in units of L) of the generated KK-gravitons $\omega^{\rm out}_{n,k}\mathcal{N}^{\rm out}_{n,k,\bullet}$ binned in mass intervals $\Delta m = 1$ is shown [6]. One observes that, as expected, the energy transferred into the production of KK-gravitons of a particular mass range is the same (within the region where the numerical results are stable), independent of the number of KK-modes lying in the interval. This is in particular evident for $y_s = 30, 100$. The discrepancy for $y_s = 10$ is due to the binning. As we shall see below in detail, the particle spectrum can be split into two different parts. The first part is dominated by the coupling of the zero-mode to the KK-modes (as already seen before) whereas the second part is dominated by the KK-intermode couplings and is practically independent of the wave number k. As long as the coupling of the zero-mode to the KK-modes is the dominant contribution to their

[6] The energy for the case $y_s = 3$ is not shown because no KK-mode belongs to the first mass interval.

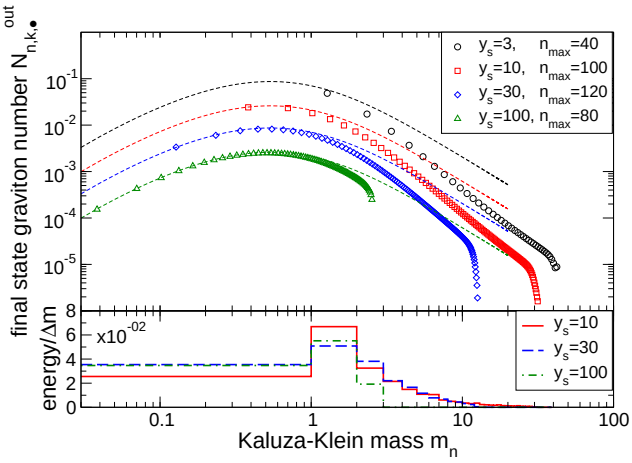

FIG. 15: Upper panel: Final state KK-particle spectra for $k = 0.01$, $v_b = 0.1$ and different $y_s = 3, 10, 30$ and 100. The analytical prediction Eq. (6.33) is shown as well (dashed line). Lower panel: Energy $\omega^{out}_{n,k}\mathcal{N}^{out}_{n,k,\bullet}$ of the produced final state gravitons binned in mass intervals $\Delta m = 1$ for $y_s = 10, 30, 100$.

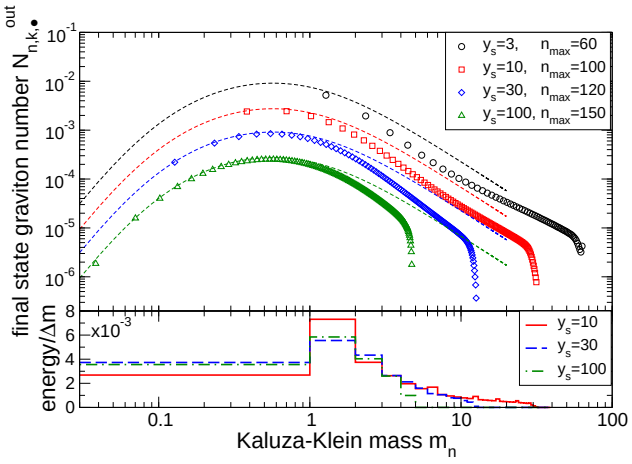

FIG. 16: Upper panel: Final state KK-particle spectra for $k = 0.1$, $v_b = 0.1$ and different $y_s = 3, 10, 30$ and 100. The analytical prediction Eq. (6.33) is shown as well (dashed line). Lower panel: Energy $\omega^{out}_{n,k}\mathcal{N}^{out}_{n,k,\bullet}$ of the produced final state gravitons binned in mass intervals $\Delta m = 1$ for $y_s = 10, 30, 100$.

creation we have [cf. Eq. (6.33)] $\mathcal{N}^{out}_{n,k,\bullet} \propto 1/k$. Hence, $\mathcal{E}^{out}_{n,k,\bullet} = \omega^{out}_{n,k}\mathcal{N}^{out}_{n,k,\bullet} \propto 1/k$ if $m_n \gg k$. This explains why the energy per mass interval Δm is one order larger for $k = 0.01$ [cf Fig. 15] than for $k = 0.1$ [cf Fig. 16] .

Let us now discuss the KK-graviton spectrum for large masses. As we have just seen, the shape and qualitative behaviour of the spectrum $\mathcal{N}^{out}_{n,k,\bullet}$ is independent of the position y_s of the static brane and thus the mass at which the decline of the spectrum changes is independent of y_s. This is demonstrated in Figure 17 where we show the numerically calculated KK-mode spectrum for $v_b = 0.1$, $k = 0.1$ and $y_s = 10$ [cf Fig. 14] and $y_s = 3$ [cf Fig. 16]. In addition to the results obtained by taking all intermode-couplings into account we show the results of simulations where we have switched off the coupling of the KK-modes to each other, i.e. $M_{ij} = 0$, as well as their self-coupling, i.e. $M_{ii} = 0$. Furthermore we display the results for the KK-spectrum obtained by taking only the KK-intermode couplings into account, i.e. $M_{i0} = 0$ as well as $M_{ii} = 0$. One observes that for the lowest masses the spectra obtained with the full coupling are identical to the ones obtained without the KK-intermode ($M_{ij} = 0$) and self-couplings ($M_{ii} = 0$). Hence, as already seen before, the primary source of the production of light KK-gravitons is their coupling to the evolution of the four-dimensional graviton mode. In this mass range, the contribution to the particle creation coming from the KK-intermode couplings is very much suppressed and negligibly small.

For masses $m_n \simeq 4$ a change in the decline of the spectrum sets in and the spectrum obtained without the coupling of the KK-modes to the zero-mode starts to diverge from the spectrum computed by taking all the couplings into account. While the spectra without the KK-intermode couplings decrease roughly like a power law $\mathcal{N}_{n,k,\bullet} \propto m_n^{-3}$ the spectra corresponding to the full coupling case change their slope towards a power law decline with less power. At this point the KK-intermode couplings gain importance and the coupling of the KK-modes to the zero-mode looses influence. For a particular mass $m_c \simeq 9$ the spectra obtained including the KK-intermode couplings only cross the onces calculated by taking into account exclusively the coupling of the KK-modes to the zero-mode. After the crossing, the spectra obtained by taking only the KK-intermode couplings into account approach the spectra corresponding to the full coupling case. For larger masses, both agree. Thus for large masses $m_n > m_c$ the production of KK-gravitons is dominated by the couplings of the KK-modes to each other and is not influenced anymore by the evolution of the four-dimensional graviton. This crossing defines the transition between the two regimes mentioned before: for masses $m_n < m_c$ production of KK-gravitons takes place due to their coupling to the zero-mode M_{i0} while it is entirely caused by the intermode couplings M_{ij} for masses $m_n > m_c$.

The decoupling of the evolution of the KK-modes from the dynamics of the four-dimensional graviton for large masses implies that the KK-spectra obtained for the same maximal velocity are independent of the three-momentum k. This is demonstrated in Fig. 18 where we compare spectra obtained for $v_b = 0.1$ and $y_s = 3$ but different k. As expected, all spectra converge towards the same behavior for masses $m_n > m_c$.

In Fig. 19 we show the KK-particle spectra for three-momentum $k = 0.1$, maximum brane velocity $v_b = 0.1$ and $y_s = 3$ obtained for different coupling combinations. This plot visualizes the effects of each different coupling on the production of KK-gravitons. It shows, as al-

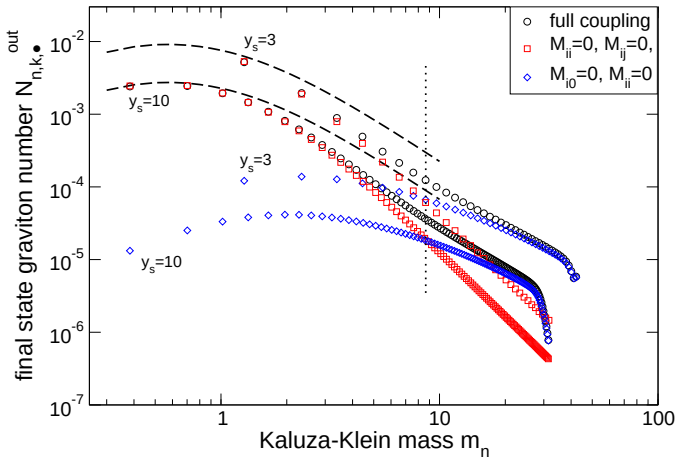

FIG. 17: KK-particle spectra for three-momentum $k = 0.1$, maximum brane velocity $v_b = 0.1$ and $y_s = 3$ and 10 with different couplings taken into account. The dashed lines indicates again the analytical expression Eq. (6.33).

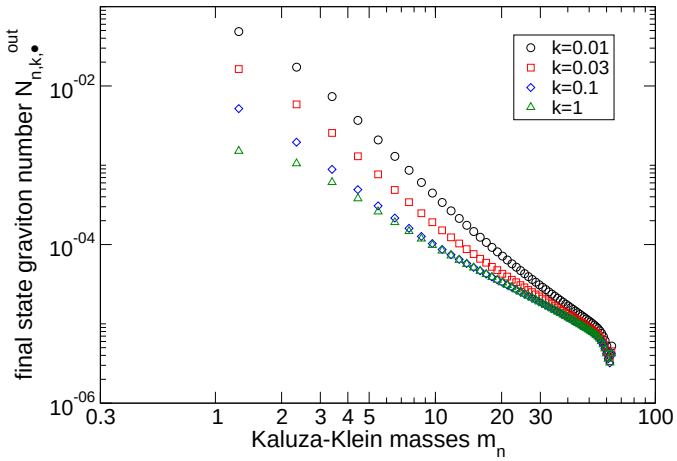

FIG. 18: Comparison of KK-particle spectra for $y_s = 3$, $v_b = 0.1$ and three-momentum $k = 0.01,\ 0.03,\ 0.1$ and 1 demonstrating the independence of the spectrum on k for large masses. $n_{\max} = 60$ KK-modes have been taken into account in the simulations.

ready mentioned before but not shown explicitly, that the M_{ii} coupling which is the rate of change of the corresponding KK-mass [cf. Eqs. (2.34),(A8)] is not important for the production of KK-gravitons. Switching it off does not affect the final graviton spectrum. In addition we show the result obtained with full coupling but with $\alpha^+_{ii}(t) = \omega^{\rm in}_{i,k}$ and $\alpha^-_{ii}(t) = 0$, i.e. we neglect the time-dependence of the frequency [cf. Eq. (3.36)]. We observe that for this case the spectrum for larger masses is changed slightly but shows the same qualitative behaviour. If, on the other hand, all the couplings are switched off $M_{i0} = M_{ij} = M_{ii} = 0$ and only the time-dependence of the frequency $\omega_{i,k}$ is taken into account,

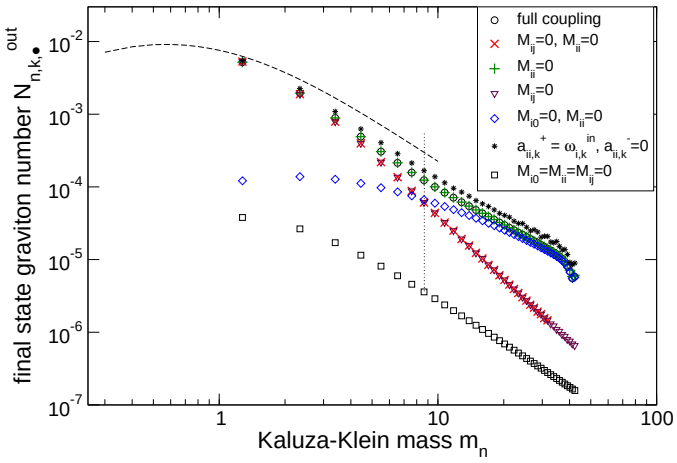

FIG. 19: KK-particle spectra for three-momentum $k = 0.1$, maximum brane velocities $v_b = 0.1$ and $y_s = 3$ for $n_{\max} = 40$ obtained for different coupling combinations.

the spectrum changes drastically. Not only the number of produced gravitons is now orders of magnitude smaller but also the spectral tilt changes. For large masses it behaves now as $\mathcal{N}_{n,k,\bullet} \propto m_n^{-2}$. Consequently, the time-dependence of the graviton frequency itself plays only an inferior role for production of KK-gravitons. The bottom line is that the main sources of the production of KK-gravitons is their coupling to the evolution of the four-dimensional graviton (M_{i0}) and their couplings to each other (M_{ij}) for small and large masses, respectively. Those effects are caused entirely by the time-dependent boundary conditions. The time-dependence of the oscillator frequency $\omega_{j,k} = \sqrt{m_j^2(t) + k^2}$ is practically irrelevant. Note that this situation is very different from ordinary inflation where there are no boundaries and particle production is due entirely to the time dependence of the the frequency [7].

The behavior of the KK-spectrum, in particular the mass m_c at which the KK-intermode couplings start to dominate over the coupling of the KK-modes to the zero-mode can only depend on the three-momentum $k = |\mathbf{k}|$ and the maximal brane velocity v_b. This is now discussed. In Figure 20 we show the KK-particle spectra for $y_s = 10$, $v_b = 0.1$, $n_{\max} = 100$ and three-momenta $k = 0.01$ and 0.1. Again, the spectra obtained by taking all the couplings into account are compared to the case where only the coupling to the zero-mode is switched on. One observes that for $k = 0.01$ the spectrum is dominated by the coupling of the KK-modes to the zero-mode up to larger masses than it is the case for $k = 0.1$. For $k = 0.01$ the spectrum obtained taking into account M_{i0} only is iden-

[7] Note however, that the time-dependent KK-mass $m_j(t)$ enters the intermode-couplings.

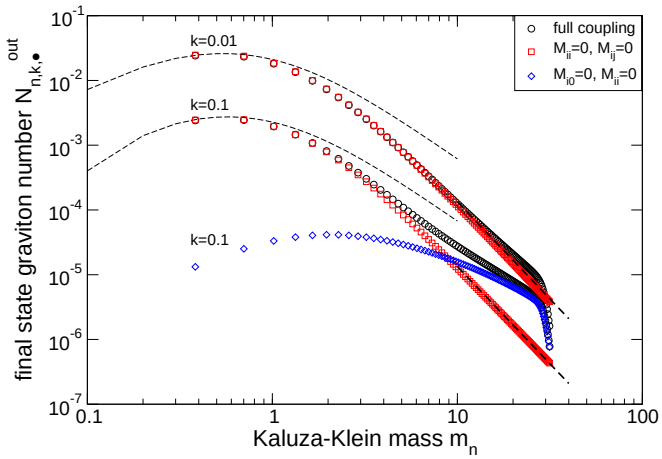

FIG. 20: KK-particle spectra for $y_s = 10$, $v_b = 0.1$, $n_{\max} = 100$ and three-momentum $k = 0.01$ and 0.1 with different couplings taken into account. The thin dashed lines indicates Eq. (6.33) and the thick dashed line Eq. (5.5).

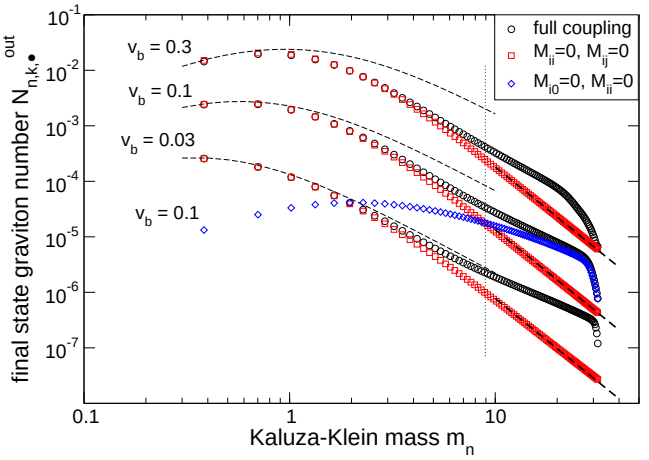

FIG. 21: KK-particle spectra for three-momentum $k = 0.1$,$y_s = 10$ and maximum brane velocities $v_b = 0.03, 0.1$ and 0.3 with $n_{\max} = 100$. As in Fig. 20 different couplings have been taken into account and thin dashed lines indicates Eq. (6.33) and the thick dashed line Eq. (5.5).

tical to the spectrum obtained with the full coupling up to $m_n \simeq 10$. In case of $k = 0.1$ instead, the spectrum is purely zero-mode dominated only up to $m_n \simeq 5$. Hence, the smaller the three-momentum k, the larger is the mass range for which the KK-intermode coupling is suppressed and the coupling of the zero-mode to the KK-modes is the dominant source for the production of KK-gravitons. We find that as long as the coupling to the zero-mode is the primary source of particle production, the spectrum declines with a power law $\propto m_n^{-3}$. Therefore, in the limiting case $k \to 0$ when the coupling of the zero-mode to the KK-modes dominates particle production also for very large masses we have $\mathcal{N}^{\rm out}_{n\gg 1,k\to 0,\bullet} \propto 1/m_n^3$.

In Figure 21 we show KK-graviton spectra obtained for the same parameters as in Fig. 20 but for fixed $k = 0.1$ and different maximal brane velocities v_b. Again, the spectra obtained by taking all the couplings into account are compared with the spectra to which only the coupling of the KK-modes to the zero-mode has contributed. One observes that the mass up to which the spectra obtained with the different couplings are identical changes slightly with the maximal brane velocity. Therefore the dependence on the velocity is rather small even if the velocity is changed by an order of magnitude, but nevertheless evident.

This behavior of the spectrum can indeed be understood qualitatively. In Section VI we will show that the strength of the coupling of the KK-modes to the zero-mode at the bounce $t = 0$ where production of KK-gravitons takes place, is proportional to

$$\frac{\sqrt{v_b}}{k}. \tag{5.3}$$

The larger this term, the stronger is the coupling of the KK-modes to the zero-mode and thus the larger is the mass up to which this coupling dominates over the KK-intermode couplings. Consequently, the mass at which the decline of the KK-particle spectrum changes strongly depends on the three-momentum k but only weakly on the maximal brane velocity due to the square root. This explains qualitatively the behavior obtained from the numerical simulations.

An (approximate) analytical expression for $m_c(k, v_b)$ in terms of k and v_b is obtained from the numerical simulations. In Figure 22 we show the KK-particle spectra for three-momentum $k = 0.01$, 0.03, 0.1 and 1 for $y_s = 3$ and maximum brane velocities $v_b = 0.1$ with different couplings taken into account. The legend is like in Fig. 21. From the crossing of the $M_{ii} = M_{ij} = 0$- and $M_{ii} = M_{i0} = 0$ results we determine the k-dependence of m_c. Note that the spectra are not numerically stable for large masses, but they are stable in the range where m_c lies [cf., e.g., Fig. 24, for $k = 0.1$]. Using the data for $k = 0.01, 0.03$ and 0.1 one finds $m_c(k, v_b) \propto 1/\sqrt{k}$. In Fig. 23 KK-graviton spectra are displayed for $k = 0.1$,$y_s = 3$ and maximal brane velocities $v_b = 0.3, 0.2, 0.1, 0.08, 0.05$ and 0.03 with different couplings taken into account. From the crossing of the $M_{ii} = M_{ij} = 0$- and $M_{ii} = M_{i0} = 0$ results it is in principle possible to determine the v_b-dependence of m_c. As the values for m_c displayed in the Figures indicate, that the dependence of m_c on v_b is very weak. From the given data it is not possible to obtain a good fitting formula (as a simple power law) for the v_b-dependence of m_c. (In the range $0.1 \le v_b \le 0.3$ a very good fit is $m_c = 1.12\pi v_b^{0.13}/\sqrt{k}$.) The reason is twofold. First of all, given the complicated coupling structure, it is *a priori* not clear that a simple power law dependence exists. Recall that also the analytical expression for the particle number Eq. (6.33) has not a simple power law dependence of the velocity . More importantly, for the number of modes taken into account

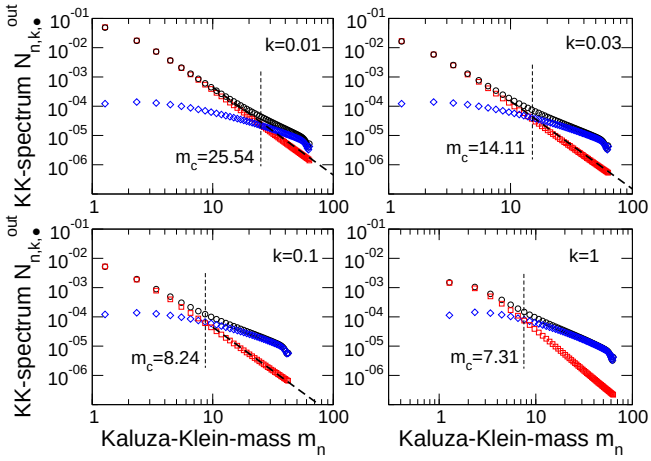

FIG. 22: KK-particle spectra for three-momentum $k = 0.01$, 0.03, 0.1 and 1 for $y_s = 3$ and maximum brane velocities $v_b = 0.1$ with different couplings taken into account where the notation is like in Fig. 21. From the crossing of the $M_{ii} = M_{ij} = 0$- and $M_{ii} = M_{i0} = 0$ results we determine the k-dependence of $m_c(k, v_b)$. The thick dashed line indicates Eq. (5.5).

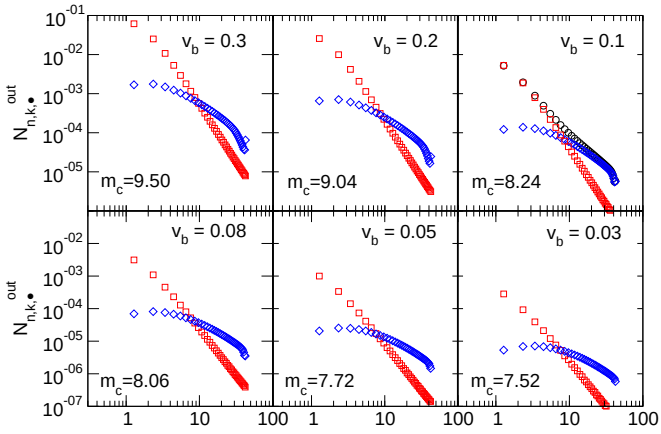

FIG. 23: KK-graviton spectra for three-momentum $k = 0.1$, $y_s = 3$ and maximal brane velocities $v_b = 0.3, 0.2, 0.1, 0.08, 0.05$ and 0.03 with different couplings taken into account where the notation is like in Fig. 21. From the crossing of the $M_{ii} = M_{ij} = 0$- and $M_{ii} = M_{i0} = 0$ results we determine the v_b-dependence of m_c.

($n_{\max} = 40$) the numerical results are not stable enough to resolve the weak dependence of m_c on v_b with a high enough accuracy. (But it is good enough to perfectly resolve the k-dependence.) The reason for the slow convergence of the numerics will become clear below. As we will see, the corresponding energy density is dominated by masses much larger than m_c. Consequently the weak dependence of m_c on v_b is not very important in that respect and therefore we do not have to determine it more precisely. However, combinig all the date we can give as fair approximation

$$m_c(k, v_b) \simeq \frac{\pi\, v_b^\alpha}{\sqrt{k}}, \quad \text{with} \quad \alpha \simeq 0.1. \tag{5.4}$$

Taking $\alpha = 0.13$ for $0.1 \le v_b \le 0.3$ and $\alpha = 0.08$ for $0.03 \le v_b \le 0.1$ fits the given data reasonably well.
As we have seen, as long as the zero-mode is the dominant source of KK-particle production, the final KK-graviton spectrum can be approximated by a power law decrease m_n^{-3}. We can combine the presented numerical results to obtain a fitting formula valid in this regime:

$$\mathcal{N}^{\rm out}_{n\gg 1, k\ll 1, \bullet} = \frac{\pi}{k\, y_s} \frac{(v_b)^{2.37}}{(L\, m_n)^3}, \quad \text{for} \quad 1 < m_n < m_c. \tag{5.5}$$

This fitting formula is shown in Figs. 20 21 and 22 and is in reasonable good agreement with the numerical results.
Of particular interest is the slope of the KK-graviton spectrum for masses $m_n \to \infty$ since it determines the contribution of the heavy KK-modes to the energy density. In Figure 24 we show KK-graviton spectra obtained for three-momentum $k = 0.1$, second brane position $y_s = 3$ and maximal brane velocities $v_b = 0.01, 0.03$ and 0.1. Up to $n_{\max} = 100$ KK-modes have been taken into account in the simulations. One immediately is confronted with the observation that the convergence of the KK-graviton spectra for large m_n is very slow. This is not surprising since those modes, which are decoupled from the evolution of the four-dimensional graviton-mode, are stronlgy affected by the kink in the brane motion. Recall that the production of "light" KK-gravitons with masses $m_n \ll m_c$ is practically driven entirely by the evolution of the massless mode. Those light modes are not so sensitive to the discontinuity in the velocity of the brane motion. A discontinuity in the motion will always lead to a divergent total particle number. Arbitrary high frequency modes are excited by the kink since the acceleration diverges there. Due to the excitation of KK-gravitons of arbitrarily high masses one cannot expect that the numerical simulations show a satisfactory convergence which would allow to determine the slope by fitting the data. However, it is nevertheless possible to give an quantitative expression for the behavior of the KK-graviton spectrum for large masses.
In the context of the dynamical Casimir effect for a real scalar field on a time-dependent interval $[0, y(t)]$ it has been shown analytically that a discontinuity in the motion will lead to a divergent particle number [38, 39]. Furthermore, it is known analytically that for a linear boundary motion $y(t) = y_0 + vt$ the particle spectrum behaves as $\propto v^2 n^{-1}$ where n determines the frequency [39]. The discontinuities in the velocity when it is switched on and off are responsible for this divergent behaviour. More details are collected in Appendix D. where we also present particle spectra obtained numerically. Those spectra show an identical slow convergence behaviour as the KK-graviton spectra depicted in Fig. 24. For the

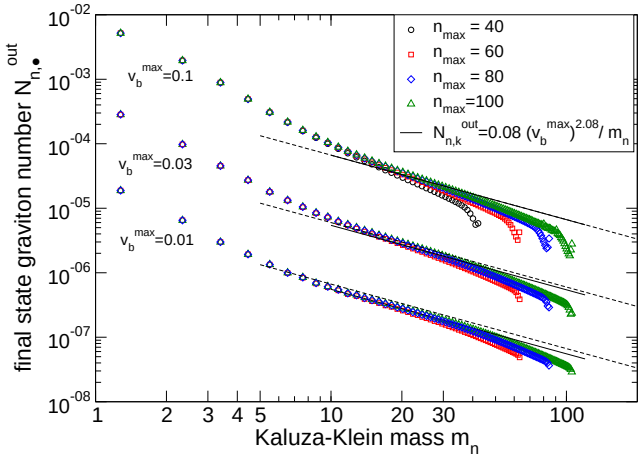

FIG. 24: KK-particle spectra for $k = 0.1$, $y_s = 3$ and maximal brane velocities $v_b = 0.01, 0.03, 0.1$ up to KK-masses $m_n \simeq 100$ compared with an $1/m_n$ decline. The dashed lines indicate the approximate expression (5.7) which describes the numerical results reasonably well.

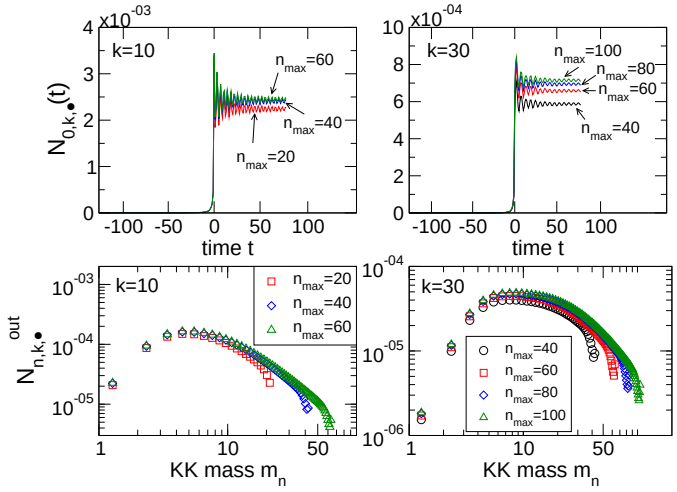

FIG. 25: Evolution of the zero-mode particle number $\mathcal{N}_{0,k,\bullet}(t)$ and final KK-graviton spectra $\mathcal{N}^{out}_{n,k,\bullet}$ for $y_s = 3$, maximal brane velocity $v_b = 0.1$ and three-momenta $k = 10$ and 30.

kink in the brane-motion the total change of the velocity during the bounce is $2v_b$ as it is the case for the linear motion. Consequently one may conclude that for large KK-masses, i.e. after the evolution of the KK-modes is no longer affected by their coupling to the four-dimensional graviton [8], the KK-graviton spectrum should behave as

$$\mathcal{N}^{out}_{n\geq n_c,k,\bullet} \propto \frac{(v_b)^2}{m_n}. \tag{5.6}$$

Thereby n_c is defined by the KK-mass after which the spectrum is independent of the three-momentum k, i.e. the KK-mode dynamics is no longer coupled to the zero-mode. If one assumes that the spectrum declines like $1/m_n$ and uses that the numerical results for the mass $m_{29} = 30.686$ are practically stable one finds $\mathcal{N}^{out}_{n,\bullet} = 0.08 \times (v_b)^{2.08}/m_n$ which is plotted in Fig. 24. As for the dynamical Casimir effect for a uniform motion as discussed in Appendix D, the slow convergence of the numerical results towards the $1/m_n$ behaviour is well visible [cf. Fig. 33]. We consider this as a strong indication that the final graviton spectrum for large masses behaves indeed like (5.6). It is therefore possible to give a single simple expression for the final KK-particle spectrum for large masses which comprises all the features of the spectrum even quantitatively reasonably well [cf. dashed lines in Fig. 24]

$$\mathcal{N}^{out}_{n,k,\bullet} \simeq 0.2\frac{v_b^2}{\omega_{n,k}\, y_s}. \tag{5.7}$$

The $1/y_s$-dependence is compelling. It follows immediately from the considerations on the energy and the scaling behaviour discussed above [cf. Figs. 15 and 16]. For completeness we now write $1/\omega_{n,k}$ instead of the KK-mass m_n only, since what matters is of course the total energy of a mode. Throughout this section this has not been important since we considered only $k \ll 1$ and the spectrum becomes independent of k for larger masses [cf. Fig. 18].

E. Short wavelengths $k \gg 1$

For short wave lengths $k \gg 1$, i.e. short compared to the AdS-curvature scale L set here to one, a completely new and very interesting effect appears. The behavior of the four-dimensional graviton mode changes drastically. We find that the zero-mode now couples to the KK-gravitons and no longer evolves (effectively) independently of the KK-modes, contrary to the behavior of long wavelengths. In Fig. 25 we show the evolution of the zero-mode particle number $\mathcal{N}_{0,k,\bullet}(t)$ and final KK-graviton spectra $\mathcal{N}^{out}_{n,k,\bullet}$ for $y_s = 3$, maximal brane velocity $v_b = 0.1$ and three-momentum $k = 10$ and 30. One observes that the evolution of the four-dimensional graviton depends on the number of KK-modes n_{max} taken into account. Hence the zero-mode couples to the KK-gravitons. For $k = 10$ the first 60 KK-modes have to be included in the simulation in order to obtain a numerically stable result for the zero-mode. In the case of $k = 30$ we already need $n_{max} \simeq 100$ to obtain a numerically stable result for $\mathcal{N}_{0,k,\bullet}(t)$

[8] Note that the analytical calculation in [39] is carried out for Dirichlet boundary conditions. For Neumann boundary conditons considered here the zero-mode and its asymmetric coupling play certainly a particular role. However, as we have shown, for large masses only the KK-intermode couplings are important. Consequently, there is no reason to expect that the qualitative behaviour of the spectrum for large masses depends on the particular kind of boundary condition.

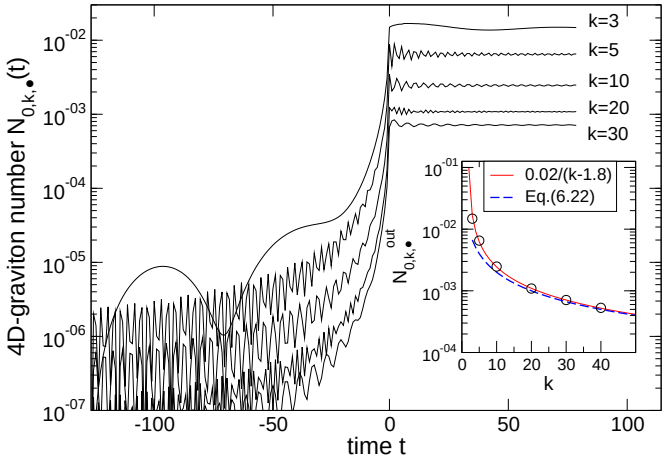

FIG. 26: 4D-graviton number $\mathcal{N}_{0,k,\bullet}(t)$ for $k = 3, 5, 10, 20$ and 30 with $y_s = 3$ and maximal brane velocity $v_b = 0.1$. The small plot shows the final graviton spectrum $\mathcal{N}^{\rm out}_{0,k,\bullet}$ together with a fit to the inverse law $a/(k+b)$. For $k = 10$ and 30 the corresponding KK-graviton spectra are shown in Fig. 25.

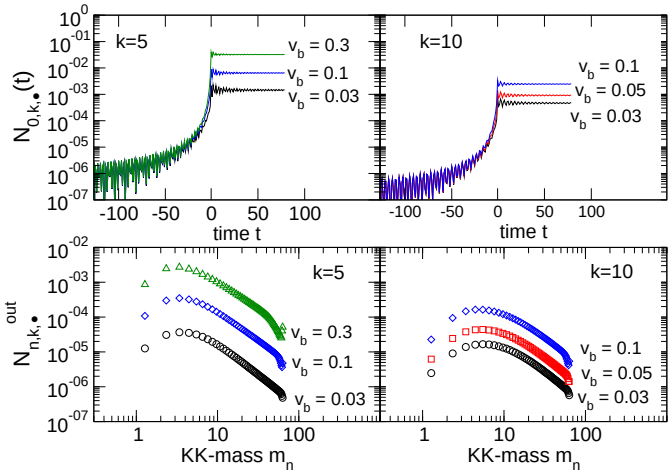

FIG. 27: Zero-mode particle number $\mathcal{N}_{0,k,\bullet}(t)$ and corresponding final KK-particle spectra $\mathcal{N}^{\rm out}_{n,k,\bullet}$ for $y_s = 3$, $k = 5, 10$ and different maximal brane velocities v_b. $n_{\rm max} = 60$ guarantess numerically stable solutions for the zero-mode.

Figure 26 displays the time-evolution of the number of produced zero-mode gravitons $\mathcal{N}_{0,k,\bullet}(t)$ for $y_s = 3$ and $v_b = 0.1$. For large k the production of massless gravitons takes place only at the bounce since these short wavelength modes are sub-horizon right after the bounce. The corresponding KK-particle spectra for $k = 10, 30$ are depicted in Fig. 25 and the insert in Fig. 26 shows the resulting final 4D-graviton spectrum $\mathcal{N}^{\rm out}_{0,k,\bullet}$. It turns out that 4D-graviton spectrum is very well fitted by an inverse power law[9] $\mathcal{N}^{\rm out}_{0,k,\bullet} = 0.02/(k - 1.8)$. Consequently for $k \gg 1$ the zero-mode particle number $\mathcal{N}^{\rm out}_{0,k,\bullet}$ will decline like $1/k$ only, in contrast to the $1/k^2$ behaviour found for $k \ll 1$. The dependence of $\mathcal{N}^{\rm out}_{0,k,\bullet}$ on the maximal brane velocity v_b also changes. In Fig. 27 we show $\mathcal{N}_{0,k,\bullet}(t)$ together with the corresponding KK-graviton spectra for $y_s = 3$, $k = 5$ and 10 in each case for different v_b. Using $n_{\rm max} = 60$ KK-modes in the simulation guarantees numerical stability for the zero-mode. We find that the velocity dependence of $\mathcal{N}^{\rm out}_{0,k,\bullet}$ is not given by a simple power law as it is the case for $k \ll 1$. This is not very suprising since now the zero-mode couples strongly to the KK-modes. For $k = 10$, for example, we find $\mathcal{N}^{\rm out}_{0,k,\bullet} \propto v_b^{1.37}$ if $v_b \leq 0.1$.

As in the long wavelengths case the zero-mode particle number does not depend on the position of the static brane y_s even though the zero-mode now couples to the KK-modes. This is demonstrated in Fig. 28 where we show the evolution of the zero-mode particle number $\mathcal{N}_{0,k,\bullet}(t)$ and the corresponding KK-graviton spectra with $k = 10$, $v_b = 0.1$ for the two values $y_s = 3$ and 10. One needs $n_{\rm max} = 60$ for $y_s = 30$ in order to obtain a stable result for the zero-mode which is not sufficent in the case $y_s = 10$. Only for $n_{\rm max} = 120$ the zero-mode solution approaches the stable result which is identical to the result obtained for $y_s = 3$. What is therefore important is not the number of the KK-modes the four-dimensional graviton couples to, but rather a particular mass $m_{\rm zm} \simeq k$. The zero-mode couples to all KK-modes of masses below $m_{\rm zm}$ no matter how many KK-modes are lighter. Recall that the value of y_s just determines how many KK-modes belong to a given mass interval Δm since, roughly, $m_n \simeq n\pi/y_s$. Thus the KK-spectra for $k \geq 1$ show the same scaling behaviour as demonstrated for long wavelengths in Figs. 15 and 16.

The production of 4D-gravitons of short wavelengths takes place on the expense of the KK-modes. In Fig. 29 we show the numerical results for the final KK-particle spectra with $v_b = 0.1$, $y_s = 3$ and $k = 3, 5, 10$ and 30 obtained for different coupling combinations. These spectra should be compared with those shown in Fig. 22 for the long wavelength case. For $k \gtrsim 10$ the number of the produced lightest KK-gravitons is smaller in the full coupling case compared to the situation where only the KK-intermode coupling is taken into account. In case $k = 30$, for instance, the numbers of produced gravitons for the first four KK-modes are smaller for the full coupling case. This indicates that the lightest KK-modes couple strongly to the zero-mode. Their evolution is damped and graviton production in those modes is suppressed. The production of zero-mode gravitons on the other hand is enhanced compared to the long wavelengths case. For short wavelengths, the evolution of the KK-modes therefore contributes to the production of 4D-gravitons. This can be interpreted as creation of 4D-gravitons out of KK-

[9] The momenta $k = 5, 10, 20, 30$ and 40 have been used to obtain the fit. Fitting the spectrum for $k = 20, 30$ and 40 to a power spectrum fit gives $\mathcal{N}^{\rm out}_{0,k,\bullet} \propto k^{-1.1}$

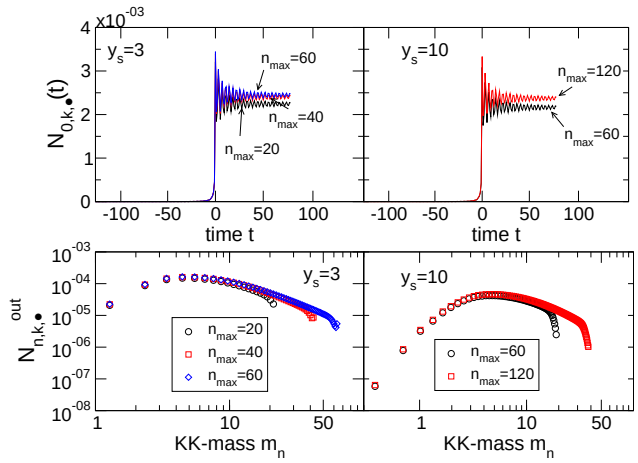

FIG. 28: Zero-mode particle number $\mathcal{N}_{0,k\bullet}(t)$ and corresponding KK-graviton spectra for $k = 10$, $v_b = 0.1$ and 2nd brane positions $y_s = 3$ and 10.

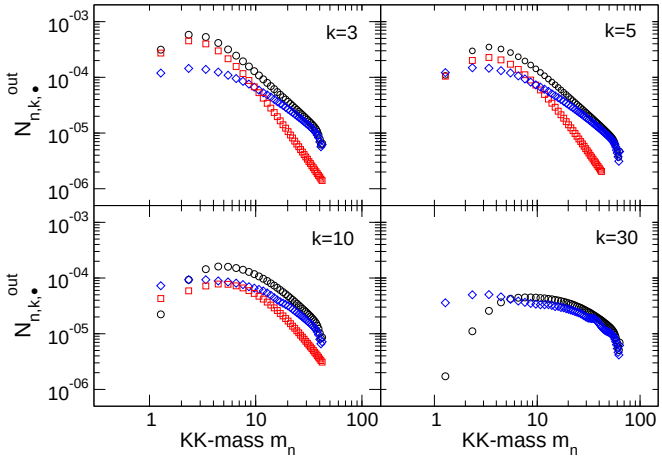

FIG. 29: Final KK-particle spectra $\mathcal{N}^{\rm out}_{n,k,\bullet}$ for $v_b = 0.1$, $y_s = 3$ and $k = 3, 5, 10$ and 30 and different couplings. Circles correspond to the full coupling case, squares indicate the results if $M_{ij} = M_{ii} = 0$, i.e. no KK-intermode couplings and diamonds correspond to $M_{i0} = 0$, i.e. no coupling of KK-modes to the zero-mode.

mode vacuum fluctuations.

As in the long wavelength case, the KK-particle spectrum becomes independent of k if $m_n \gg k$ and the evolution of the KK-modes is dominated by the KK-intermode coupling. This is visible in Fig. 29 for $k = 3$ and 5. Also the bend in the spectrum when the KK-intermode coupling starts to dominate is observable. For $k = 10$ and 30 this regime with $m_n \gg k$ is not reached. As we have shown before, in the regime $m_n \gg k$ the KK-particle spectrum behaves as $1/\omega_{n,k}$ which will dominate the energy density of produced KK-gravitons.

If $1 \ll m_n \lesssim k$, however, the zero-mode couples to the KK-modes and the KK-graviton spectrum does not decay like $1/\omega^{\rm out}_{n,k}$. This is demonstrated in Fig. 30 where the

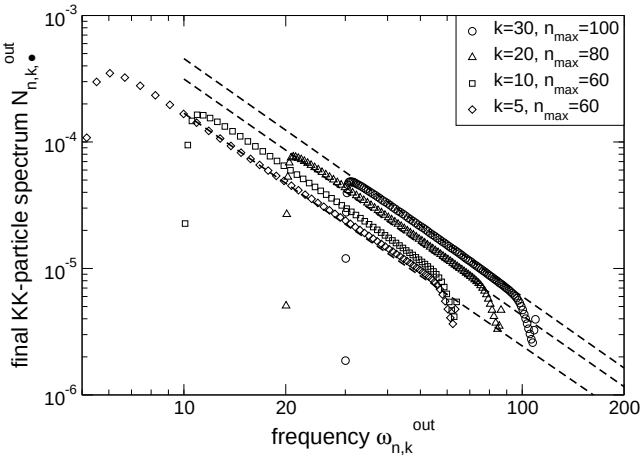

FIG. 30: Final KK-particle spectra $\mathcal{N}^{\rm out}_{n,k,\bullet}$ for $v_b = 0.1$, $y_s = 3$ and $k = 5, 10, 20$ and 30. The dashed lines indicate Eq. (6.34).

number of produced final state gravitons $\mathcal{N}^{\rm out}_{n,k,\bullet}$ is plotted over their frequency $\omega^{\rm out}_{n,k}$ for parameters $v_b = 0.1$, $y_s = 3$ and $k = 5, 10, 20$ and 30. While for $k = 5$ the KK-intermode coupling dominates for large masses [cf. Fig. 29] leading to a bending over in the spectrum and eventually to an $1/\omega^{\rm out}_{n,k}$-decay, the spectra for $k = 20$ and 30 show a different behaviour. Most of the modes are still coupled to the zero-mode leading to a power-law decrease $\propto 1/(\omega^{\rm out}_{n,k})^\alpha$ with $\alpha \simeq 2$. The case $k = 10$ corresponds to an intermediate regime. Also shown is the simple analytical expression given in Eq. (6.34) which describes the spectra reasonably well for large k (dashed line). The KK-particle spectra in the region $1 \ll m_n \lesssim k$ will also contribute to energy density since we chose the cut-off scale to be the same for the integration over k and the summation over the KK-tower (see section VI.D).

F. A smooth transition

Let us finally investigate how the KK-graviton spectrum changes when the kink-motion (2.16) is replaced by the smooth motion (5.2). In Fig. 31 we show the numerical results for the final KK-graviton spectrum for $y_s = 3$, $v_b = 0.1$ and $k = 0.1$ for the smooth motion (5.2) with $t_s = 0.05, 0.015$ and 0.005. $n_{\rm max} = 60$ modes have been taken into account in the simulation and the results are compared to the spectrum obtained with the kink-motion (2.16). The parameter t_s defines the scale L_s at which we smooth the kink. They are related by $L_s \simeq 2t_s$, i.e. L_s corresponds to the width of the transition from contraction to expansion. From the numerical results we observe that KK-modes of masses smaller than $m_s = 1/L_s$ are not affected but the production of KK-particles of masses larger than m_s is exponentially suppressed. This is in particular evident for $t_s = 0.05$ where the particle spectrum for masses $m_n > 10$ has been fitted to a exponential

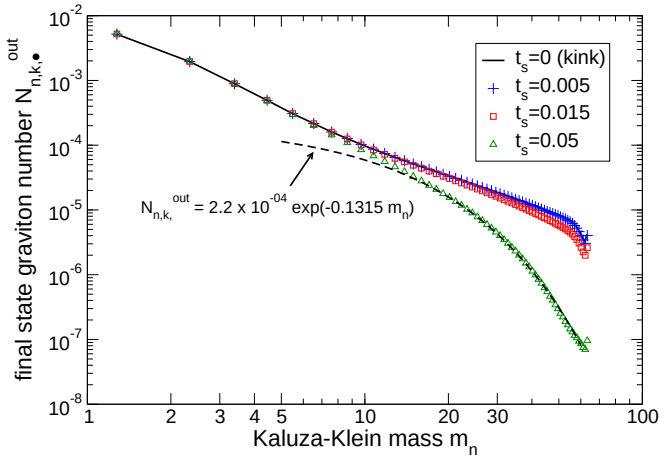

FIG. 31: KK-particle spectrum for $y_s = 3$, $v_b = 0.1$ and $k = 0.1$ for the bouncing as well as smooth motions with $t_s = 0.005, 0.015$, and 0.05 to demonstrate the influence of the bounce. $n_{\max} = 60$ KK-modes have been taken into account in the simulations and the result for the kink motion is shown as well.

decrease. Going to the smaller value $t_s = 0.015$ the suppression of KK-mode production sets in for masses larger than $m_s \simeq 33$. Finally, for the last shown example with $t_s = 0.005$ the KK-particle spectrum is identical to the one obtained with the kink-motion within the depicted mass range. In this case the exponential suppression of particle production sets in only for masses $m_n > 100$. Note that the exponential decay of the spectrum for the smooth transition from contraction to expansions also shows that no additional spurious effects due to the discontinuities in the velocity when switching the brane dynamics on and off occur. Consequently, $t_{\rm in}$ and $t_{\rm out}$ are appropriately chosen.

VI. ANALYTICAL CALCULATIONS AND ESTIMATES

A. The zero-mode: long wavelengths $k \ll 1/L$

The numerical simulations show that the evolution of the zero-mode at large wavelength is not affected by the KK-modes. To find an analytical approximation to the numerical result for the zero-mode, we neglect all the couplings of the KK-modes to the zero-mode by setting $M_{jk} = 0$ and keeping M_{00} only. Then only the evolution equation for $\epsilon_0^{(\alpha)} \equiv \delta_0^\alpha \epsilon$ is important; it decouples and reduces to

$$\ddot{\epsilon} + [k^2 + \mathcal{V}(t)]\epsilon = 0 \,, \tag{6.1}$$

with "potential"

$$\mathcal{V} \;=\; \dot{M}_{00} - M_{00}^2 \,. \tag{6.2}$$

A brief calculation using the expression for M_{00} given in Appendix A yields

$$\mathcal{V} \;=\; \frac{y_s^2}{y_s^2 - y_b^2}\left[\frac{\ddot{y}_b}{y_b} + \frac{\dot{y}_b^2}{y_b^2}\frac{3y_b^2 - 2y_s^2}{y_s^2 - y_b^2}\right] \tag{6.3}$$

$$\;=\; -\frac{y_s^2}{y_s^2 - y_b^2}\left[\mathcal{H}^2\left(1 - \frac{y_b^2}{y_s^2 - y_b^2}\right) + \dot{\mathcal{H}}\right]. \tag{6.4}$$

The vacuum initial conditions are

$$\lim_{t\to-\infty} \epsilon \;=\; 1 \,, \quad \lim_{t\to-\infty} \dot{\epsilon} = -ik. \tag{6.5}$$

To evaluate $\mathcal{V}$ we use the scale factor is given by (2.15) so that

$$\mathcal{H} \;=\; \frac{\dot{a}}{a} = \frac{\mathrm{sign}(t)}{|t| + t_b} \qquad \text{and} \tag{6.6}$$

$$\dot{\mathcal{H}} \;=\; \frac{2\delta(t)}{t_b} - \frac{1}{(|t| + t_b)^2} \tag{6.7}$$

$$\dot{\mathcal{H}} + \mathcal{H}^2 \;=\; \frac{2\delta(t)}{t_b} \,. \tag{6.8}$$

Here δ denotes the Dirac delta function. If we also assume that the static brane is much further away from the Cauchy horizon than the physical brane, $y_s \gg y_b$, we obtain

$$\mathcal{V} = \dot{M}_{00} - M_{00}^2 \simeq -\frac{2\delta(t)}{t_b} = -\frac{2\sqrt{v_b}}{L}\delta(t) \,, \tag{6.9}$$

where v_b is given in Eq (5.1). The approximated potential $\mathcal{V}$ vanishes for all $t < 0$. With the initial condition (6.5) we therefore have

$$\epsilon(t) = e^{-ikt} \,, \quad t < 0 \,. \tag{6.10}$$

Assuming continuity of ϵ through $t = 0$, the differential equation gives

$$0 \;=\; \int_{0_-}^{0_+}\left[\ddot{\epsilon} + \left(k^2 - \frac{2\sqrt{v_b}}{L}\delta(t)\right)\epsilon\right]$$

$$\;=\; \dot{\epsilon}(0_+) - \dot{\epsilon}(0_-) - \frac{2\sqrt{v_b}}{L}\epsilon(0) \,. \tag{6.11}$$

This jump of $\dot{\epsilon}$ at $t = 0$ leads to particle creation. Using $\epsilon(0_+) = \epsilon(0) = \epsilon(0_-)$ and $\dot{\epsilon}(0_+) = \dot{\epsilon}(0_-) - \frac{2\sqrt{v_b}}{L}\epsilon(0)$ as initial conditions for the solution for $t > 0$, we obtain

$$\epsilon(t) = Ae^{-ikt} + Be^{ikt} \,, \quad t > 0 \tag{6.12}$$

with

$$A \;=\; 1 + i\frac{\sqrt{v_b}}{kL} \tag{6.13}$$

$$B \;=\; -i\frac{\sqrt{v_b}}{kL} \,. \tag{6.14}$$

The Bogoliubov coefficient $\mathcal{B}_{00}(t)$ is given by

$$\mathcal{B}_{00}(t \geq 0) = \frac{e^{-ikt}}{2}\left[\left(1 + i\frac{\mathcal{H}}{k}\right)\epsilon(t) - \frac{i}{k}\dot{\epsilon}(t)\right] \tag{6.15}$$

where we have used that $M_{00} = -\mathcal{H}$ if $y_s \gg y_b$. At this point the importance of the coupling matrix M_{00} becomes obvious. Even though the solution ϵ to the differential equation (6.1) is a plane wave right after the bounce, $|\mathcal{B}_{00}(t)|^2$ is not a constant due to the motion of the brane itself. Only after the mode is inside the horizon, i.e. $\mathcal{H}/k \ll 1$, $|\mathcal{B}_{00}(t)|^2$ is constant and the number of generated final state gravitons (for both polarizations) is given by

$$\begin{aligned}\mathcal{N}^{\rm out}_{0,k} &= 2|\mathcal{B}_{00}(kt \gg 1)|^2 = \frac{1}{2}\left[|\epsilon|^2 + \frac{|\dot\epsilon|^2}{k^2}\right] - 1 \\ &= \frac{2v_b}{(kL)^2} \end{aligned} \tag{6.16}$$

where we have used that the Wronskian of ϵ, ϵ^* is $2ik$. As illustrated in Fig. 8 the expression (6.16) is indeed in excellent agreement with the (full) numerical results, not only in its k-dependence but also the amplitude agrees without any fudge factor. The evolution of the four-dimensional graviton mode and the associated generation of massless gravitons with momentum $k < 1/L$ can therefore be understood analytically.

$\mathcal{N}^{\rm out}_{0,k}$ is dimensionless and its integral over d^3k gives the particle number density in real space. However, we have to take into account that our approximation of an exactly radiation dominated universe with an instant transition breaks down on small scales. We assume this break down to occur at some lengths scale L_s which we expect to be the string scale, much smaller than L. It is the true width of the transition from collapse to expansion, which we have set to zero in our treatment. Modes with mode numbers $k \gg (2\pi)/L_s$ will not 'feel' the potential and are not generated. We therefore choose $k_{\rm max} = (2\pi)/L_s$ as our cutoff scale so that the zero-mode particle density is

$$n_0 = \frac{4\pi}{a^3}\int_0^{2\pi/L_s} \frac{dk k^2}{(2\pi)^3}\mathcal{N}_{0,k}\ . \tag{6.17}$$

With Eq (4.21) we obtain correspondingly for the energy density

$$\rho_0 = \frac{1}{\pi^2 a^4}\int_0^{2\pi/L_s} dk k^3 \mathcal{N}_{0,k}\ . \tag{6.18}$$

For small wave numbers, $k < 1/L$, we can use the above analytical result for the zero-mode particle number. However, as we have seen in our numerical analysis, as soon as $k \geq 1/L$, coupling to the KK-modes becomes important and at large wave numbers, $\mathcal{N}_{0,k}$ decays only like $1/k$. Hence both integrals (6.17) and (6.18) are entirely dominated by the upper cutoff. The contribution from long wavelengths to the energy density are negligible.

For the power spectrum, on the other hand, we are interested in cosmologically large scales, $1/k \simeq$ several Mpc or more but not in short wavelengths $kL > 1$ dominating the energy density. Inserting the expression for the number of produced long wavelength gravitons (6.16) into (4.11), the gravity wave power spectrum at late time becomes

$$\mathcal{P}_0(k) = \frac{4v_b}{(2\pi)^3}\frac{\kappa_4}{(aL)^2} \ \text{ for } \ kt \gg 1. \tag{6.19}$$

This is the *asymptotic* power spectrum, when ϵ starts oscillating, hence inside the Hubble horizon, $kt \gg 1$. On super Hubble scales, $kt \ll 1$ when the asymptotic outstate of the zero-mode is not yet reached, we have to use Eq. (4.10) with

$$\mathcal{R}_{0,k}(t) = \frac{|\epsilon(t)|^2 - 1}{k} \simeq \frac{4v_b a^2}{k}\ . \tag{6.20}$$

For the $\simeq$ sign we assume $t \gg L$ and $t \gg t_b$ so that we may neglect terms of order t/L in comparison to $\sqrt{v_b}(t/L)^2$, we have also approximated $a = (t+t_b)/L \simeq t/L$. Inserting this in Eq. (4.8) yields

$$\mathcal{P}_0(k) = \frac{\kappa_4}{\pi^3} v_b\, k^2\ , \qquad kt \ll 1\ . \tag{6.21}$$

The gravity wave spectrum on large, super Hubble scales is blue $\propto k^2$ and therefore very suppressed on scales relevant for the anisotropies of the cosmic microwave background. Both expressions (6.19) and (6.21) are in good agreement with the corresponding numerical results, see Figs. 8,9 and 10.

B. The zero-mode: short wavelengths $k \gg 1/L$

As we have seen in our numerical analysis, as soon as $k \geq 1/L$, coupling of the zero-mode to the KK-modes becomes important and for large wave numbers, $\mathcal{N}_{0,k} \propto 1/k$. We obtain a good asymptotic behavior if we set

$$\mathcal{N}_{0,k,\bullet} \simeq \frac{v_b}{5(kL)}. \tag{6.22}$$

This function and Eq. (6.16) (divided by two for one polarization) meet at $kL = 5$. Even though the approximation is not good in the intermediate regime it is very reasonable for large k [cf. Fig. 26]. The integral in Eq. (6.17) is entirely dominated by the upper cutoff and we obtain

$$n_0 \simeq \frac{2}{5}\frac{v_b}{a^3 L L_s^2}\ . \tag{6.23}$$

Inserting our approximation for $\mathcal{N}_{0,k}$ into Eq (6.18) for the energy density, we again find that the integral is dominated entirely by the blue, high energy modes:

$$\rho_0 \simeq \frac{16}{15}\frac{\pi}{a^4}\frac{v_b}{L L_s^3}. \tag{6.24}$$

The power spectrum associated with the short wavelengths $k > 1/L$ is not of interest since the gravity wave spectrum is measured on cosmologically large scales only, $k \ll 1/L$.

C. Light Kaluza-Klein modes and long wavelengths $k \ll 1/L$

The numerics indicates that light ($m_n \lesssim 1$) long wavelength Kaluza-Klein modes become excited mainly due to their coupling to the zero-mode. We take only this coupling into account and neglect also the time-dependence of the frequency setting $\omega_n(t) \equiv \omega_n^0 \equiv \omega_n$. The Bogoliubov coefficients are then determined by the equations

$$\dot{\xi}_n + i\omega_n^0 \xi_n = \frac{k}{2\omega_n^0} S_n(t;k) \tag{6.25}$$

$$\dot{\eta}_n - i\omega_n^0 \eta_n = -\frac{k}{2\omega_n^0} S_n(t;k) \tag{6.26}$$

with the "source"

$$S_n(t;k) = (\xi_0 - \eta_0)\, M_{n0} \ . \tag{6.27}$$

This source is known. From the result for ϵ above and the definition of ξ and η in terms of ϵ we obtain

$$\xi_0 - \eta_0 = \frac{2i}{k}\left[-ik + \frac{1}{|t| + t_b}\right] e^{-itk} \ , \quad t < 0 \tag{6.28}$$

$$\xi_0 - \eta_0 = 2\left[1 + \frac{i}{kt_b} + \frac{1 - ikt_b}{k^2 t_b (t + t_b)}\right] e^{-itk} + 2\left[\frac{i}{kt_b} - \frac{1}{k^2 t_b (t + t_b)}\right] e^{itk} \ , \quad t > 0 \ . \tag{6.29}$$

Furthermore, if $y_s \gg y_b$ (see appendix) we have

$$M_{n0} = 2\frac{\dot{y}_b}{y_b} \sqrt{\frac{Y_1(m_n y_s)^2}{Y_1(m_n y_b)^2 - Y_1(m_n y_s)^2}} \ . \tag{6.30}$$

Assuming $y_s m_n \gg 1$ and $y_b m_n \ll 1$ we can expand the Bessel functions and arrive at

$$M_{n0} \simeq \sqrt{\pi}\sqrt{\frac{m_n}{y_s}}\dot{y}_b = -\sqrt{\frac{\pi m_n L^2}{y_s}} \frac{L\,\mathrm{sign(t)}}{(|t| + t_b)^2} \ .$$

To determine the number density we only need to calculate η_n since

$$\lim_{t\to\infty} N_n \equiv \mathcal{N}_{n,k}^{out} = \frac{\omega_n}{4k}|\eta_n|^2 \ .$$

The vacuum initial conditions require $\lim_{t\to-\infty} \eta_n = 0$ so that η_n is given by the particular solution

$$\eta_n(t) = \frac{k}{\omega_n} \int_{-\infty}^{t} S_j(t';k) e^{-it'\omega_n} dt' \ , \tag{6.31}$$

and

$$\mathcal{N}_{n,k}^{out} = \frac{k}{4\omega_n} \left| \int_{-\infty}^{\infty} S_n(t;k) e^{-it\omega_j} dt \right|^2 \ . \tag{6.32}$$

This integral can be solved exactly. A somewhat lengthy but straight forward calculation gives

$$\mathcal{N}_{n,k}^{out} = \frac{\pi m_n^5 L^4}{2\omega_n k y_s} \Big| 2i\mathrm{Re}\left(e^{i(\omega_n+k)t_b} E_1(i(\omega_n + k)t_b)\right) + (kt_b)^{-1} e^{i(\omega_n - k)t_b} E_1(i(\omega_n - k)t_b) - e^{i(\omega_n+k)t_b} E_1(i(\omega_n + k)t_b) \Big|^2 \ . \tag{6.33}$$

Here E_1 is the exponential integral, $E_1(z) \equiv \int_z^\infty t^{-1} e^{-t} dt$. This function is holomorphic in the complex plane with a cut along the negative real axis, and the above expression is therefore well defined. Note that this expression does not give rise to a simple dependence of $\mathcal{N}_{n,k}^{out}$ on the velocity $v_b = (L/t_b)^2$. In the preceding section we have seen that, within its range of validity, Eq. (6.33) is in excellent agreement with the numerical results (cf., for instance, Figs. 11 and 12).

D. Kaluza-Klein modes: asymptotic behaviour and energy density

The numerical simulations show that the asymptotic KK-graviton spectra (i.e. for masses $m_n \gg 1$) decay like $1/\omega_{n,k}^{\mathrm{out}}$ if $m_n \gg k$ and like $\left(1/\omega_{n,k}^{\mathrm{out}}\right)^\alpha$ with $\alpha \simeq 2$ if $m_n \lesssim k$. The corresponding energy density on the brane is given by the summation of Eq. (4.23) over all KK-modes up to the cut-off. Since the mass m_n is simply the momentum into the extra dimension, it makes sense to choose the same cut-off scale for both, the k-integral and the summation over the KK-modes, namely $2\pi/L_s$. The main contribution to the 4-dimensional particle density and energy density comes from $m_n \sim 2\pi/L_s$ and $k \sim 2\pi/L_s$, i.e. the blue end of the spectrum.
The large-frequency behaviour of the final KK-spectrum can be approximated by

$$\mathcal{N}_{n,k,\bullet}^{\mathrm{out}} \simeq \frac{0.2 v_b^2}{y_s} \begin{cases} \dfrac{1}{\omega_{n,k}^{\mathrm{out}}} & \text{if } \ 1/L \lesssim k \lesssim m_n \\ 2^{(\alpha-1)/2} \dfrac{k^{\alpha-1}}{(\omega_{n,k}^{\mathrm{out}})^\alpha} & \text{if } \ m_n \lesssim k \lesssim 2\pi/L_s \end{cases} \tag{6.34}$$

with $\alpha \simeq 2$ which is in particular good for large k. Both expression match at $m_n = k$ and are indicated in Figures 24 and 30 as dashed lines. Given the complicated coupling structure of the problem and the multitude of features visible in the particle spectra those compact expressions describe the numerical results reasonable well for all parameters. The deviation from the numerical results is at most a factor of two. This accuracy is sufficient in order to obtain a useful expression for the energy density from which bounds on the involved energy scales can be derived.
The energy density on the brane associated with the KK-

gravitons is given by [cf. Eq. (4.23)]

$$\rho_{\rm KK} \simeq \frac{L^2}{2\pi a^6 y_s} \sum_n \int dk k^2 \, \mathcal{N}^{\rm out}_{n,k,\bullet} \, \omega^{\rm out}_{n,k} m_n \ . \qquad (6.35)$$

Splitting the momentum integration into two integrations from 0 to m_n and m_n to the cut-off $2\pi/L_s$, and replacing the sum over the KK-masses by an integral one obtains

$$\rho_{KK} \simeq C(\alpha) \frac{\pi^5 v_b^2}{a^6 y_s} \frac{L^2}{L_s^5}. \qquad (6.36)$$

The power α in Eq. (6.34) enters the final result for the energy density only through the pre-factor $C(\alpha)$ which is of order unity.

In the limit $y_s \to \infty$ we can recover the 1-brane scenario. Eq. (6.36) implies that a bouncing model with only one brane has vanishing KK-energy density on the brane. Even though KK-modes are produced in the bulk.

VII. DISCUSSION

A. The zero-mode

1. Power spectrum

We finally summarize our results and draw some conclusions. Let us first consider the zero-mode. On scales on which we observe cosmological fluctuations, i.e. scales of Mpc and larger, we have obtained for $t \gg L$ and t_b, in the radiation dominated era

$$\mathcal{P}_0(k) = \frac{\kappa_4}{\pi^3} v_b \begin{cases} k^2 & \text{if } kt \ll 1 \\ \frac{1}{2}(La)^{-2} & \text{if } kt \gg 1 \end{cases} \qquad (7.1)$$

Hence, we find a blue spectrum of tensor perturbations on super Hubble scales. The amplitude of perturbations on CMB scales is of the order of $(H_0/m_{Pl})^2$, hence unobservably small. The fluctuations induced by these Casimir gravitons are much too small to leave any observable imprint on the CMB.

2. Energy density

For the zero-mode graviton energy density at late times, $kt \gg 1$, we have obtained [cf Eq. (6.24)]

$$\rho_{h0} \simeq \frac{16}{15} \frac{\pi}{a^4} \frac{v_b}{L L_s^3}. \qquad (7.2)$$

Here we denote the energy density of the zero-mode by ρ_{h0} in order not to confuse it with the present density of the Universe. The string scale L_s is related to the scale L via Eq. (2.13). It is the scale at which our kinky approximation (2.15) of the scale factor breaks down, i.e. the width of the bounce. If this width is taken to zero, the energy density of gravitons is very blue and diverges. This is not so surprising, since the kink in $a(t)$ allows us to generate gravitons of arbitrary high energies. The numerical simulations have shown that when we smooth the kink at some scale L_s, the production of modes with energies larger than about $1/L_s$ is exponentially suppressed [cf. Fig. 31]. We have therefore used L_s as a cutoff scale. Below we use apart from v_b the quantities

$$\begin{aligned} a_{\rm min} &= \frac{L}{y_b^{\rm min}} = \frac{t_b}{L} = \frac{1}{\sqrt{v_b}} \quad \text{and} \\ H_{\rm max} &= \left.\frac{\dot a}{a^2}\right|_{t=0} \simeq \frac{v_b}{L} \ . \end{aligned}$$

Here $a_{\rm min}$ is the minimal scale factor and $H_{\rm max}$ is the maximal Hubble parameter, i.e. the Hubble parameter right after the bounce, and we have made use of the low energy approximation, $\dot a \simeq da/dt$. During the radiation era, curvature and/or a cosmological constant can be neglected so that the density is

$$\rho_{\rm rad} = \frac{3}{\kappa_4} H^2_{\rm max} \left(\frac{a_{\rm min}}{a}\right)^4 = \frac{3}{\kappa_4 L^2} a^{-4} \ . \qquad (7.3)$$

We want to determine the density parameter of the generated gravitons today, i.e., at $t = t_0$. For this we use $\Omega_{h0} \equiv \rho_{h0}(t_0)/\rho_c(t_0) = [\rho_{h0}(t_0)/\rho_{\rm rad}(t_0)] \times [\rho_{\rm rad}(t_0)/\rho_c(t_0)]$. The second factor is the present radiation density parameter $\Omega_{\rm rad} = \rho_{\rm rad}(t_0)/\rho_c(t_0)$. For the factor $\rho_{h0}/\rho_{\rm rad}$, which is time independent since both ρ_{h0} and $\rho_{\rm rad}$ scale like $1/a^4$, we insert the above results and obtain

$$\begin{aligned} \Omega_{h0} &= \frac{\rho_{h0}}{\rho_{\rm rad}} \Omega_{\rm rad} = \frac{16}{15} \frac{\pi}{3} v_b \left(\frac{L_{Pl}}{L_s}\right)^2 \frac{L}{L_s} \Omega_{\rm rad} \\ &\simeq v_b \left(\frac{L_{Pl}}{L_s}\right)^2 \frac{L}{L_s} \Omega_{\rm rad} \ . \end{aligned} \qquad (7.4)$$

The nucleosynthesis bound [37] requests that

$$\Omega_{h0} \lesssim 0.1 \Omega_{\rm rad} \ , \qquad (7.5)$$

which translates into

$$v_b \left(L_{Pl}/L_s\right)^2 (L/L_s) \lesssim 0.1 \ . \qquad (7.6)$$

The scale dependent term in this equation is exactly 1 due to the RS fine tuning condition (2.13). Consequently all scale dependencies drop out of the equation and we are left with the condition

$$v_b \lesssim 0.1 \ . \qquad (7.7)$$

All we have to require to be consistent with the nucleosynthesis bound is a small brane velocity. This justifies our low energy approach. In all, we conclude that the model is not severely constrained by the zero-mode. This result itself is remarkable. If there would be no coupling of the zero-mode to the KK-modes for small wavelengths the number of produced 4D gravitons would behave as $\propto k^{-2}$ as it is the case for long wavelengths.

The production of high energy zero-mode gravitons from KK-gravitons enhances the total energy density by a factor of about L/L_s. Without this enhancement, the nucleosynthesis bound would not lead to any meaningful constraint and would not require $v_b < 1$.

The coupling of the 4D graviton to the KK-modes for short wavelengths is also directly responsible for the scale independence of the nucleosynthesis bound.

B. The KK-modes

In our setup the more stringent bounds come from the KK-modes. The energy density of KK-gravitons on the brane is dominated by high enegy gravitons and can be approximated by Eq. (6.36)

$$\rho_{KK} \simeq \frac{\pi^5 v_b^2}{a^6 y_s}\frac{L^2}{L_s^5}. \tag{7.8}$$

The most surprising fact is that the energy density of these massive modes decays like $1/a^6$. At first this seems very disturbing. How can it be that massive modes on the brane scale like stiff matter rather than like ordinary massive particles, $\propto 1/a^3$. The reason for this is twofold. First of all, the mass of the modes, m_n is a 'comoving' mass. The dispersion relation of the particles is $\omega_n^2 = k^2 + m_n^2$, where k and ω are comoving momentum and frequency. This comes from the fact that the 5D time t corresponds to the *conformal* 4D time and not the the physical time τ on the brane. Therefore, the mass of the KK-particles, which is simply their momentum in the direction transverse to the branes, is redshifted like their kinetic energy from the point of view of an observer sitting on the brane measuring physical time $d\tau \simeq a dt$. This is true for all massive modes on an AdS braneworld.

Alone, this would imply a $1/a^4$ behavior of the energy density, as for the massless mode. But there is an additional factor $1/a^2$ coming from the value of the mode function ϕ_n on the brane. This function is normalized in the bulk but its value on the brane decreases. Physically this means, as time evolves, the probability that a KK-graviton is concentrated close to the brane becomes smaller and smaller, see Fig. 4. The KK-gravitons escape into the bulk. The wave function of massive gravitons is repulsed away from the brane. This is an expression of the confinement of gravity: the five dimensional aspects of it, like the KK-gravitons become less and less 'visible' on the brane. If the inter-brane distance which is given by y_s is large, the KK-gravitons have more space in the bulk and their density on the brane decreases. In the limit $y_s \to \infty$ they disappear completely from the brane, even though they are still present in the bulk.

At first, one might be surprised by this decay law since we know that the energy density corresponding to the 5D Weyl tensor projected onto the brane decays like $1/a^4$ in a FRW braneworld, from where its name 'dark radiation' stems. But here we do not consider a component which is homogeneous on the physical brane, but a perturbation. Furthermore, the graviton energy momentum tensor is quadratic in the perturbation field h_{ij}.

Finally, let us evaluate the constraint induced from the requirement that the KK-energy density on the brane be smaller than the radiation density $\rho_{\rm KK}(t) < \rho_{\rm rad}(t)$ at all times. If this is not satisfied, back-reaction cannot be neglected and our results are no longer valid. Clearly, at early times this condition is more stringent than at late times since $\rho_{\rm KK}$ decays faster then $\rho_{\rm rad}$. Inserting the value of the scale factor directly after the bounce, $a_{\rm min}^{-2} = v_b$, we find, using again the RS fine tuning condition (2.13),

$$\left(\frac{\rho_{\rm KK}}{\rho_{\rm rad}}\right)_{\rm max} \simeq 100\, v_b^3 \left(\frac{L}{y_s}\right)\left(\frac{L}{L_s}\right)^2 . \tag{7.9}$$

If we use the largest value for the brane velocity v_b admitted by the nucleosynthesis bound $v_b \simeq 0.1$ and require that $\rho_{\rm KK}/\rho^{\rm rad}$ be (much) smaller than one for back-reaction effects to be negligible we obtain the very stringent condition

$$\frac{L}{y_s} \ll \left(\frac{L_s}{L}\right)^2 . \tag{7.10}$$

Let us first the largest allowed value for $L \simeq 0.1$mm. The Randall-Sundrum fine tuning condition then determines $L_s = (LL_{Pl}^2)^{1/3} \simeq 10^{-22}$mm $\simeq 1/(10^6$TeV). In this case the brane tension is $\mathcal{T} = 6\kappa_4/\kappa_5^2 = 6L_{Pl}^2/L_s^6 = 6/(LL_s^3) \sim (10\text{TeV})^4$. Furthermore, we have $(L/L_s)^2 \simeq 10^{42}$ so that $y_s > L(L/L_s)^2 \simeq 10^{41}$mm $\simeq 3\times 10^{15}$Mpc which is about 12 orders of magnitude larger than the present Hubble scale.

Also, since $y_b(t) \ll L$ in the low energy regime, and $y_s \gg L$ according to the inequaltiy (7.10), the physical brane and the static brane are very far apart at all times. Note that the distance between the physical and the static brane is

$$d = \int_{y_b}^{y_s} \frac{L}{y} dy = L\log(y_s/y_b) \gtrsim L \gg L_s .$$

This situation is probably not very realistic. We need some high energy, stringy effects to provoke the bounce and we expect these to be relevant only when the branes are sufficiently close, i.e. at a distance of order L_s. But in this case the constraint (7.10) will be violated which implies that back-reaction will be relevant.

On the other hand, if we want that $y_s \simeq L$ and back-reaction to be unimportant, then Eq. (7.9) implies that the bounce velocity has to be exceedingly small, $v_b \lesssim 10^{-15}$.

One might hope to find a way out of these conclusions by allowing the bounce to happen in the high energy regime. But then $v_b \simeq 1$ and the nucleosynthesis bound is violated since too many zero-mode gravitons are produced. Even if we disregard this limit for a moment, saying that our calculation only applies in the low energy regime, $v_b \ll 1$, the modification coming from

the high energy regime are not expected to alleviate the bounds. In the high energy regime we have to perform a y-dependent boost in y direction in order to obtain coordinates with respect to which the gravitons satisfy Neumann boundary condition at the physical brane $y_b(t)$ and at the static brane y_s along the lines of Ref. [40]. In this work, which considers the generation of scalar particles and TM photons in an oscillating cavity, it is found that particle creation at high speed is rather somewhat more efficient than the low velocity result which neglects the time derivative in the boundary condition. We therefore expect the energy densities of both, the zero-mode and the KK-mode gravitons to be rather larger than in the case analysed here.

In the high energy regime we may of course have $y_b(t) \gg L$ and therefore the physical brane can approach the static brane arbitrarily closely without the latter having to violate (7.10).

VIII. CONCLUSIONS

The dynamical Casimir effect from two bouncing branes leads to a blue spectrum of gravitons which has much too little power on large scales to affect the fluctuations of the CMB. Also the energy density of the generated massless gravitons is small for natural choices of the parameters. However, requiring that also the energy density of KK-gravitons is always smaller than the radiation density leads to interesting constraints on the ratios between the string and AdS scales and between the AdS scale and the position of the static brane.

The energy density of the KK gravitons decays very fast when the universe expands, like stiff matter, $\propto 1/a^6$. All KK-modes of a (massless) bulk field in an AdS braneworld have this property and they can therefore not provide the dark matter.

The present model is not ruled out by observations and backreaction is negligible as long as $y_s \gg L(L/L_s)^2$. In the low energy regime where $y_b(t) \ll L$, this makes a bounce unlikely. Therefore, either back reaction from KK-gravitons is very important or the bounce takes place in the high energy regime where particle creation is rather more abundant. The detailed calculation of the graviton spectrum in the high energy regime is reserved for future work.

If back-reaction is important we expect it to affect the bulk geometry. This model might be appropriate to study this issue, since particle creation happens only at the bounce.

On the other hand, at the level discussed here, this model does not provide a mechanism to generate initial fluctuations nor can it explain the origin of dark matter. In principle, however one can add an inflationary phase after the bounce which then leads to a scale invariant spectrum of perturbations in the same way as ordinary inflation [22].

The results obtained in this work are summarized in a letter [41].

Acknowledgment

We thank Cyril Cartier who participated in the early stages of this work and Kazuya Koyama for discussions. We are grateful for the use of the 'Myrinet'-cluster of Geneva University on which most of the quite intensive numerical computations have been performed. This work is supported by the Swiss National Science Foundation.

APPENDIX A: THE COUPLING MATRICES $M_{\alpha\beta}$ AND $N_{\alpha\beta}$

The coupling matrices $M_{\alpha\beta}$ and $N_{\alpha\beta}$ are given by [21]

$$M_{\alpha\beta}(t) \equiv (\partial_t\phi_\alpha, \phi_\beta) \ , \quad N_{\alpha\beta}(t) \equiv (\partial_t\phi_\alpha, \partial_t\phi_\beta) \ . \quad \text{(A1)}$$

The completeness of the eigenfunctions ϕ_α implies

$$\sum_\gamma \phi_\gamma(y)\phi_\gamma(\tilde{y}) = \delta(y-\tilde{y})y^3 \ , \quad \text{(A2)}$$

so that

$$\begin{aligned}\sum_\gamma M_{\alpha\gamma}M_{\beta\gamma} =& \sum_\gamma [(\partial_t\phi_\alpha, \phi_\gamma)(\partial_t\phi_\beta, \phi_\gamma)] \\ =& (\partial_t\phi_\alpha, \partial_t\phi_\beta) = N_{\alpha\beta} \ . \end{aligned} \quad \text{(A3)}$$

The use of several identities of Bessel functions leads to

$$M_{00} = \widehat{y}_{\rm b}\frac{y_{\rm s}^2}{y_{\rm s}^2 - y_{\rm b}^2} \ , \quad \text{(A4)}$$

$$M_{0j} = 0 \ , \quad \text{(A5)}$$

$$M_{i0} = \frac{2N_i}{\pi m_i}\frac{\hat{y}_b}{y_b}\phi_0 = \hat{y}_b\,\frac{2\sqrt{2}}{\pi m_i}\,N_i\,\frac{y_s}{\sqrt{y_s^2 - y_b^2}} \ , \quad \text{(A6)}$$

$$M_{ii} = \widehat{\rm m}_i \ , \quad \text{(A7)}$$

$$M_{ij} = M_{ij}^{\rm A} + M_{ij}^{\rm N} \quad \text{(A8)}$$

with

$$\begin{aligned} M_{ij}^{\rm A} =& (\hat{y}_b + \hat{m}_i)y_b\frac{m_i^2 N_i N_j}{m_j^2 - m_i^2}\times \\ &\times [y_s\,\mathcal{C}_2(m_j y_s)\,\mathcal{J}_1(m_i y_s) - y_b\,\mathcal{C}_2(m_j y_b)\,\mathcal{J}_1(m_i y_b)] \end{aligned} \quad \text{(A9)}$$

where

$$\mathcal{J}_1(m_i\,y) = [J_2(m_i y_b)Y_1(m_i y) - Y_2(m_i y_b)J_1(m_i y)] \quad \text{(A10)}$$

and

$$M_{ij}^{\rm N} = N_i N_j m_i \hat{m}_i \int_{y_b}^{y_s} dy y^2 \mathcal{C}_1(m_i y)\mathcal{C}_2(m_j y). \quad \text{(A11)}$$

This integral has to be solved numerically. Note that, because of the boundary conditions, on has the identity

$$\int_{y_b}^{y_s} dy y^2 \mathcal{C}_1(m_i y)\mathcal{C}_2(m_j y) = -\int_{y_b}^{y_s} dy y^2 \mathcal{C}_1(m_i y)\mathcal{C}_0(m_j y). \tag{A12}$$

Furthermore, one can simplify

$$\mathcal{J}_1(m_i\, y_b) = \frac{2}{\pi m_i y_b}\ ,\ \ \mathcal{J}_1(m_i\, y_s) = \frac{2}{\pi m_i y_b}\frac{Y_1(m_i y_s)}{Y_1(m_i y_b)} \tag{A13}$$

where the limiting value has to be taken for the last term whenever $Y_1(m_i y_b) = Y_1(m_i y_s) = 0$.

APPENDIX B: ON POWER SPECTRUM AND ENERGY DENSITY CALCULATION

1. Instantaneous vacuum

In Section III the in - out state approach to particle creation has been presented. The definition of the in - and out- vacuum states Eq. (3.9) is unique and the particle concept is well defined and meaningful. It is also possible to interpret $t_{\rm out}$ as continous time variable. Then we can write the Bogoliubov transformation Eq. (3.23) as

$$\hat{a}_{\alpha,\mathbf{k},\bullet}(t) = \sum_\beta \left[\mathcal{A}_{\beta\alpha,k}(t)\hat{a}^{\rm in}_{\beta,\mathbf{k},\bullet} + \mathcal{B}^*_{\beta\alpha,k}(t)\hat{a}^{\rm in\,\dagger}_{\beta,-\mathbf{k},\bullet}\right]. \tag{B1}$$

where at any time t we have introduced a set of operators $\{\hat{a}_{\alpha,\mathbf{k}\bullet}(t), \hat{a}^\dagger_{\alpha,\mathbf{k},\bullet}\}(t)$. Vacuum states defined at any time t can be associated with those operators via

$$\hat{a}_{\alpha,\mathbf{k},\bullet}(t)|0,t\rangle = 0\ \ \forall\, \alpha, \mathbf{k}\ \bullet\,. \tag{B2}$$

Similar to Eq. (3.11) a "particle number" can be introduced through

$$\mathcal{N}_{\alpha,k}(t) = \sum_\bullet \langle 0,{\rm in}|\hat{a}^{t\,\dagger}_{\alpha,\mathbf{k}\bullet}\hat{a}^t_{\alpha,\mathbf{k},\bullet}|0,{\rm in}\rangle = 2\sum_\beta |\mathcal{B}_{\beta\alpha,k}(t)|^2 \tag{B3}$$

We shall denote $|0,t\rangle$ as the instantaneous vacuum state and the quantity $\mathcal{N}_{\alpha,k}(t)$ as instantaneous particle number [10]. However, even if we call it "particle number" and plot it in section V for illustrative reasons, we consider only the particle definitions for the initial and final state (asymptotic regions) outlined in section III as physically meaningful particles.

[10] It could be interpreted as the number of particles which would have been created if the motion of the boundary (the brane) stops at time t.

2. Power spectrum

In order to calculate the power spectrum Eq. (4.7) we need to evaluate the expectation value

$$\langle \hat{h}_\bullet(t,y_b,\mathbf{k})\hat{h}^\dagger_\bullet(t,y_b,\mathbf{k}')\rangle_{\rm in} = \frac{\kappa_5}{L^3}\sum_{\alpha\alpha'}\phi_\alpha(t,y_b)\phi_{\alpha'}(t,y_b)\langle \hat{q}_{\alpha,\mathbf{k},\bullet}(t)\hat{q}^\dagger_{\alpha',\mathbf{k}',\bullet}(t)\rangle_{\rm in} \tag{B4}$$

where we have introduced the shortcut $\langle ...\rangle_{\rm in} = \langle 0,{\rm in}|...|0,{\rm in}\rangle$. Using the expansion (3.15) of $\hat{q}_{\alpha',\mathbf{k}'\bullet}(t)$ in itital state operators and complex functions $\epsilon^{(\gamma)}_{\alpha,k}(t)$ one finds

$$\langle \hat{q}_{\alpha,\mathbf{k}\bullet}(t)\hat{q}^\dagger_{\alpha',\mathbf{k}'\bullet}(t)\rangle_{\rm in} = \sum_\beta \frac{\epsilon^{(\beta)}_{\alpha,k}(t)\,\epsilon^{(\beta)*}_{\alpha',k}(t)}{2\omega^{\rm in}_{\beta,k}}\,\delta^{(3)}(\mathbf{k}-\mathbf{k}'). \tag{B5}$$

From the initial conditions (3.20) it follows that the sum in (B4) diverges at $t = t_{\rm in}$. This divergence is related to the usual normal ordering problem and can be removed by a substraction scheme. However, in order to get a well defined power spectrum at all times, it is not sufficient just to substract the term $(1/2)(\delta_{\alpha\alpha'}/\omega^{\rm in}_{\alpha,k})\delta^{(3)}(\mathbf{k}-\mathbf{k}')$ which corresponds to $\langle \hat{q}_{\alpha,\mathbf{k},\bullet}(t_{\rm in})\hat{q}^\dagger_{\alpha',\mathbf{k}',\bullet}(t_{\rm in})\rangle_{\rm in}$ in the above expression. In order to identify all terms contained in it we use the instantaneous particle concept which allows us to treat the Bogoliubov coefficients (3.24) and (3.25) as continuos functions of time. First we express the complex functions $\epsilon^{(\beta)}_{\alpha,k}$ in (B5) in terms of $\mathcal{A}_{\gamma\alpha,k}(t)$ and $\mathcal{B}_{\gamma\alpha,k}(t)$. This is of course equivalent to calculating the expectation value using [cf. Eq.(3.7)]

$$\hat{q}_{\alpha,k\bullet}(t) = \frac{1}{\sqrt{2\omega_{\alpha,k}(t)}}\left[\hat{a}_{\alpha,\mathbf{k},\bullet}(t)\Theta_{\alpha,k}(t) + \hat{a}^\dagger_{\alpha,-\mathbf{k},\bullet}(t)\Theta^*_{\alpha,k}(t)\right] \tag{B6}$$

and the Bogoliubov transformation Eq. (B1). The result consists of terms involving the Bogoliubov coefficients and the factor $(1/2)(\delta_{\alpha\alpha'}/\omega_{\alpha,k}(t))\delta^{(3)}(\mathbf{k}-\mathbf{k}')$, leading potentially to a divergence at all times. This term corresponds to $\langle 0,t|\hat{q}_{\alpha,\mathbf{k},\bullet}(t)\hat{q}^\dagger_{\alpha',\mathbf{k}',\bullet}(t)|0,t\rangle$, i.e. it is related to the normal ordering problem (zero-point energy) with respect to the instantaneous vacuum state $|0,t\rangle$. It can be removed by the substraction scheme

$$\langle \hat{q}_{\alpha,\mathbf{k}\bullet}(t)\hat{q}^\dagger_{\alpha',\mathbf{k}'\bullet}(t)\rangle_{\rm in,phys} = \langle \hat{q}_{\alpha,\mathbf{k}\bullet}(t)\hat{q}^\dagger_{\alpha',\mathbf{k}'\bullet}(t)\rangle_{\rm in} - \langle 0,t|\hat{q}_{\alpha,\mathbf{k}\bullet}(t)\hat{q}^\dagger_{\alpha',\mathbf{k}'\bullet}(t)|0,t\rangle \tag{B7}$$

where we use the substript "phys" to denote the physically meaningful expectation value. Inserting this expectation value into (B4), and using Eq. (4.2) on finds

$$\langle \hat{h}_\bullet(t,\mathbf{k},y_b)\hat{h}_\bullet(t,\mathbf{k}',y_b)\rangle_{\rm in} = \frac{1}{a^2}\frac{\kappa_5}{L}\sum_\alpha \mathcal{R}_{\alpha,k}(t)\mathcal{Y}^2_\alpha(a)\delta^{(3)}(\mathbf{k}-\mathbf{k}') \tag{B8}$$

with $\mathcal{R}_{\alpha,k}(t)$ defined in Eq. (4.9). The function $\mathcal{O}^{\mathcal{N}}_{\alpha,k}$ appearing in Eq. (4.9) is explicitely given by

$$\mathcal{O}^{\mathcal{N}}_{\alpha,k} = 2\,\Re\sum_{\beta}\Big\{\Theta^2_{\alpha,k}\mathcal{A}_{\beta\alpha,k}\mathcal{B}^*_{\beta\alpha,k} + \Theta_{\alpha,k}\sum_{\alpha'\neq\alpha}\times \\ \times\sqrt{\frac{\omega_{\alpha,k}}{\omega_{\alpha',k}}}\frac{\mathcal{Y}_{\alpha'}(a)}{\mathcal{Y}_{\alpha}(a)}\left[\Theta^*_{\alpha',k}\mathcal{B}^*_{\beta\alpha}\mathcal{B}_{\beta\alpha'} + \Theta_{\alpha',k}\mathcal{A}_{\beta\alpha}\mathcal{B}^*_{\beta\alpha'}\right]\Big\} \tag{B9}$$

and $\mathcal{O}^{\epsilon}_{\alpha,k}$ appearing in Eq. (4.10) reads

$$\mathcal{O}^{\epsilon}_{\alpha,k} = \sum_{\beta,\alpha'\neq\alpha}\frac{\mathcal{Y}_{\alpha'}(a)}{\mathcal{Y}_{\alpha}(a)}\frac{\epsilon^{(\beta)}_{\alpha,k}\epsilon^{(\beta)^*}_{\alpha',k}}{\omega^{\rm in}_{\beta,k}}. \tag{B10}$$

3. Energy density

In order to calculate the energy density we need to evaluate the expectation value $\langle\dot{\hat{h}}_{ij}(t,\mathbf{x},y_b)\dot{\hat{h}}^{ij}(t,\mathbf{x},y_b)\rangle_{\rm in}$. Using (2.19) and the relation $e^{\bullet}_{ij}(-\mathbf{k}) = (e^{\bullet}_{ij}(\mathbf{k}))^*$ one finds

$$\langle\dot{\hat{h}}_{ij}(t,\mathbf{x},y_b)\dot{\hat{h}}^{ij}(t,\mathbf{x},y_b)\rangle_{\rm in} = \sum_{\bullet\bullet'}\int\frac{d^3k}{(2\pi)^{3/2}}\frac{d^3k'}{(2\pi)^{3/2}}\times \tag{B11}$$

$$\times\,\langle\dot{\hat{h}}_{\bullet}(t,y_b,\mathbf{k})\dot{\hat{h}}^{\dagger}_{\bullet'}(t,y_b,\mathbf{k}')\rangle_{\rm in}e^{i(\mathbf{k}-\mathbf{k}')\cdot\mathbf{x}}e^{\bullet}_{ij}(\mathbf{k})\,\left(e^{\bullet' ij}(\mathbf{k}')\right)^*.$$

By means of the expansion (3.17) the expectation value $\langle\dot{\hat{h}}_{\bullet}(t,y_b,\mathbf{k})\dot{\hat{h}}^{\dagger}_{\bullet'}(t,y_b,\mathbf{k}')\rangle_{\rm in}$ becomes

$$\langle\dot{\hat{h}}_{\bullet}(t,y_b,\mathbf{k})\dot{\hat{h}}^{\dagger}_{\bullet'}(t,y_b,\mathbf{k}')\rangle_{\rm in} \tag{B12}$$
$$= \frac{\kappa_5}{L^3}\sum_{\alpha\alpha'}\langle\hat{p}_{\alpha,\mathbf{k},\bullet}(t)\hat{p}^{\dagger}_{\alpha',\mathbf{k}',\bullet'}(t)\rangle_{\rm in}\phi_{\alpha}(t,y_b)\phi_{\alpha'}(t,y_b).$$

From the definition of $\hat{p}_{\alpha,\mathbf{k},\bullet}(t)$ in Eq. (3.18) it is clear that this expectation value will in general contain terms proportional to the coupling matrix and its square when expressed in terms of $\epsilon^{(\beta)}_{\alpha,k}$. However, since we are interested in the expectation value at late times only when the brane moves very slowly such that the mode couplings go to zero and a physical meaningful particle definition can be given, we can set

$$\langle\hat{p}_{\alpha,\mathbf{k},\bullet}(t)\hat{p}^{\dagger}_{\alpha',\mathbf{k}',\bullet'}(t)\rangle_{\rm in} = \left\langle\dot{\hat{q}}_{\alpha,\mathbf{k},\bullet}(t)\dot{\hat{q}}^{\dagger}_{\alpha',\mathbf{k}',\bullet'}(t)\right\rangle_{\rm in}. \tag{B13}$$

Calculating this expectation value by using Eq. (3.15) leads to an expression which, as for the power spectrum calculation before, has a divergent part related to the zero-point energy of the instantaneous vacuum state (normal ordering problem). We remove this part by a subtraction scheme similar to Eq (B7). The final result reads

$$\langle\dot{\hat{q}}_{\alpha,\mathbf{k}\bullet}(t)\dot{\hat{q}}^{\dagger}_{\alpha',\mathbf{k}'\bullet'}(t)\rangle_{\rm in,phys} \tag{B14}$$
$$= \frac{1}{2}\left[\sum_{\beta}\frac{\dot{\epsilon}^{(\beta)}_{\alpha,k}(t)\dot{\epsilon}^{(\beta)^*}_{\alpha',k'}(t)}{\sqrt{\omega^{\rm in}_{\beta,k}\omega^{\rm in}_{\beta,k'}}} - \omega_{\alpha,k}(t)\delta_{\alpha\alpha'}\right]\delta_{\bullet\bullet'}\delta^{(3)}(\mathbf{k}-\mathbf{k}').$$

Inserting this result into Eq. (B12), splitting the summations in sums over $\alpha=\alpha'$ and $\alpha\neq\alpha'$ and neglecting the oscillating $\alpha\neq\alpha'$ contributions having averaging over several oscillations in mind, leads to

$$\langle\dot{\hat{h}}_{\bullet}(t,y_b,\mathbf{k})\dot{\hat{h}}^{\dagger}_{\bullet'}(t,y_b,\mathbf{k}')\rangle_{\rm in} \tag{B15}$$
$$= \frac{1}{a^2}\frac{\kappa_5}{L}\sum_{\alpha}\mathcal{K}_{\alpha,k}(t)\mathcal{Y}^2_{\alpha}(a)\delta_{\bullet\bullet'}\delta^{(3)}(\mathbf{k}-\mathbf{k}')$$

where the function $\mathcal{K}_{\alpha,k}(t)$ is formally given by

$$\mathcal{K}_{\alpha,k}(t) = \sum_{\beta}\frac{|\dot{\epsilon}^{(\beta)}_{\alpha,k}(t)|^2}{\omega^{\rm in}_{\beta,k}} - \omega_{\alpha,k}(t) = \omega_{\alpha,k}(t)\mathcal{N}_{\alpha,k}(t). \tag{B16}$$

and we have made use of Eq. (4.2). The relation between $\sum_{\beta}|\dot{\epsilon}^{(\beta)}_{\alpha,k}(t)|^2/\omega^{\rm in}_{\beta,k}$ and the number of created particles can easily be established. Using this expression in Eq. (B11) leads eventually to

$$\langle 0,{\rm in}|\dot{\hat{h}}_{ij}(t,\mathbf{x},y_b)\dot{\hat{h}}^{ij}(t,\mathbf{x},y_b)|0,{\rm in}\rangle \tag{B17}$$
$$= \frac{2}{a^2}\frac{\kappa_5}{L}\sum_{\alpha}\int\frac{d^3k}{(2\pi)^3}\mathcal{K}_{\alpha,k}(t)\mathcal{Y}^2_{\alpha}(a)$$

where we have used that

$$\sum_{\bullet}e^{\bullet}_{ij}(\mathbf{k})\,\left(e^{\bullet\,ij}(\mathbf{k})\right)^* = 2. \tag{B18}$$

The final expression for the energy density Eq. (4.18) is then obtained by exploiting that $\kappa_5/L = \kappa_4$.

APPENDIX C: NUMERICS

In order to calculate the number of produced gravitons the system of coupled differential equations (3.34) and (3.35) is solved numerically. The complex functions $\xi^{(\beta)}_{\alpha,k}$, $\eta^{(\beta)}_{\alpha,k}$ are decomposed into their real and imaginary parts:

$$\xi^{(\beta)}_{\alpha,k} = u^{(\beta)}_{\alpha,k} + iv^{(\beta)}_{\alpha,k}\,,\quad \eta^{(\beta)}_{\alpha,k} = x^{(\beta)}_{\alpha,k} + iy^{(\beta)}_{\alpha,k}. \tag{C1}$$

The system of coupled differential equations is then written as (cf. Eq. (A2) of [29])

$$\dot{\mathbf{X}}^{(\beta)}_{k}(t) = \mathbf{W}_k(t)\mathbf{X}^{(\beta)}_{k}(t) \tag{C2}$$

where

$$\mathbf{X}^{(\beta)}_{k} = \\ \left(u^{(\beta)}_{0,k}...u^{(\beta)}_{n_{\rm max},k}x^{(\beta)}_{0,k}...x^{(\beta)}_{n_{\rm max},k}v^{(\beta)}_{0,k}...v^{(\beta)}_{n_{\rm max},k}y^{(\beta)}_{0,k}...y^{(\beta)}_{n_{\rm max},k}\right)^{\rm T}. \tag{C3}$$

The matrix $\mathbf{W}_k(t)$ is given by Eq. (A4) of [29] but here indices start at zero. The number of produced gravitons can be calculated direclty from the solutions to this

system using Eqs. (3.28) and (3.32). Note that for a given truncation parameter $n_{\max}$ the above system of size $4(n_{\max}+1)\times 4(n_{\max}+1)$ has to be solved $n_{\max}+1$ - times, each time with different initial conditions (3.38). The main difficulty in the numerical simulations is that most of the entries of the matrix $\mathbf{W}_k(t)$ [Eq. (A4) of [29]] are not known analytically. This is due to the fact that Eq. (2.33) which determines the time-dependent KK-masses $m_i(t)$ does not have an (exact) analytical solution. Only the 00-component of the coupling matrix $M_{\alpha\beta}$ is known analytically. We therefore have to determine the time-dependent KK-spectrum $\{m_i(t)\}_{i=1}^{n_{\max}}$ by solving Eq. (2.33) numerically. In addition, also the part M_{ij}^N [Eq. (A11)] has to be calculated numerically since the integral over the particular combination of Bessel functions can not be found analytically.

We numerically evaluate the KK-spectrum and the integral M_{ij}^N for discrete time-values t_i and use spline routines to assemble $\mathbf{W}_k(t)$. The system (C2) can then be solved using standard routines. We chose the separation of the t_i's in a non-uniform way. A more dense mesh close to the bounce and a less dense mesh at early and late times. The independence of the numerical results on the particular separation is checked. In order to implement the bounce as realistic as possible we do not spline the KK-spectrum very close to the bounce but recalculate it numerically at every time t needed in differential equation solver. This minimizes possible artificial effects caused by using a spline in the direct vicinity of the bounce. The same is done for M_{ij}^N and we find that splining M_{ij}^N when propagating through the bounce does not affect the numerical results.

Entirely routines provided by the GNU Scientific Library (GSL) [42] have been employed. Different routines for root finding, and integration and several differential equation solvers have been compared. The code has been parallelized (MPI) in order to deal with the intensive numerical computations.

The accuracy of the numerical simulations can be assessed by checking the validity of the Bogoliubov relations

$$\sum_\beta \left[\mathcal{A}_{\beta\alpha,k}(t)\mathcal{A}^*_{\beta\gamma,k}(t) - \mathcal{B}^*_{\beta\alpha,k}(t)\mathcal{B}_{\beta\gamma,k}(t)\right] = \delta_{\alpha\gamma} \quad \text{(C4)}$$

$$\sum_\beta \left[\mathcal{A}_{\beta\alpha,k}(t)\mathcal{B}^*_{\beta\gamma,k}(t) - \mathcal{B}^*_{\beta\alpha,k}(t)\mathcal{A}_{\beta\gamma,k}(t)\right] = 0. \quad \text{(C5)}$$

In the following we demonstrate the accuracy of the numerical simulations by considering the diagonal part of (C4). The deviation of the quantity

$$d_{\alpha,k}(t) = 1 - \sum_\beta \left[|\mathcal{A}_{\beta\alpha,k}(t)|^2 - |\mathcal{B}_{\beta\alpha,k}(t)|^2\right] \quad \text{(C6)}$$

from zero gives a measure for the accuracy of the numerical result. We consider this quantity at final times $t_{\rm out}$ and compare it with the corresponding final particle spectrum. In Fig. 32 we compare the final KK-graviton spectrum $\mathcal{N}^{\rm out}_{n,k,\bullet}$ with the expression $d_{n,k}(t_{\rm out})$ for two different cases. We observe that the accuracy of the numerical simulations is very good. Even if the particle number is only of order 10^{-7} to 10^{-6}, the deviation of $d_{n,k}(t_{\rm out})$ from zero is at least one order of magnitude smaller. This demonstrates the reliability of our numerical simulations and that we can trust the numerical results presented in this work.

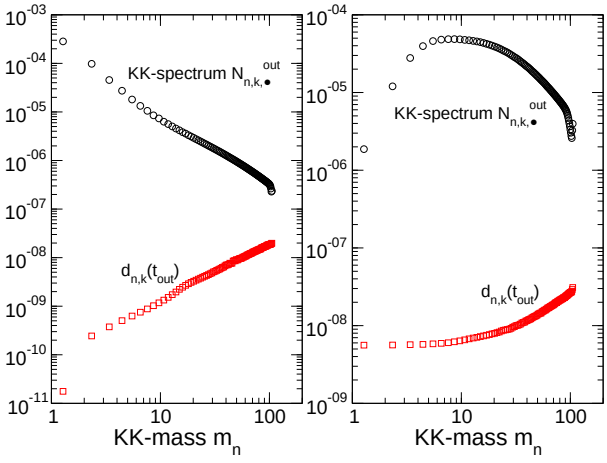

FIG. 32: Comparison of the final KK-graviton spectrum $\mathcal{N}^{\rm out}_{n,k,\bullet}$ with the expression $d_{n,k}(t_{\rm out})$ describing to what accuracy the diagonal part of the Bogoliubov relation (C4) is satisfied. Left panel: $y_s=3$, $k=0.1$, $v_b=0.03$ and $n_{\max}=100$ [cf. Fig. 24]. Right panel: $y_s=3$, $k=30$, $v_b=0.1$ and $n_{\max}=100$ [cf. Fig. 25].

APPENDIX D: DYNAMICAL CASIMIR EFFECT FOR A UNIFORM MOTION

Consider a massless scalar field on a time-dependent interval $[0,y(t)]$. The time-evolution of its mode functions are described by a system of differential equation like (2.37) where the specific form of $M_{\alpha\beta}$ depends on the particular boundary condition the field is subject to. In [28, 30] a method has been introduced to study particle creation due to the motion of the boundary $y(t)$ (i.e. the dynamical Casimir effect) fully numerically. We refer the interested reader to those publications for more details. If the boundary undergoes a uniform motion $y(t)=1+vt$ (in units of some reference length) it was shown in [38, 39] that the total number of created scalar particles diverges caused by the discontinuities in the velocity at the beginning and at the end of the motion. In particular (in case of Dirichlet boundary conditions) it was found in [39] that $\langle 0,\text{in}|\hat{N}^{\rm out}_n|0,\text{in}\rangle \propto v^2/n$ if $n>6$ and $v\ll 1$. Thereby in- and out- vacuum states are defined like in the present work and the frequency of a mode function is given by $\omega_n = \pi\, n\ ,\quad n=1,2,\ldots$. In Figure 33 we show spectra of created scalar particles obtained numerically with the method of [30] for this particular case. One observes that, as for our bouncing motion, the convergence is very

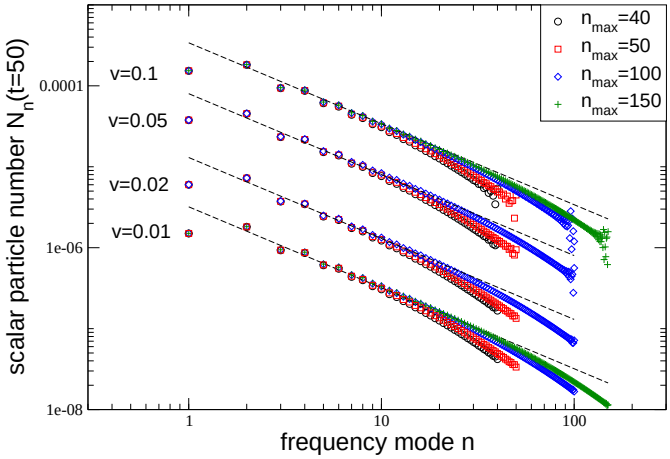

FIG. 33: Spectra of massless scalar particles produced under the influence of the uniform motion $y(t) = 1 + vt$ for velocities $v = 0.01, 0.02, 0.05$ and 0.1. The numerical results are compared to the expression $N_n = 0.035v^2/n$ (dashed lines) which agrees with the analytical prediction $N_n \propto v^2/n$.

slow. As already explained in Section V.D, the discontinuities in the velocity lead to the excitation of arbitrary high frequnecy modes. Nevertheless it is evident from Fig. 33 that the numerically calculated spectra approach the analytical prediction also shown in the plot. The linear motion discussed here and the brane-motion (2.16) are very similar with respect to the discontinuities in the velocity. In both cases, the total discontinous change of the velocity is $2v$ and $2v_b$, respectively. The resulting divergence of the acceleration is responsible for the excitation and therefore creation of particles of all frequency modes. Consequently we expect the same $\propto v^2/\omega_n$ behaviour for the bouncing motion (2.16).

[1] J. Polchinski, *String theory. An introduction to the bosonic string, Vol. I* (Cambridge University Press, Cambridge, UK, 1998).
[2] J. Polchinski, *String theory. Superstring theory and beyond, Vol. II* (Cambridge University Press, Cambridge, UK, 1998).
[3] N. Arkani-Hamed, S. Dimopoulos, and G. R. Dvali, Phys. Lett. **B429**, 263 (1998), hep-ph/9803315.
[4] J. Polchinski, Phys. Rev. Lett. **75**, 4724 (1995),KY hep-th/9510017.
[5] L. Randall and R. Sundrum, Phys. Rev. Lett. **83**, 3370 (1999), hep-ph/9905221.
[6] L. Randall and R. Sundrum, Phys. Rev. Lett. **83**, 4690 (1999), hep-th/9906064.
[7] P. Kraus, JHEP **12**, 011 (1999), hep-th/9910149.
[8] M. Bordag, *Quantum Field Theory under the Influence of External Conditions* (Teuber, Stuttgart, 1996).
[9] C. Lanczos, Ann. Phys. (Leipzig) **74**, 518 (1924).
[10] N. Sen, Ann. Phys. (Leipzig) **73**, 365 (1924).
[11] G. Darmois, *Mémorial des sciences mathématiques, fascicule 25 chap. 5* (Gauthier-Villars, Paris, 1927).
[12] W. Israel, Nuovo Cimento **B44**, 463 (1966).
[13] C. W. Misner, K. S. Thorne, and J. A. Wheeler, *Gravitation* (W.H. Freeman and Compagny, San Francisco, USA, San Francisco, USA, 1973).
[14] N. Deruelle, T. Dolezel, and J. Katz, Phys. Rev. **D63**, 083513 (2001), hep-th/0010215.
[15] S. Mukohyama, Phys. Rev. **D64**, 064006 (2001), hep-th/0104185.
[16] R. Maartens, Living Rev. Rel. **7**, 7 (2004), gr-qc/0312059.
[17] P. Binetruy, C. Deffayet, U. Ellwanger, and D. Langlois, Phys. Lett. **B477**, 285 (2000), hep-th/9910219.
[18] S. W. Hawking, T. Hertog, and H. S. Reall, Phys. Rev. **D62**, 043501 (2000), hep-th/0003052.
[19] S. W. Hawking, T. Hertog, and H. S. Reall, Phys. Rev. **D63**, 083504 (2001), hep-th/0010232.
[20] D. Langlois, R. Maartens, and D. Wands, Phys. Lett. **B489**, 259 (2000), hep-th/0006007.
[21] C. Cartier, R. Durrer, M. Ruser, Phys. Rev. **D72**, 104018 (2005), hep-th/0510155.
[22] D. S. Gorbunov, V. A. Rubakov, and S. M. Sibiryakov, JHEP **10**, 015 (2001), hep-th/0108017.
[23] J. Khoury, P.J. Steinhardt, N. Turok, Phys. Rev. Lett. **92**, 031302 (2004), hep-th/0307132.
[24] J. Khoury, P.J. Steinhardt and N. Turok, Phys. Rev. Lett. **91** 161301 (2003), astro-ph/0302012.
[25] A. V. Frolov and L. Kofman (2002), hep-th/0209133.
[26] C. Cartier and R. Durrer, Phys. Rev. **D71**, 064022 (2005), hep-th/0409287.
[27] R. Durrer, *Braneworlds*, at the XI Brazilian School of Cosmology and Gravitation, Edt. M. Novello and S.E. Perez Bergliaffa, AIP Conference Proceedings 782 (2005), hep-th/0507006.
[28] M. Ruser, J. Opt. B: Quantum Semiclass. Opt. **7**, S100 (2005), quant-ph/0408142.
[29] M. Ruser, Phys. Rev. A **73**, 043811 (2006) [arXiv:quant-ph/0509030].
[30] M. Ruser, J. Phys. A **39** (2006) 6711.
[31] T. Kobayashi, H. Kudoh, and T. Tanaka, Phys. Rev. **D68**, 044025 (2003), gr-qc/0305006.
[32] K. Koyama, JCAP **0409**, 010 (2004), astro-ph/0407263.
[33] T. Kobayashi and T. Tanaka, Phys. Rev. D **71**, 124028 (2005).
[34] T. Kobayashi and T. Tanaka, Phys. Rev. D **73**, 044005 (2006).
[35] S. Seahra, Phys. Rev. D **74**, 044010 (2006).
[36] M. Abramowitz and I. Stegun, *Handbook of Mathematical Functions*, 9th Edition (Dover Publications, NY, 1970).
[37] M. Maggiore. Phys. Rept. **331**, 283 (2000).
[38] G. T. Moore, J. Math. Phys. **11**, 2679 (1970).
[39] M. Castagnino and R. Ferraro, Ann. Phys. **154**, 1 (1984).
[40] M. Crocce, D.A.R. Dalvit and F.D. Mazzitelli, Phys. Rev.

A66, 033811 (2002).
[41] R. Durrer and M. Ruser, `arXiv:0704.0756` (2007).
[42] http://www.gnu.org/software/gsl